INFORMATION TO USERS

This manuscript has been reproduced from the microfilm master. UMI films the text directly from the original or copy submitted. Thus, some thesis and dissertation copies are in typewriter face, while others may be from any type of computer printer.

The quality of this reproduction is dependent upon the quality of the copy submitted. Broken or indistinct print, colored or poor quality illustrations and photographs, print bleedthrough, substandard margins, and improper alignment can adversely affect reproduction.

In the unlikely event that the author did not send UMI a complete manuscript and there are missing pages, these will be noted. Also, if unauthorized copyright material had to be removed, a note will indicate the deletion.

Oversize materials (e.g., maps, drawings, charts) are reproduced by sectioning the original, beginning at the upper left-hand corner and continuing from left to right in equal sections with small overlaps. Each original is also photographed in one exposure and is included in reduced form at the back of the book.

Photographs included in the original manuscript have been reproduced xerographically in this copy. Higher quality 6" x 9" black and white photographic prints are available for any photographs or illustrations appearing in this copy for an additional charge. Contact UMI directly to order.

UMI

A Bell & Howell Information Company
300 North Zeeb Road, Ann Arbor MI 48106-1346 USA
313/761-4700 800/521-0600

Reconstructing the Oceanic ^{13}C Suess Effect

by

Rolf Erik Sonnerup

A dissertation submitted in partial
fulfillment of the requirements for the
degree of

Doctor of Philosophy

University of Washington

1999

Approved by: Paul Quay
Chairperson of Supervisory Committee

Program Authorized
to Offer Degree Oceanography

Date March 16, 1999

UMI
300 North Zeeb Road
Ann Arbor, MI 48103

Doctoral Dissertation

In presenting this thesis in partial fulfillment of the requirements for the Doctoral degree at the University of Washington, I agree that the Library shall make its copies freely available for inspection. I further agree that extensive copying of the dissertation is allowable only for scholarly purposes, consistent with "fair use" as prescribed in the U.S. Copyright Law. Requests for copying or reproduction of this dissertation may be referred to UMI Dissertation Services, 300 North Zeeb Road, P.O. Box 1346, Ann Arbor, MI 48106-1346, to whom the author has granted "the right to reproduce and sell (a) copies of the manuscript in microform and/or (b) printed copies of the manuscript made from microform."

Signature Rolf

Date March 16 1999

UNIVERSITY OF WASHINGTON

ABSTRACT

Reconstructing the Oceanic ^{13}C Suess Effect

by Rolf Erik Sonnerup

Chairperson of the Supervisory Committee: Professor Paul D. Quay
Department of Oceanography

This dissertation consists of two components: deriving along-isopycnal advection rates in the North Pacific from chlorofluorocarbon (CFC) distributions and determining $^{13}C/^{12}C$ changes in the global ocean due to oceanic uptake of anthropogenic CO_2.

Thermocline ventilation rates for the subtropical North Pacific were determined using a 1-dimensional (meridional) along-isopycnal model tuned to (CFC) concentrations measured along 152°W in 1991. Mean southward advection rates in the subtropics ranged from 1.0 to 0.6 cm s^{-1} between σ_θ = 25.5 and 26.6, and ventilation times for the subtropical gyre increased from about 10 to 27 years over that isopycnal range. Oxygen utilization rates (OURs) determined with the model decreased from 6.6 to 3.2 μmol kg^{-1} yr^{-1} between $\sigma_\theta = 25.5$ and 26.6. Extrapolation of the OUR versus depth trend to the base of the euphotic zone and integration from 500 to 100 meters depth implied a carbon export rate of 2.2 ± 0.5 moles C m^{-2} yr^{-1} from overlying surface waters at 30°N, 152°W.

The rate of anthropogenic $\delta^{13}C$ change in the oceans during 1968 to 1991 was determined from trends in preformed $^{13}C/^{12}C$ of dissolved inorganic carbon (DIC) and CFC-derived water ages on isopycnal surfaces, and, in the Indian Ocean, using a multiparameter linear regression (MLR) comparison of 1978 GEOSECS and 1995 WOCE $\delta^{13}C$ of DIC, hydrographic and nutrient data. The change rate of $\delta^{13}C$ in the surface ocean increased from about -0.13 ‰ decade^{-1} in the tropics to approximately -0.2 ‰ decade^{-1} within the subtropics, and then decreased to around -0.1 ‰ decade^{-1} in the subpolar oceans. Our reconstructions implied ocean-wide average surface ocean and depth-integrated $\delta^{13}C$ change rates of -0.15 to -0.17 ‰ decade^{-1} and -7.9 ± 3.1 μmol kg^{-1} yr^{-1}, respectively, using extrapolations based on ocean model predictions (Bacastow et al., 1996) and correlations with GEOSECS bomb ^{14}C inventories, respectively. The integrated $\delta^{13}C$ change implied global ocean CO_2 uptake rates during 1970-1990 of 1.3 ± 1 Gt. C yr^{-1} and 2.0 ± 0.9 Gt. C yr^{-1} using the $^{13}CO_2$ and $^{12}CO_2$ budget of Quay et al. (1992) and dynamic constraint method of Heimann and Maier Reimer (1996), respectively.

Table of contents

List of figures

Number *Page*

List of tables

Number *Page*

Acknowledgments

I would like to thank Paul Quay for his generosity and flexibility as an advisor, and for the constructive and insightful comments he provided on the many, many drafts of this manuscript. John Bullister provided open access to his CFC datasets and lots of encouragement during the early stages of this dissertation. I thank Susan Hautala for her enthusiasm; it provided a much needed shot in the arm down the stretch. Ann McNichol shared the WOCE $\delta^{13}C$ data from the National Ocean Sciences AMS facility.

My dissertation work benefited substantially from discussions with Anthony Aufdenkampe, Fiammetta Straneo, Emmanuel Boss and Jianrong Zhang. Several fellow students spent many long afternoons helping me with oral presentations, foremost among them were Amy Snover, Steven Gerst, Sherry Wilhelm, John Dunne, Hilairy Hartnett, Roberta Hamme, Jennifer Morford, Thomas Chapin, Jay Brandes and Michael McClain. Paul Quay also exceeded the call of duty in this regard. The North Pacific modeling study benefited from discussions with Steve Emerson, Mark Warner and Bill Jenkins.

Tania Westby and Heather Anderson made access to the $\delta^{13}C$ datasets easy and enjoyable. Dave Wilbur, Johnny Stutsman and David White are always a pleasure to work with. Also, many thanks to my officemates Jianrong Zhang, Amy Snover, and Steve Gerst for your friendship.

My Parents, Ulla and Bengt, and my sisters, Anna and Malin, supported me on all fronts in this endeavor. Finally, I thank my wife, Linda Kjarstad, for helping me keep my dissertation work in its proper perspective.

Chapter 1 : The oceanic ^{13}C Suess effect estimated by three independent methods

Introduction

Over the past 200 years fossil fuel combustion and deforestation have increased the CO_2 content of the atmosphere from its pre-industrial concentration of ~ 280 μatm to about 360 μatm today (Fig. 1.1). The increase, while substantial, represents only about half of the total amount of CO_2 released due to industrial activities alone, however (Keeling et al., 1989). Determining the fate of the remaining anthropogenic CO_2 is one of the most important problems in the science of global change. Without improvements in our understanding of the present budget for atmospheric CO_2, predictions of future CO_2 levels based on various emission scenarios remain highly uncertain.

The carbon reservoirs that are large enough and exchange with the atmosphere rapidly enough to be viable sinks for the missing fossil-fuel CO_2 are the terrestrial biosphere and the oceans. The terrestrial biosphere contains ~ 2,000 Gt. C (1 Gt. = 10^{12} g) primarily in trees and soils, and exchanges ~ 100 Gt. C yr $^{-1}$ with the atmosphere via photosynthesis and respiration. The ocean contains ~ 39,000 Gt. of dissolved inorganic carbon, and exchanges ~ 90 Gt. yr $^{-1}$ with the atmosphere via air-sea CO_2 gas exchange (Siegenthaler and Sarmiento, 1993). The distinction between the two sinks is important because any anthropogenic carbon sequestered in the oceans is unlikely to re-enter the

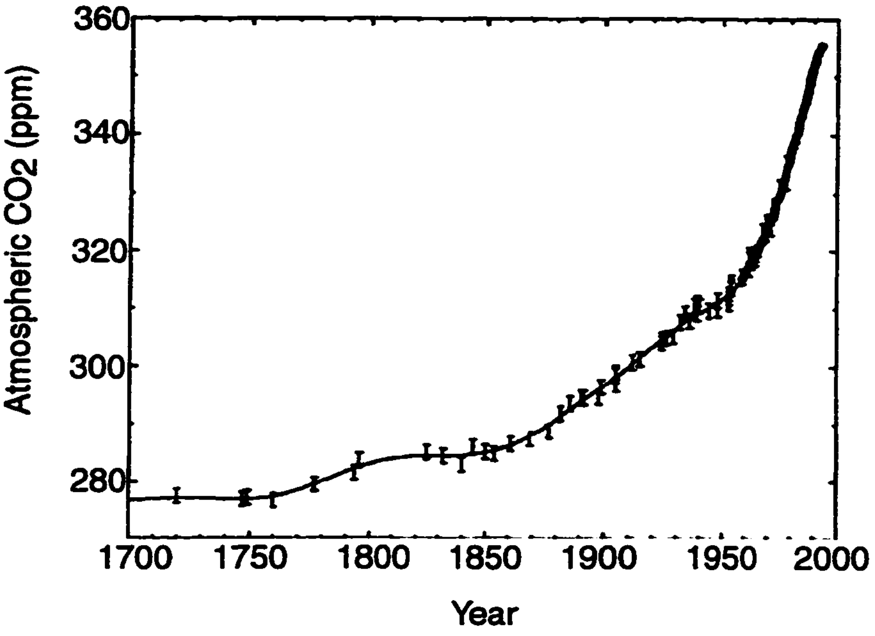

Figure 1.1. Atmospheric pCO_2 from air samples dated 1700-1995. The pre-1950 values are based on measurements of gasses trapped in bubbles in ice cores (Joos and Bruno, 1998).

atmosphere in the foreseeable future. Excess CO_2 stored in the terrestrial biosphere, on the other hand, is likely more vulnerable to re-release due to changes in climate or human activities. Recent studies have come to opposite conclusions regarding the fate of the CO_2 that is "missing" from the atmosphere. Calculations based on changes in atmospheric O_2 levels (Keeling et al., 1996) or on ocean models tuned to bomb ^{14}C (Siegenthaler and Sarmiento, 1993) generally indicate that of the 2.2 Gt. C yr^{-1} of missing anthropogenic CO_2, the oceans account for ~ 1.5 to 2 Gt. C yr^{-1} during 1970-1990, with a typical uncertainty of ± 1 Gt. C yr^{-1}. On the other hand, recent studies based on transport models and atmospheric distributions of CO_2 and $^{13}CO_2$ have concluded that terrestrial uptake of fossil fuel CO_2 has been the major sink, responsible for sequestration of 50 to 70 % (Ciais et al., 1995) or even up to 100 % (Tans and White, 1998) of the "missing" CO_2.

Direct determination of changes in the carbon inventory of the terrestrial biosphere is very difficult due to its heterogeneous nature. The magnitude of the oceanic CO_2 sink has been difficult to determine because the net CO_2 flux into the oceans due to atmospheric CO_2 increases is small relative to gross CO_2 exchange fluxes between the atmosphere, oceans and the terrestrial biosphere (Broecker and Peng, 1993). The above-ground detonation of nuclear bombs during the 1950s and 1960s resulted in a doubling of atmospheric $^{14}CO_2$ levels by 1963 (Fig. 1.2). Because this signal was so large, measurements of the penetration of bomb ^{14}C into the oceans have provided a relatively high signal-to-noise analog to the ocean's uptake of anthropogenic CO_2 (Broecker et al., 1985; Broecker et al., 1995). As a result, oceanic bomb ^{14}C inventories have been widely used for testing and calibrating models of oceanic CO_2 uptake (e.g., Siegenthaler and Sarmiento, 1993). Recently, however, Heimann and Maier Reimer (1996) have shown that because the time scales of the atmospheric perturbation histories of $^{12}CO_2$ and $^{14}CO_2$ are distinctly different (Figs. 1.1 and 1.2, respectively), oceanic $^{12}CO_2$ uptake and $^{14}CO_2$ uptake are poorly correlated in an ocean general circulation model (OGCM) simulation of the 20th century CO_2 perturbation.

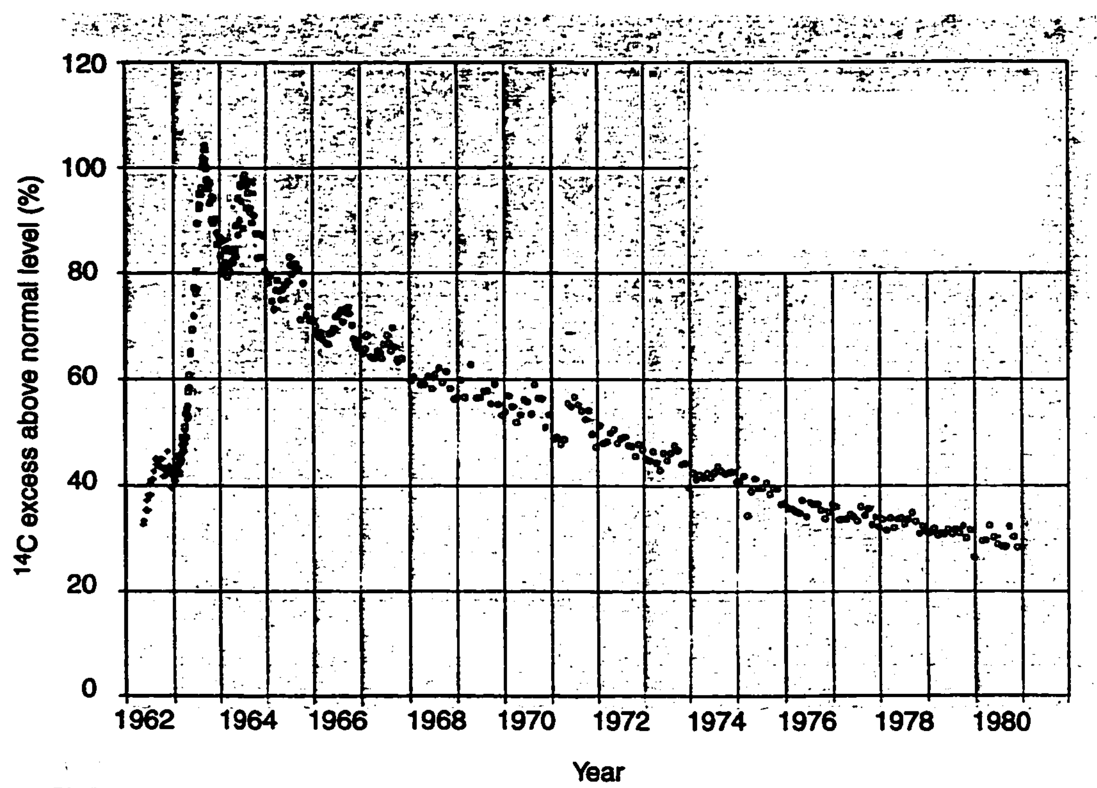

Figure 1.2. Atmospheric $\Delta^{14}C$ values measured during 1962-1981 (Nydal et al., 1983).

The oceanic ^{13}C Suess effect

The addition of anthropogenic CO_2 to the atmosphere has caused a decrease in the $^{13}C/^{12}C$ ratio[Ψ] of atmospheric CO_2 (Fig. 1.3), the so called "Suess effect", because fossil fuel and terrestrial biomass burning derived CO_2

[Ψ] $^{13}C/^{12}C$ ratios in this dissertation are expressed in parts per thousand using δ notation: $\delta(‰)=\left\{\frac{{}^{13}C/{}^{12}C_{sample}}{{}^{13}C/{}^{12}C_{standard}}-1\right\}\cdot 1000$ where the standard is the Pee Dee Belemnite (PDB) marine carbonate (Craig, 1957). In δ notation, positive numbers denote samples enriched in ^{13}C relative to PDB, and vice versa.

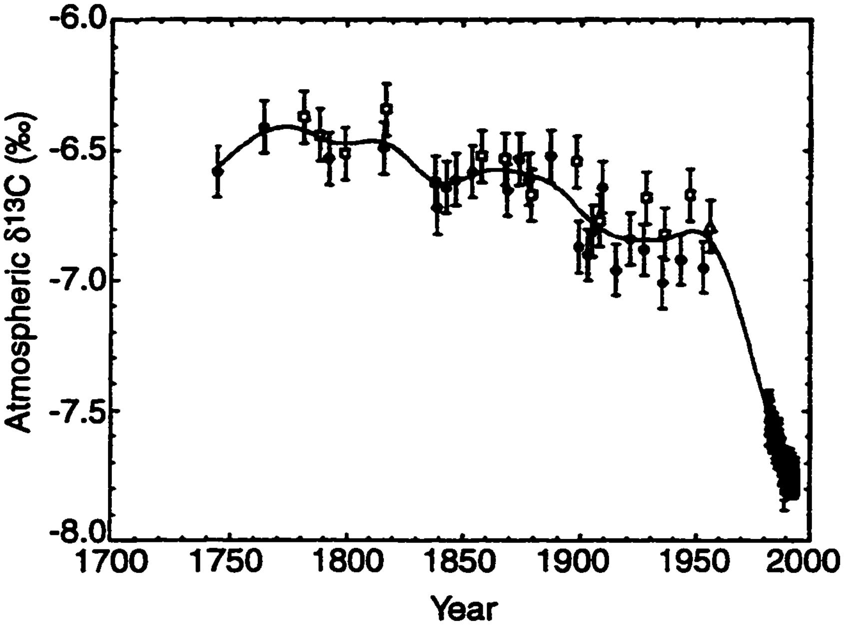

Figure 1.3. Atmospheric $\delta^{13}C$ of CO_2 from air samples dated 1700-1995. The pre-1950 values are based on measurements of gasses trapped in bubbles in ice cores (Joos and Bruno, 1998).

are depleted ($\delta^{13}C \approx -28$ ‰) relative to atmospheric CO_2 ($\delta^{13}C \approx -8$ ‰, presently). The observation that the $\delta^{13}C$ of oceanic DIC ($\delta^{13}C \approx 1$ ‰) is also decreasing has provided a means for calculating the ocean's uptake of fossil-fuel CO_2 (Druffel and Benavides, 1986; Quay et al., 1992; Heimann and Maier Reimer, 1996; Bacastow et al., 1996). $\delta^{13}C$ is a useful tracer of fossil fuel CO_2 uptake because the atmospheric perturbations of $^{12}CO_2$ and $^{13}CO_2$ are caused by the same processes, so the perturbation histories of the two isotopes are similar in the atmosphere (Figs. 1.1 and 1.3) and oceans. There is a signal-to-noise advantage in detecting the ocean's $\delta^{13}C$ change rather than the $^{12}CO_2$ change directly (Tans et al., 1993). Heimann and Maier Reimer (1996) showed that in contrast to the situation for bomb ^{14}C, the oceanic $^{13}CO_2$ and $^{12}CO_2$ perturbations were very well correlated (r^2=0.96) in an OGCM simulation. Knowledge of the ocean's $\delta^{13}C$ perturbation, therefore, can potentially provide a much stronger constraint on ocean CO_2 uptake rates than can the oceanic bomb ^{14}C perturbation.

Although the oceanic CO_2 uptake rate cannot be determined directly from the oceanic $\delta^{13}C$ change, there are two approaches that yield CO_2 uptake from $\delta^{13}C$ changes. First, CO_2 uptake can be determined from $\delta^{13}C$ changes using the slope of the $^{13}CO_2$ versus $^{12}CO_2$ changes predicted in ocean models (e.g., Heimann and Maier-Reimer, 1996; Bacastow et al., 1996). Second, atmospheric $^{13}CO_2$ and $^{12}CO_2$ budgets provide estimates of oceanic CO_2 uptake rates. The budgeting approach is based on the observation that isotopic exchange with the ocean dilutes (slows) the atmospheric $\delta^{13}C$ change rate and that this isotopic exchange depends on the ocean's net CO_2 uptake rate. The oceanic and terrestrial biosphere's net CO_2 uptake rate can thus be determined using an atmospheric $^{12}CO_2$ and $^{13}CO_2$ budget, measurements of the $\delta^{13}C$ of fossil fuels, and the atmospheric and oceanic $\delta^{13}C$ time rates of change (Quay et al., 1992). A complication in this approach results from the fact that the CO_2 presently taken up by the terrestrial biosphere is isotopically lighter than that respired because the $\delta^{13}C$ of CO_2 in the atmosphere is decreasing. This "terrestrial biosphere Suess effect" needs to be quantified because CO_2 exchange with the terrestrial biosphere also dilutes the atmospheric change. Quay et al. (1992) combined an estimate of the mean lifetime of carbon in the terrestrial biosphere (~ 10 yrs) with the time rate of change of $\delta^{13}C$ of CO_2 in the atmosphere (~ -0.02 ‰ yr^{-1}) to estimate that the

CO_2 currently released is 0.2 ‰ enriched relative to that taken up by the terrestrial biosphere. Combining this estimate with an estimate of terrestrial net primary production (~ 60 Gt. C yr^{-1}) yielded a terrestrial biosphere Suess effect estimate of ~ 12 Gt. C ‰ yr^{-1}. For the ocean, they estimated a global $\delta^{13}C$ change rate of -10.4 ± 2.3 ‰ m yr^{-1} based on a regression of depth-integrated $\delta^{13}C$ and bomb ^{14}C (GEOSECS) changes measured at seven locations in the Pacific Ocean. The globally averaged oceanic and terrestrial biospheric $\delta^{13}C$ change rates, described above, were applied to the atmospheric $^{13}CO_2$ and $^{12}CO_2$ mass balance to derive an oceanic uptake rate of CO_2 of 2.1 ± 0.8 Gt. C yr^{-1} during 1970-1990 (Quay et al., 1992). Most (75 percent) of the uncertainty in the oceanic CO_2 uptake rate resulted from uncertainty in the ocean's integrated $\delta^{13}C$ change rate.

Goal of dissertation

The oceanic $\delta^{13}C$ Suess effect has been poorly known due to a lack of high quality $\delta^{13}C$ data from the past with which we can compare present day $\delta^{13}C$ measurements. Prior to this dissertation, global coverage of the time rate of change of oceanic $\delta^{13}C$ of DIC consisted of one subtropical time series site each in the North Pacific (P. Quay, unpublished data) and North Atlantic (Bacastow et al., 1996), a comparison between surface water $\delta^{13}C$ measurements from 1970 (Kroopnick et al., 1977) and 1990-1991 (Quay et al., 1992) along ~ 150°W in the Pacific Ocean, seven depth profiles of $\delta^{13}C$ reoccupied ~ 20 years apart in time in the Pacific Ocean as above (Quay et al., 1992), and two reconstructions based on the $\delta^{13}C$ of aragonite incorporated into a sclerosponge at Jamaica (18°N, 78°W in the Caribbean; Druffel and Benavides, 1986; Böhm et al., 1996).

The primary goal of this dissertation research was to improve the estimated global oceanic ^{13}C Suess effect and, in turn, improve the accuracy of the $\delta^{13}C$ derived oceanic CO_2 uptake rate. In this work, I made extensive use of oceanic $\delta^{13}C$ and ^{14}C distributions and a third oceanic tracer, chlorofluorocarbons, or CFCs. I used CFCs as a tool for diagnosing water ages (chapters two and three), and as a diagnostic tool for detecting ^{13}C and ^{12}C changes in the oceans (chapter four). Because all of this work relied, to varying extents, on oceanic CFC measurements, I introduce those briefly here.

CFCs are stable and conservative in oxic seawater (Lee, 1998), and recent advances in at-sea analytical techniques make it possible to obtain oceanic distributions of CFC-11 and CFC-12 at resolutions comparable to that of other chemical tracers, such as O_2 and nutrients. As a result, CFCs have emerged as perhaps the most widely used transient tracer for studying decadal time-scale ventilation and water mass formation processes in the oceans (e.g., Doney and Bullister, 1992; Wallace and Lazier, 1988; Warner and Weiss, 1992). One advantage of CFCs as a tracer of ocean ventilation is that, like O_2, they are generally near saturation equilibrium with the atmosphere in the surface ocean. This feature, coupled with the fact that the time scales of thermocline ventilation and oxygen consumption are similar to that of the atmospheric CFC source history (Fig. 1.4), allows fairly simple and direct estimations of thermocline ventilation and in-situ oxygen consumption rates (e.g., Doney and Bullister, 1992). I took advantage of this feature in chapters two and three. In addition, CFCs are useful as indicators of waters that have been in

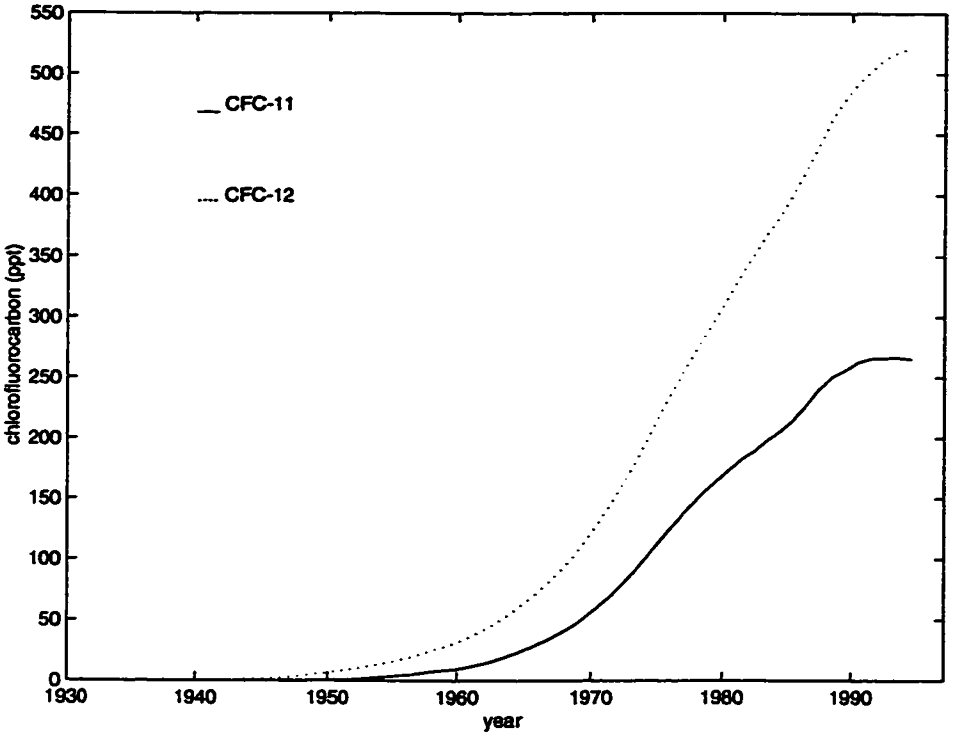

Figure 1.4. Atmospheric CFC-11 (solid line) and CFC-12 (dotted line) in the Northern Hemisphere. During the time period 1930-1981, these values are based on industrial production and release estimates, while the post-1980 values are based on direct measurements (Walker et al., 1995).

contact with the atmosphere since the 1930s (Fig. 1.4), and thus serve as unambiguous tracers of waters likely to contain substantial amounts of anthropogenic CO_2. I took advantage of this feature in chapter four.

Outline of dissertation research

This dissertation consists of two main bodies of work. The first (chapter two) is a regional study of thermocline ventilation rates in the subtropical North Pacific Ocean. My goal was to address two problems: 1) Dynamical calculations based on climatological data (Huang and Qiu, 1994) indicate that the advective turnover rate of the North Pacific subtropical gyre is much slower than implied by the extent of contamination of these waters with anthropogenic tracers (Fine et al., 1981; Watanabe et al., 1994). 2) Calculated rates of organic carbon export from the subtropical mixed layer (~ 2 moles C m^{-2} yr^{-1}) apparently exceed the rate of nutrient supply to the euphotic zone (Emerson et al., 1997). In chapter two I used a simple one-dimensional advection-diffusion model, tuned to CFC distributions, to determine thermocline ventilation rates in the North Pacific subtropical gyre. I found that the degree of ventilation of CFCs was consistent with previous estimates of flow and mixing rates in the North Pacific thermocline. I then applied the model's CFC-tuned flow and mixing parameters to the O_2 distribution in order to calculate in-situ oxygen consumption rates. I found that the depth-integrated rate of oxygen consumption in the thermocline independently corroborated the carbon export rates determined for the subtropical North Pacific at the time series station ALOHA (22°45'N, 158°W). From the perspective of the $\delta^{13}C$ Suess effect determinations (chapter three), the most important finding of this work was that water ages calculated based on CFC-11 or CFC-12 concentrations alone are relatively unaffected by mixing when waters are less than 20 years old in 1991.

In chapters three and four I focus on the problem of determining the oceanic ^{13}C Suess effect. In chapter three I used the CFC-derived water age calculation to quantify the anthropogenic change rates of $\delta^{13}C$ in the thermocline. Since high-quality $\delta^{13}C$ of DIC data from the past are limited, I quantified $\delta^{13}C$ changes by evaluating subsurface trends in present day $\delta^{13}C$ data only. This approach greatly expands the geographic extent of the oceanic ^{13}C Suess effect estimate. To use $\delta^{13}C$ as a tracer of fossil-fuel CO_2, I first had to remove the biological component of oceanic $\delta^{13}C$ distributions by calculating preformed $\delta^{13}C$ distributions. Preformed $\delta^{13}C$ ($\delta^{13}C^{\circ}$) equals the measured $\delta^{13}C$ with remineralization's effects on the $\delta^{13}C$ removed using AOU, an assumed Redfield O_2/C ratio of remineralization, and the measured $\delta^{13}C$ of marine organic matter. Variability in $\delta^{13}C^{\circ}$ due to gas-exchange and circulation (mixing) effects were accounted for via concurrent isopycnal analyses of salinity and preformed nitrate distributions. The time rate of oceanic $\delta^{13}C$ change was determined by regressing isopycnal trends in $\delta^{13}C^{\circ}$ against trends in CFC ages. I performed these reconstructions in the North Pacific, North Atlantic, South Pacific and South Indian Oceans. In the Pacific Ocean, the reconstructed surface $\delta^{13}C$ changes compared well with the $\delta^{13}C$ Suess effect that I calculated from the difference between two meridional sections of $\delta^{13}C$ occupied in 1970 and reoccupied in 1993. The major contributions of this work were an independent corroboration of the $\delta^{13}C$ change estimates of Quay et al. (1992) and an expansion of the $\delta^{13}C$ Suess effect estimates to the North Atlantic and South Indian Oceans.

Unfortunately, the GEOSECS $\delta^{13}C$ data from the Atlantic and Pacific Oceans were not measured precisely enough to resolve the Suess effect by direct comparisons with modern $\delta^{13}C$ data. However, the GEOSECS Indian Ocean data appear to be of very good quality (Kroopnick, 1985). The emerging WOCE $\delta^{13}C$ data set in the Indian Ocean (1994-1995) afforded an opportunity for comparison to GEOSECS (1978) $\delta^{13}C$ data. Because the closest station pairs available for $\delta^{13}C$ comparisons during GEOSECS and WOCE were often separated by up to 15° longitude, calculations of the oceanic $\delta^{13}C$ change from a simple subtraction of GEOSECS from nearby WOCE $\delta^{13}C$ values was not straightforward. In addition, since WOCE measurements were collected in boreal spring and fall and GEOSECS data were collected in boreal winter-spring, a seasonal cycle in surface water $\delta^{13}C$ (Bacastow et al., 1996) may have aliased the anthropogenic $\delta^{13}C$ change as well.

In chapter four I adopt a multiparameter linear regression (MLR) approach, previously used by Wallace (1995) and Slansky et al. (1997) for anthropogenic CO_2 reconstructions, to reduce the impacts spatial and temporal variability on the $\delta^{13}C$ Suess effect determination. My MLR approach used $\delta^{13}C$ correlations with steady-state nutrient and hydrographic data (T, S, oxygen and nutrients) at one time (GEOSECS) to predict, based on nutrient and hydrographic data measured during WOCE, the $\delta^{13}C$ at a later time (1994-1995). To estimate the temporal change, these predictions were then compared with predictions based only on the later $\delta^{13}C$ measurements and nutrient and hydrographic data. The MLR approach accounts for biases due to spatial and seasonal variability of $\delta^{13}C$ and seasonal and interannual variability in water mass ventilation and biological metabolic rates to the extent that such variability is reflected in differences in the nutrient and hydrographic data sets. I used the MLR approach to estimate the changes over a ~17 year period in the meridional and depth distributions of $\delta^{13}C$ from 65°S to 5°N in the Indian Ocean. The datasets were collected during WOCE (1994-1995) along 80°E to 115°E and during GEOSECS (1978) along 50°E to 100°E.

The MLR approach affords a much more extensive and higher resolution $\delta^{13}C$ change estimate for the Indian Ocean than preformed $\delta^{13}C$ reconstructions or direct station comparisons. When I compared the MLR-derived depth-integrated $\delta^{13}C$ changes with those calculated from isopycnal

$\delta^{13}C^{\circ}$ versus CFC age trends (chapter three) and from direct WOCE to GEOSECS $\delta^{13}C$ station comparisons, I found excellent agreement among the Suess effect determinations. The agreement is encouraging because each approach relies on substantial, but independent, assumptions. Furthermore, the agreement provides support for the preformed $\delta^{13}C$ changes I reconstructed in the Atlantic Ocean (chapter three), where few Suess effect estimates are currently available. Finally, I combined all of our individual basin estimates of the $\delta^{13}C$ Suess effect (chapters three and four; Quay et al., 1992) to derive global estimates of $-0.16 \pm .025$ ‰ decade^{-1} for the surface ocean $\delta^{13}C$ change rate and -7.9 ± 3.1 ‰ m yr^{-1} for the depth-integrated $\delta^{13}C$ change rate during ~1970 to ~1990. This integrated $\delta^{13}C$ change rate implies an oceanic CO_2 uptake rate of 1.3 ± 1.0 Gt. C yr^{-1} using the atmospheric $^{13}CO_2$ and $^{12}CO_2$ budgeting approach discussed above (Quay et al., 1992).

Although my $\delta^{13}C$ Suess effect estimates based on the preformed $\delta^{13}C$ and MLR approaches significantly improved the spatial coverage, I was still forced to rely on the analogy between $\delta^{13}C$ and bomb $\Delta^{14}C$ changes in the ocean (discussed above) to derive the most representative estimate of the global ^{13}C change. In chapter five I take a closer look at the relationship between the CO_2, $^{13}CO_2$ and $^{14}CO_2$ anthropogenic perturbations in the oceans. Focusing on the $^{13}CO_2$ and $^{12}CO_2$ perturbations only, I evaluate the possibility that determination of the ratio of the $\delta^{13}C$ to CO_2 perturbations in the oceans can be used as a constraint on CO_2 exchange fluxes through the biosphere, as discussed above, and, when coupled with the measured surface ocean-atmosphere $\delta^{13}C$ disequilibrium, as a constraint on the ocean-atmosphere

pCO_2 disequilibrium. Then, I summarize the relative strengths and weaknesses of $\delta^{13}C^{\circ}$ and MLR approaches presented in chapters three and four. I use this discussion to make recommendations on how to improve the MLR and preformed $\delta^{13}C$ reconstruction methods so they can be used to further extend our global coverage of the $\delta^{13}C$ Suess effect, and to highlight their most promising future applications.

Chapter 2 : Thermocline ventilation and oxygen utilization rates in the subtropical North Pacific based on CFC distributions during WOCE[Ψ]

Introduction

Recent advances in observations and understanding of the circulation of the North Pacific have been compiled by Talley (1995). Many of the efforts aimed at understanding the ventilation of the subtropical North Pacific have focused on subtropical mode water formation in the western Pacific (Masuzawa 1969, Suga 1989), the shallow salinity minimum of the eastern and central subtropical Pacific (Reid 1973, Talley 1985, Yuan and Talley 1992), or on the formation and circulation of North Pacific intermediate water (Talley 1993, Reid 1965).

Maps of isopycnal potential vorticity in the North Pacific thermocline show relatively uniform water mass structure within the subtropics from 25.0 to 26.8 σ_θ. On isopycnals that outcrop only in the subpolar gyre (26.2 to 26.6 σ_θ), the strong potential vorticity gradients between the subtropical and the subpolar gyres reflect the separation of the subtropics from the subpolar outcrops (Talley 1988). Other features evident on these maps include the isolation of the subtropical gyre from the eastern tropical Pacific shadow zone, predicted by the theory of Luyten et al. (1983), and the northwestward shift and contraction of the subtropical gyre with depth described by Reid (1965).

[Ψ] This chapter was originally published by R. E. Sonnerup, P. D. Quay and J. L. Bullister (1999) in *Deep-Sea Research*, **46** (5), 777-805.

Subtropical mode water (STMW), a thermostad centered around 16.5°C, salinity ≈ 34.75, is observed between 100 and 300 m in the western and central subtropical gyre, and is thought to form in the northwestern subtropical gyre by sporadic winter overturning events (Masuzawa 1969, Talley 1988). In the East-central Pacific the shallow salinity minimum (salinity ≈ 34.1) is found between 25.4 and 26.2 σ_θ (100 to 300 meters) and is thought to be formed in the Northeast subtropical Pacific, generally on the heaviest isopycnal to outcrop in this region (Yuan and Talley 1992, Tsuchiya 1982).

Subtropical Pacific water mass formation rates in the upper 450 meters have been estimated by Huang and Qiu (1994), based on the three-dimensional wind driven circulation of the North Pacific calculated from the Levitus (1982) climatology and Hellerman and Rosenstein (1983) wind stress data. They calculated subduction rates due to vertical pumping and lateral induction (Woods, 1985) and derived subtropical water mass renewal times, defined as the mass of water within an isopycnal layer divided by its subduction rate. Their renewal times ranged from 5-6 years for shallow waters (23 to 25 σ_θ, maximum depth ~ 200 m), to around 10 years for subtropical mode water (25.2 to 25.4 σ_θ, maximum depth ~ 275 m), and increased rapidly with depth to about 85 years for 26.2 to 26.4 σ_θ (maximum depth ~ 550 m).

Investigations using transient tracers to study ventilation rates in the subtropical North Pacific began with observations of the penetration of bomb-produced ^{137}Cs and tritium. Folsom (1970) reported a ^{137}Cs maximum in the subtropical Pacific at 25.4 σ_θ, coincident with the shallow salinity minimum. Michel and Suess (1975) observed a major subsurface tritium and salinity maximum originating around 30°N and extending southward on ~ 25.0 σ_θ beneath the North Equatorial Current. They took this feature as evidence that along-isopycnal mixing and advection were the primary processes ventilating the subtropical and tropical North Pacific down to 26.1 σ_θ. Using an advective-diffusive balance of heat and tritium, Michel and Suess estimated southward advection rates between 400 and 600 meters (approximately 26.4 to 26.8 σ_θ) of 1.5 ± 0.5 cm s^{-1}, an along-isopycnal eddy diffusivity of 1500 $m^2\ s^{-1}$, and a maximum vertical (cross-isopycnal) eddy diffusivity of 0.3 $cm^2\ s^{-1}$ in the eastern subtropical gyre (30°N, 140°W).

Tritium distributions measured during GEOSECS (1972-1974) exhibited a major subsurface maximum in the tropical and subtropical North Pacific, confirming that the subtropical Pacific must be ventilated primarily by isopycnal processes on decadal time scales (Fine et al. 1981). The higher resolution GEOSECS tritium data set also demonstrated some finer-scale features of the subtropical circulation, such as the northwestward shift and contraction of the subtropical gyre on successively deeper isopycnals and the eastward advection of high tritium waters in the North Equatorial Counter Current (4°N-8°N) into the lower tritium waters of the eastern tropical Pacific (Fine et al. 1981). Fine et al. took advantage of the transient nature of the bomb tritium tracer to estimate ventilation times for North Pacific Intermediate Water (NPIW) of > 17 years (the time lapse between the major bomb pulse and the GEOSECS Pacific expeditions) at $\sigma_\theta = 26.81$ between 45°N and 20°N and a transit time about the subtropical gyre of < 17 years for $\sigma_\theta =$ 25.0.

Van Scoy et al. (1991) showed that by the mid-1980's the subpolar Pacific had lost tritium to the subtropics and tritium had penetrated as deep as 27.4 σ_θ in the subpolar and subtropical gyres, even though the heaviest isopycnal that outcrops in the open North Pacific is only 26.6 σ_θ (Levitus 1982, Talley 1993). Van Scoy et al. observed a homogenization of subtropical tritium concentrations on isopycnals shallower than 26.44 σ_θ and an increase in tritium inventories on 26.2 to 26.8 σ_θ since GEOSECS. They estimated that the main thermocline ($\sigma_\theta <= 26.6$) ventilates on a time scale of less than one decade.

Chlorofluorocarbons (CFCs) have been widely used to study decadal time-scale ventilation and water mass formation processes (e.g., Doney and Bullister 1992, Wallace and Lazier 1988, Warner and Weiss 1992). In the North Pacific, Watanabe et al. (1994) used the temporal evolution of the CFC-11/CFC-12 atmospheric concentration ratio to estimate ventilation times of 24 to 30 years for the subtropical gyre along 170°E between $\sigma_\theta = 26.4$ and 26.6, respectively, in rough agreement with the tritium results of Fine et al. (1981).

Recently, Warner et al. (1996) mapped CFC distributions in the North Pacific based on two zonal sections and several meridional sections completed in the mid- to late 1980's. Their age-normalized isopycnal maps showed that CFCs were not homogenized in the subtropical thermocline. The isopycnal CFC distributions in the 1980s were dominated by meridional (as opposed to zonal) gradients, presumably due to the input of CFCs on these isopycnals at their northern outcrops. A distinct CFC maximum associated with subtropical mode water was observed between 25.0 and 26.0 σ_θ as far east as 170°W, and a second maximum was observed between 26.4 and 26.6 σ_θ along

152°W. Both of these features were deeper than the deepest winter mixed layer in the North Pacific, in agreement with the early tritium observations (Michel and Suess 1975). These subsurface maxima imply that along-isopycnal mixing is important in ventilating the subtropical North Pacific. Using CFC-11 concentrations to calculate water mass ages, Warner et al. estimated subtropical ventilation times that increased from about 8 to 22 years between $\sigma_\theta = 25.4$ and 26.8. Warner et al. calculated a mean oxygen utilization rate (OUR) of ~8 μmol kg^{-1} yr^{-1} from the AOU versus CFC-11 age relationship along a zonal transect at 24°N for waters less than 20 years old only.

The purpose of this work is to use the emerging WOCE CFC and radiocarbon data sets to estimate rates of thermocline ventilation and oxygen utilization in the subtropical North Pacific. We use a one-dimensional along isopycnal advective-diffusive model calibrated to the meridional CFC-11 gradients. The ventilation rates are used to calculate water mass residence times, which are compared to water mass ages calculated using CFC-11 concentrations only. We make use of the model-calibrated ventilation rates, in conjunction with concurrent oxygen measurements, to calculate in-situ oxygen utilization rate depth trends. The depth integrated oxygen utilization rates are compared to independent estimates of overlying organic carbon export rates. Lastly, we test the usefulness of the advective-diffusive model by incorporating bomb radiocarbon, a transient tracer with a distinctly different atmospheric source history and surface ocean boundary conditions, and salinity into the model.

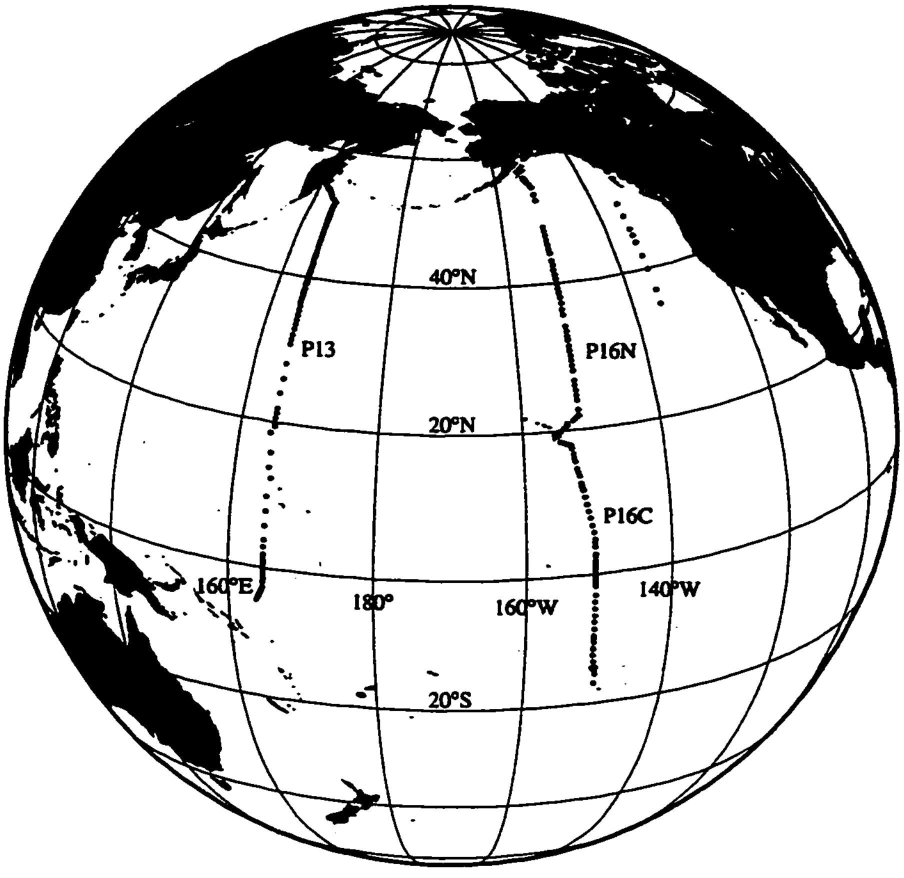

Figure 2.1. Map of the station locations for the WOCE lines P13N (late August - October, 1992), P16N (February and March, 1991) and P16C (September 1991).

Large-scale circulation features in salinity and CFC distributions

The WOCE P16C line along 152°W and P16N lines along 152°W and 135°W (Fig. 2.1) were occupied during September 1991, and February through March 1991, respectively. The WOCE P13N line along 165°E was occupied in late August through October 1992. A full discussion of the CFC analytical techniques used can be found in Bullister and Weiss (1988). Generally, the shipboard dissolved CFC-11 measurements had a detection limit of 0.005 to 0.01 pmol kg^{-1} (1 pmol = 1 picomole = 10^{-12} moles). The precision for the

CFC-11 measurements, based on analyses of replicate samples, is estimated to be 0.01 pmol kg^{-1} or 1 percent of CFC-11 concentration, whichever is greater. All CFC values presented here were adjusted to the SIO 1993 scale as outlined in Cunnold et al. (1994).

The major features evident in the meridional cross section of salinity (Fig. 2.2) are the tropical maximum occurring between 10°N and 20°N shallower than 200 meters (~25.5 σ_θ) and the broad salinity minimum centered between 400 and 600 meters (on ~26.8 σ_θ) which characterizes the NPIW (Reid 1965, Talley 1993). The subtropical-subpolar front is evident at the surface as a strong meridional salinity gradient between 30°N and 40°N. Salinity decreases northwards of 10°N on all isopycnals where $\sigma_\theta > 25.6$. Surface CFC concentrations increase northwards (Fig. 2.3) due to the strong temperature dependence of CFC-11 solubility (Warner and Weiss, 1985). The subsurface CFC-11 maximum from 25.4 to 26.0 σ_θ (150 to 300 meters) between 20°N and 40°N corresponds to the density of the subtropical central mode water described by Masuzawa (1969), the subsurface CFC maximum reported by Warner et al. (1996) using data collected in the late 1980s, and the subsurface maxima in ^{137}Cs (Folsom 1979) and tritium (Fine et al. 1981) discussed above. The penetration of CFCs gets deeper and denser towards the North in the 152°W section. Around 48°N, the 0.3 pmol kg^{-1} CFC-11 contour has penetrated to about 650 meters (27.1 σ_θ), 250 meters deeper than measured at 50°N, 140°W in 1980 (Gammon et al. 1982) and several hundred meters deeper than the depth of the densest isopycnal likely to outcrop in the open North Pacific, 26.6 σ_θ (Levitus 1982, Talley 1993). In contrast, CFCs have

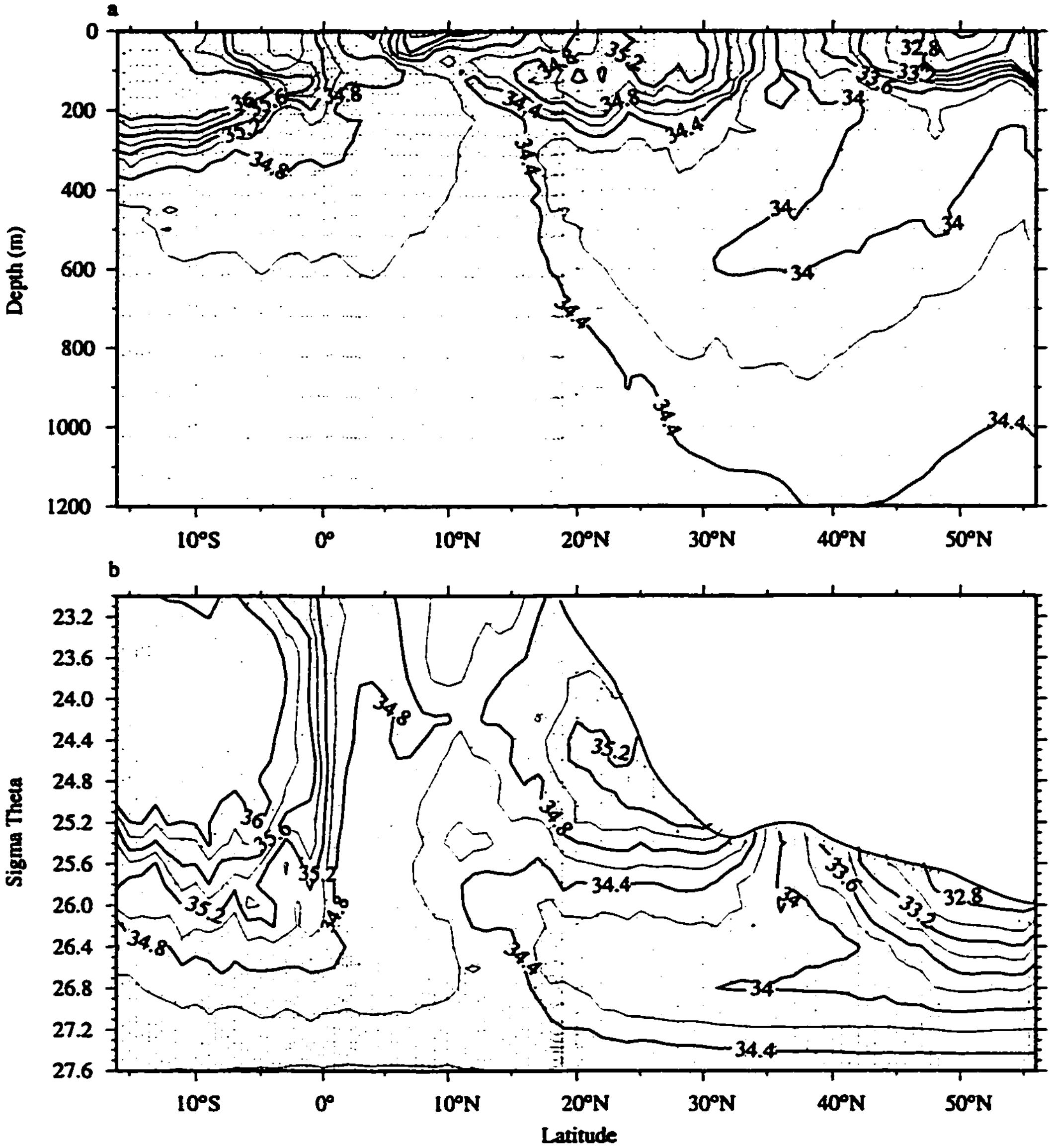

Figure 2.2. The depth (a) and density (b) distributions of salinity along 152°W measured during WOCE P16 (February and March, 1991 north of 18°N and September 1991 south of 18°N) in the North Pacific Ocean.

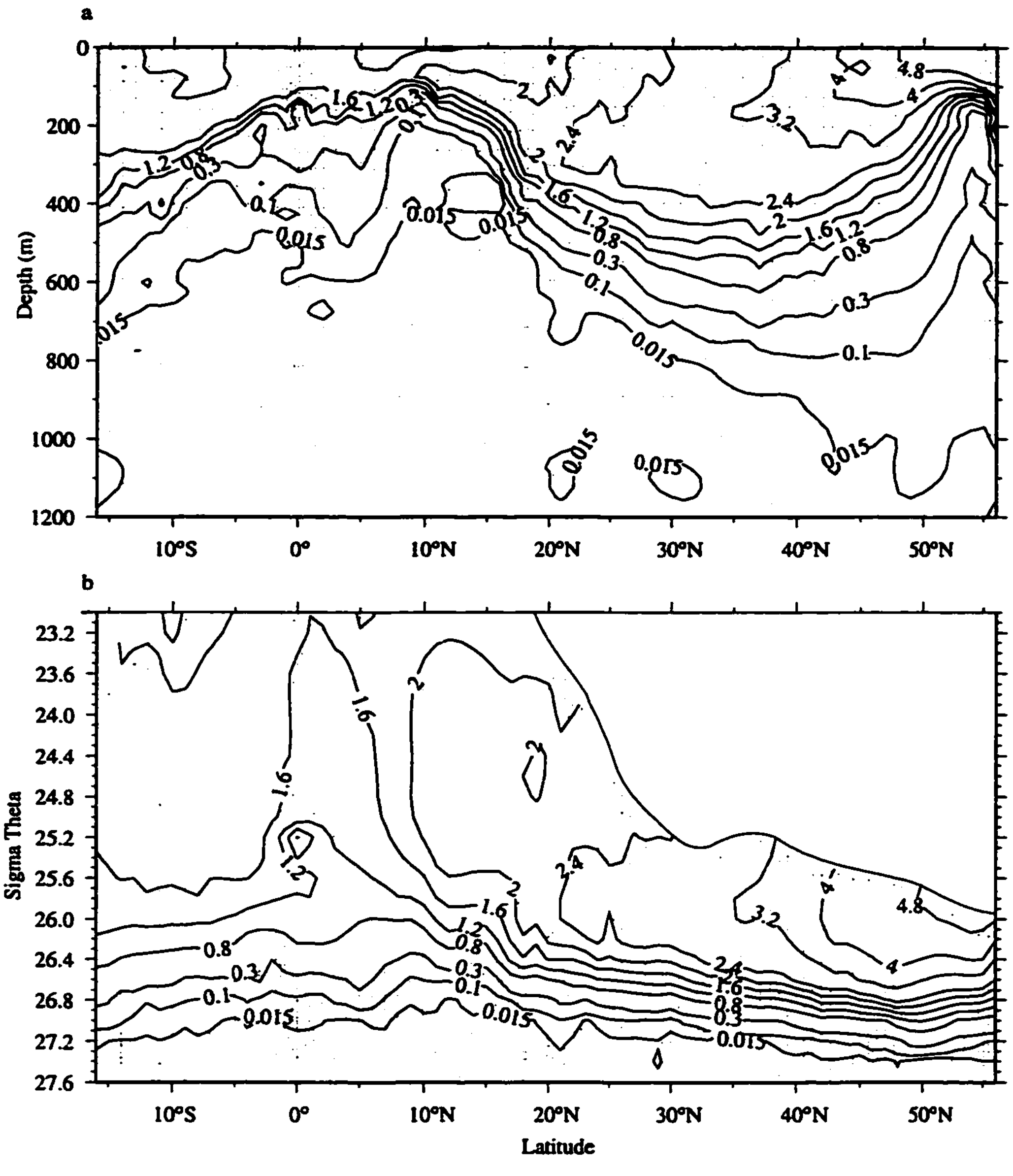

Figure 2.3. The depth (a) and density (b) distributions of CFC-11 (pmol kg^{-1}) along 152°W measured during WOCE P16 (February and March, 1991 north of 18°N and September 1991 south of 18°N) in the North Pacific Ocean.

penetrated to only 400 meters (27.0 σ_θ) at 15°N. CFC concentrations increase northward on all isopycnals to a maximum around 45-50°N, and the strongest meridional gradients occur at the southernmost extent of the subtropical gyre between 10°N and 20°N.

The CFC section along 165°E (WOCE P13N) exhibits concentrations and gradients similar to those observed along 152°W within the subtropical gyre. Deeper than 26.0 σ_θ and north of 40°N, however, CFC concentrations are much higher in the West than in the East (Fig. 2.4). The strong eastward decrease in CFC concentrations in the subpolar region at these densities is likely due to the winter outcrop of these isopycnals being located in the Northwestern Pacific only (Talley 1985). Within the subtropical gyre, zonal gradients in CFCs are generally ten times smaller than meridional gradients between 25.4 and 26.6 σ_θ (Fig. 2.4 and Warner et al. 1996). Steeper meridional CFC gradients at approximately 40°N, which are visible in salinity and potential vorticity as well, are associated with the subpolar-subtropical front (Talley 1988). The minimum in CFC observed from 5°N to 10°N along 152°W (Fig. 2.4) reflects the westward advection of waters of the slowly ventilated eastern tropical Pacific oxygen minimum zone (Warner et al. 1996).

The presence of a substantial subsurface CFC maximum (Fig. 2.3a) that is deeper than the maximum depth of wintertime convection (~100 meters) throughout the subtropical region along 152°W suggests, as previous investigators have noted (Michel and Suess 1975, Fine et al. 1981, Van Scoy et al. 1991, Warner et al. 1996), that along-isopycnal ventilation must be a dominant process ventilating the subtropical North Pacific thermocline. The lack of significant zonal CFC gradients on thermocline isopycnals throughout

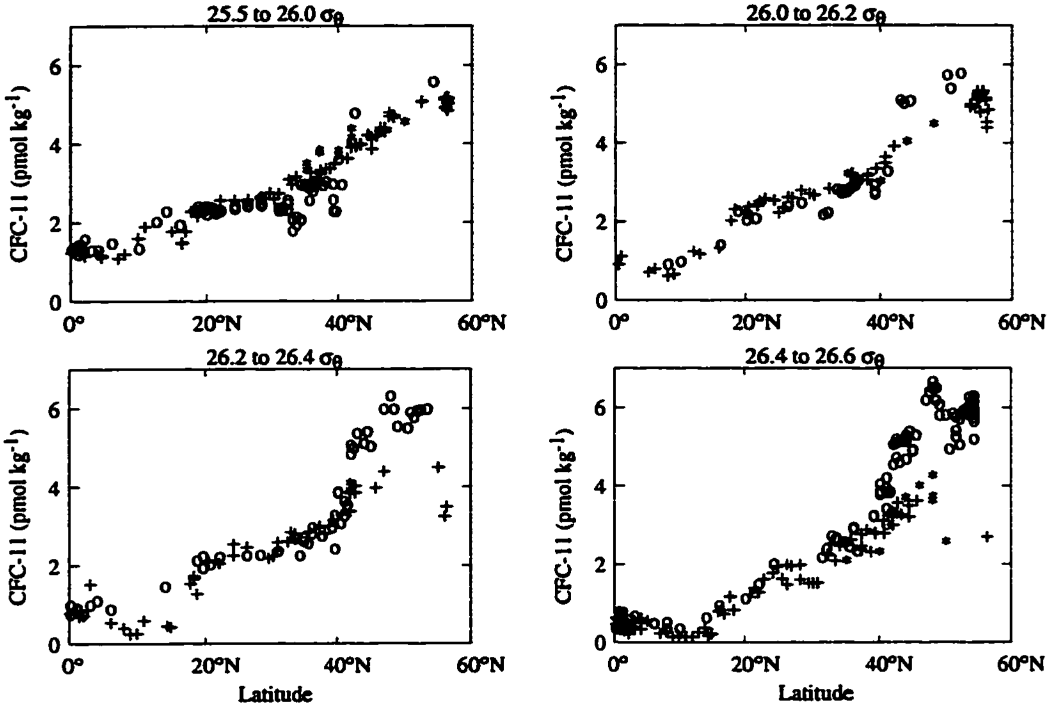

Figure 2.4. WOCE P13N and P16 CFC-11 distributions on four isopycnal layers between 25.5 and 26.6 σ_θ along 152°W (+), 135°W (*) and 165°E (o) in the North Pacific Ocean.

the subtropics suggests that either the zonal component of advection and mixing substantially exceeds the meridional component or that the meridional ventilation of tracer is zonally uniform within the subtropical gyre. The meridional distributions of CFC-11 along 165°E, 152°W and 135°W on isopycnals within the main thermocline (Fig. 2.4) show decreasing concentrations southward from the isopycnal outcrop regions. For example, in the subtropical gyre the 26.2 to 26.4 σ_θ isopycnal is gaining CFCs from the North likely from its wintertime sea surface outcrop north of 40°N (Levitus, 1982). The steep meridional CFC gradients north of 40°N imply that the zonal circulation limits the southward penetration of CFCs in this region. Once

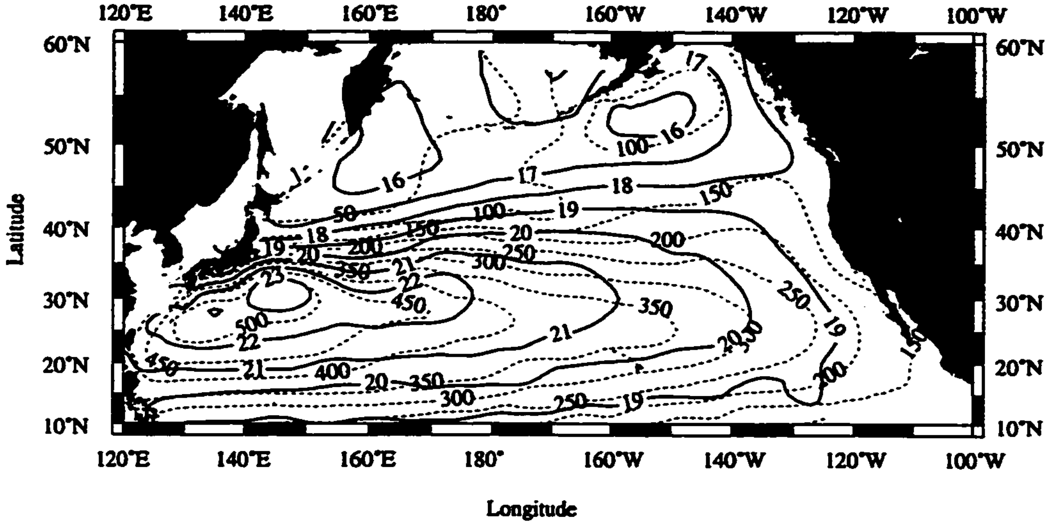

Figure 2.5. Acceleration potential ($m^{-2}\ s^{-2}$) referenced to 2000 m (solid lines) and depth contours (dashed lines) for the isopycnal surface $\sigma_\theta = 26.2$ calculated from Levitus (1982) climatology data (Huang and Qiu, 1994).

within the subtropical gyre at 152°W, the CFCs are carried southward by the predominantly southward geostrophic flow (Fig. 2.5), and this is reflected by significantly smaller meridional CFC gradients from 20°N to 40°N (Fig. 2.4). At around 15°N-20°N the mean geostrophic flow turns westward (Fig. 2.5) in the North Equatorial Current. At these latitudes the meridional gradients are larger because the meridional transport of CFCs is limited by the predominantly zonal geostrophic flow, similar to the situation in the subpolar front region.

Ventilation model

We use an advective-diffusive scheme (equation (2.1) and Fig. 2.6) to describe the meridional CFC ventilation processes on four isopycnals between

25.5 and 26.6 σ_θ (175 to 500 m depth at 30°N, 152°W) in the main thermocline of the subtropical North Pacific along 152°W.

$$\frac{dC}{dt} = -v\frac{dC}{dx} + K\frac{d^2C}{dx^2} \tag{2.1}$$

Here C represents CFC-11 concentration, K is along-isopycnal eddy diffusivity, $-v$ is the southward component of along-isopycnal velocity, t represents time and x is meridional distance. We assume that southward advection occurs only within the subtropical gyre (40°N to 18°N). Since the flow is predominantly zonal from 40°N to 45°N and south of 18°N (Fig. 2.5), we assume that meridional tracer transport is due solely to along-isopycnal eddy diffusion in these regions. These boundaries correspond to the locations of the main inflections in the meridional CFC gradients (Fig. 2.4). We assume that a constant along-isopycnal eddy diffusivity applies to all regions within each layer.

We assume that the WOCE P16N cruise (sampled February and March, 1991) represents average end-of-wintertime mixed layer temperatures and CFC-11 saturation levels with respect to the atmosphere. The wintertime outcrop positions for each isopycnal horizon were determined using either the southernmost locations of outcrops observed during P16N, as defined by the mixed layer density distribution, or the southernmost extent of Levitus' (1982) climatological average wintertime outcrop locations in the central North Pacific. The southernmost boundary of each isopycnal layer was selected as the latitude where there was no significant meridional CFC-11 gradient along 152°W in 1991 (Fig. 2.4). We applied a no-flux boundary

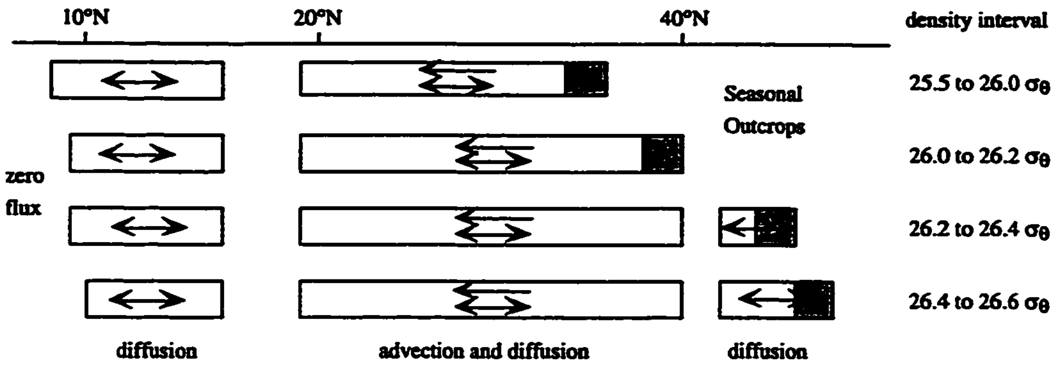

Figure 2.6. Schematic diagram of the ventilation model described in the text. The stippled areas represent seasonal outcrops. Locations of the model boundaries are outlined in Table 2.1. Southward advection and diffusion are applied to the tracer distributions within the subtropics (18°N to 40°N), and diffusion only is applied within the North Equatorial Current and the subtropical-subpolar front (south of 18°N and north of 40°N, respectively). A zero-flux boundary condition is applied at the southernmost boundary (between 6°N and 10°N). Isopycnal layers with $\sigma_\theta > 26.2$ outcrop in the subpolar gyre, and those with $\sigma_\theta < 26.2$ outcrop in the subtropical gyre.

Table 2.1. Characteristics of the domain and outcrop regions used for the advective-diffusive model.

Isopcynal Horizon	Outcropping Region	Percent Saturation	Months Outcropping	Southern Boundary
25.5 to 26.0	35 to 36°N	92 %	3	6°N
26.0 to 26.2	40 to 41°N	88 %	3	8°N
26.2 to 26.4	42 to 43°N	88 %	3	8°N
26.4 to 26.6	43 to 44°N	78 %	2	10°N

condition at this location, which moved northward between 6°N and 10°N on successively deeper isopycnal horizons (Table 2.1).

The boundary conditions applied at the outcrops assume that every year the outcrop locations are at the saturation levels observed during P16N during the outcrop period, determined from the Levitus (1982) climatology data. The CFC saturation levels were calculated from gas solubility (Warner and Weiss 1985), and time trends of atmospheric CFC concentrations (Fig. 1.4) supplied by Walker et al. (1995). In this source history, the post-1981 atmospheric values are based on direct measurements, while the pre-1981 values are based on CFC production and emission estimates applied in a two-box model of the atmosphere. Walker et al. (1995) estimate an uncertainty of < 3 % (1 σ) in atmospheric CFC-11 values reconstructed during the time period 1960-1981. A summary of the isopycnal outcrop locations, CFC-11 saturation levels, outcropping periods, and locations of model boundaries assumed is presented in Table 2.1.

The degree of saturation of CFCs in the winter mixed layer may exhibit some interannual variability. However, variations of five to ten percent have little influence on the velocities implied by the model, as these are sensitive to the gradients in CFCs, which are established over a number of years, and not to the absolute values. The zonal trend in CFCs in the outcropping region (Fig. 2.4) has little impact on the model results because we use the CFC saturation values observed along 152°W in wintertime and the zonal trend becomes much smaller south of the outcrops. The isopycnal diffusivities determined on isopycnals that outcrop in the subpolar gyre ($\sigma_\theta >$ 26.2) are sensitive, however, to the degree of saturation assumed as discussed below. The transport terms determined from the model are relatively insensitive to the length of the outcrop period assumed (Table 2.1). Another assumption inherent in our model approach is that flow and mixing rates have been constant over the time scale of the CFC transient (~50 years). On shorter time scales this has probably not been the case. For example, Van Scoy and Druffel (1993) have presented evidence based on tritium distributions that ventilation of eastern subtropical Pacific thermocline waters is retarded during El-Niño events. Since the processes of interest in our approach, i.e., ventilation and oxygen utilization, are integrated over time scales (5 years to decades) somewhat longer than these variations, however, biases due to the assumption of steady flow and mixing are likely small.

The model uses a one degree latitudinal spacing, and is marched forward in time from 1934 (prior to the introduction of atmospheric CFC-11) to March 1991 using a two week time step. The temporal evolution of CFC-11 is calculated using centered in time, centered in space (CTCS or leapfrog) differencing of the advection terms and the Dufort-Frankel scheme for the diffusion terms (Fletcher 1988):

$$\frac{C_i^{t+1} - C_i^{t-1}}{2\Delta t} = -v\frac{C_{i+1}^t - C_{i-1}^t}{2\Delta x} + K\frac{C_{i+1}^t + C_{i-1}^t - C_i^{t-1} - C_i^{t+1}}{\Delta x^2} \tag{2.2}$$

Here C_i^t represents CFC concentration at time step t, grid point i (increasing northwards). K is the along-isopycnal eddy-diffusivity, $-v$ is the southward velocity, Δt is the time step, and Δx is the grid spacing. To suppress splitting between even and odd time steps, forward-time differencing of the advective term is used every fifth time step. The truncation errors associated with the centered-leapfrog method for the advective terms cause no numerical diffusion. In the absence of explicit diffusion, however, the algorithm can generate non-physical ripples (dispersion) in the tracer field (Hecht et al. 1995). The isopycnal diffusivities fit to the data (discussed below) were sufficient to suppress dispersive effects arising from the centered-differenced advection terms.

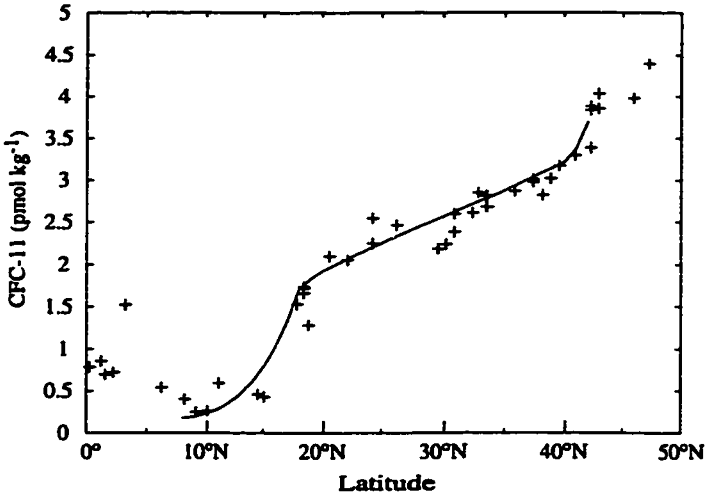

Figure 2.7. The meridional advection-diffusion model CFC-11 simulation (line) for 26.2 - 26.4 σ_θ in 1991, using a southward advection rate of 0.77 cm s^{-1} within the subtropics and an eddy diffusivity of 650 m^2 s^{-1}, compared to observations (+) made during P16 in 1991 along 152°W.

Southward velocities and along-isopycnal diffusivities were derived by fitting the model to the CFC-11 data in 1991 (P16) along 152°W (Table 2.2). The best fit model result for 26.2 to 26.4 σ_θ is shown in Fig. 2.7. Within the subtropical gyre (18°N to 40°N), where advection dominates CFC transport within the model, the model results essentially resemble a projection versus latitude of the temporal trend in atmospheric CFCs, which was roughly linear from 1970 to 1990 (Fig. 1.4). The calculated velocities are determined by the slope of the meridional CFC distribution in the subtropics, and are little

Table 2.2. Southward velocities and horizontal diffusivities (with ± 1 sd uncertainties) in the subtropical gyre (18°N to 40°N) determined by the best fit to the meridional CFC distributions measured along 152°W in 1991.

Density Interval of Isopycnal Layer (σ_θ)	Horizontal Diffusivity ($m^2 s^{-1}$)	Southward Velocity ($cm\ s^{-1}$)
25.5 to 26.0	2750 ± 250	1.03 ± 0.12
26.0 to 26.2	1200 ± 200	0.89 ± 0.07
26.2 to 26.4	650 ± 150	0.77 ± 0.06
26.4 to 26.6	700 ± 200	0.56 ± 0.08

affected by the choice of the southern and northern boundary locations of the subtropical gyre. Thus the velocities reported reflect the best fit to the meridional trend (slope) of the subtropical CFC distribution (Fig. 2.4). The errors reported only represent the range of velocities that fit within the mean slope ± 1 standard error in that trend for this model construct. As the meridional CFC gradients increase with depth (Fig. 2.3), the calculated velocities decrease from 1.03 ± 0.12 cm s^{-1} on 25.5 to 26.0 σ_θ to 0.56 ± 0.08 cm s^{-1} on 26.4 to 26.6 σ_θ. These southward velocities fall within the range of 0.5 to 1 cm s^{-1} determined by Roemmich and McCallister (1989) for waters shallower than 26.8 σ_θ from large-scale geostrophic inverse calculations across 35°N and 24°N, respectively, in the Eastern Pacific (175°W to 122°W). Coats (1981), used a variation of the beta-spiral technique to compute southward components of the absolute geostrophic velocity ranging from 0.41 to 0.56 cm s^{-1} in the same density range at 35°N, 155°W.

The along-isopycnal diffusivities were derived for each isopycnal from the least-squares fit to the meridional CFC distribution between the models' southern boundaries (Table 2.1) and 18°N and additionally, on isopycnals that outcrop north of the subtropical-subpolar front, north of 40°N as discussed above. Across these frontal regions southward advection rates are assumed to be zero. As a result, the diffusivities are sensitive to the choice of the southern boundary of the subtropical gyre and to the saturation levels assumed at the outcrops. The diffusivities estimated in this fashion decrease with depth from a maximum value of 2750 $m^2 s^{-1}$ on 25.5 to 26.0 σ_θ to 1200 $m^2 s^{-1}$ on 26.0 to 26.2 σ_θ, down to 650 $m^2 s^{-1}$ on 26.2 to 26.4 σ_θ and 700 $m^2 s^{-1}$ on 26.4 to 26.6 σ_θ (Table 2.2). The reported uncertainties represent the sensitivity of the model fit to the variability in the velocity terms reported above. As a result, the uncertainties in the velocity and diffusivity terms co-vary strongly, e.g., the lesser southward transport of CFCs implied by a smaller velocity (Table 2.2) is compensated by a correspondingly larger diffusivity, and vice-versa. The diffusivity values are, on average, in agreement with estimates of 1840 ± 440 $m^2 s^{-1}$ based on ^3He and ^3H distributions within the main thermocline of the Sargasso Sea (Jenkins 1991) and 1200 to 2400 $m^2 s^{-1}$ based on CFC distributions in Antarctic Intermediate Water in the subtropical South Atlantic (Warner and Weiss 1992). The higher diffusivities calculated for isopycnals shallower than 26.2 σ_θ may be caused by some southward advection south of 18°N which is not explicitly represented in the models. Since the minimum in CFCs around 6°N to 10°N along 152°W is due in part to the westward advection of relatively older and hence CFC depleted waters of the eastern tropical Pacific oxygen minimum zone (Warner et al. 1996), the calculated diffusivities reflect, in part, the extent of ventilation of the isopycnals in this shadow zone. The smaller diffusivities calculated with increasing depth are primarily due to the slower penetration of CFCs and larger meridional gradients within the North Equatorial Current with increasing density (Fig. 2.4). These deeper diffusivity values agree well with estimates of 500 $m^2 s^{-1}$ (Armi and Stommel 1983) and of ≤ 800 $m^2 s^{-1}$ (Jenkins 1987) from the Beta Triangle region in the eastern North Atlantic subtropical thermocline.

The model-calculated transport terms (Table 2.2) rely on the assumption that zonal transport of CFC-11 is not significant relative to meridional transport. Based on a comparison of nearly concurrent data from 165°E and 135°W with those along 152°W (Fig. 2.4), zonal gradients in CFCs are generally much smaller than meridional gradients south of the outcrop regions on all of the isopycnals we have modeled. The most notable exception is on 25.5 to 26.0 σ_θ where the zonal trend in CFC-11 is almost 1/3 the meridional trend between 30°N and the outcrop. The fact that the model neglects the influx of relatively low-CFC waters from the West means that the model underestimates the true southward transport along 152°W on 25.5 to 26.0 σ_θ within this region, and thus the velocity term (Table 2.2) may represent an underestimate.

To calculate ventilation rates or water "ages" that can be compared to the CFC-derived ages estimated by Watanabe et al. (1994) and by Warner et al. (1996) a numerical ideal age tracer, as described by Thiele and Sarmiento (1990), is incorporated into the advective-diffusive scheme. The ideal age tracer increases with each time step except at the northern boundary, where outcropped waters are reset to zero age during the winter months (Table 2.1). We assume that CFC-11 and oxygen concentrations reflect water ages, and thus assign a zero meridional age gradient at the southern boundary where there was no meridional gradient in CFC-11 and oxygen during 1991 (Table

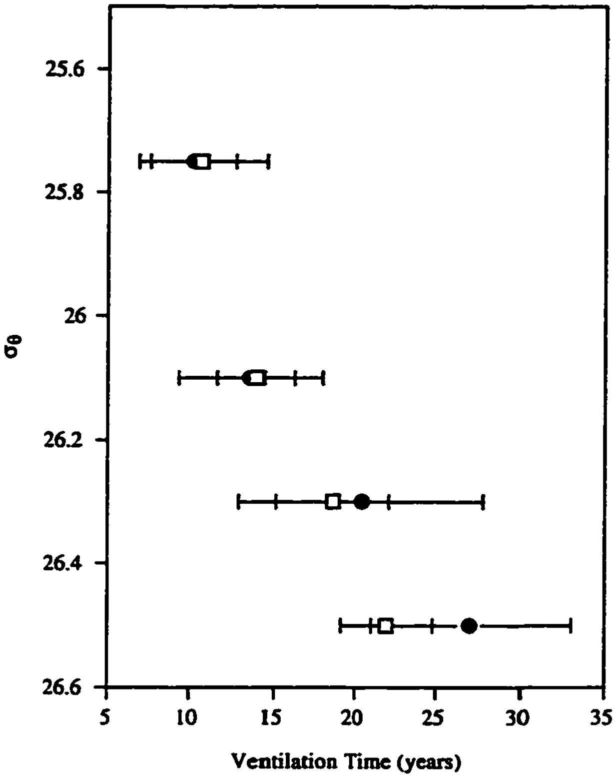

Figure 2.8. Ventilation times for the 15°N to 20°N latitude interval calculated from an ideal-age tracer incorporated into the advective-diffusive models (●), and from the CFC-11 concentration ages of waters (□) in this region. The ventilation time represents the average time since a water parcel was last in the outcropping region (see text for discussion).

2.1). We march the model forward in time until a steady-state age distribution is achieved. Ideal tracer ages for 15°N to 20°N, representing the southernmost and "oldest" waters in the subtropical gyre, are compared with CFC-11 concentration ages calculated for the same region (Fig. 2.8). The CFC-11 concentration ages are calculated by comparing each subsurface sample's CFC-11 concentration with the atmospheric source history and estimating a formation date by assuming that the water was saturated with respect to atmospheric CFCs when it outcropped (Doney and Bullister 1992). The ideal tracer ages from the advective-diffusive scheme, using the best fit velocities and diffusivities (Table 2.2), agree well with the CFC-11 ages. The ventilation times, which increase with depth from about 10 years for 25.5 to 26.0 σ_θ to about 27 years for 26.4 to 26.6 σ_θ (Fig. 2.8), represent the average time since the water from 15°N to 20°N was last in direct contact with the atmosphere. The average uncertainty in the ventilation ages is ± 25 % and is due to variability in CFC values between 15°N and 20°N and additionally, for the model calculated ages, to uncertainties in the model transport terms (Table 2.2).

The ventilation rates determined by the advective-diffusive model agree well with Fine et al.'s (1981) tritium-based estimates of less than 17 years for the subtropical gyre north of about 20°N on 26.02 σ_θ, and with Watanabe et al.'s (1994) CFC-11/CFC-12 based estimate of 23 ± 1 years for 26.4 σ_θ and 26 ± 4 years for 26.6 σ_θ from 16°N to 19°N along 170°E. Our ventilation times coincide with Warner et al.'s (1996) which were based on the same methodology as our CFC-11 apparent age derived rates, but used CFC measurements made in the late 1980s. Shallower than 26.4 σ_θ, the excellent agreement between the ideal-tracer ages and CFC-11 concentration ages is due to the nearly linear increase of atmospheric CFC-11 concentrations from the 1970s to 1990 (Fig. 1.4), and confirms that CFC-11 concentration ages suffer little from non-linearities in mixing when waters are less than 20 years old in 1991. Before 1970, the nonlinear trend in atmospheric CFC-11 causes the CFC-11 ages of mixtures of waters to be biased towards the youngest component of the mixture. A hint of this bias may be seen on 26.4 to 26.6 σ_θ, where the CFC-11 concentration ages are somewhat younger than the model calculated ages (Fig. 2.8).

Huang and Qiu (1994) calculated water mass renewal times for the subtropical North Pacific from around 25 to 85 years for the density ranges 25.5 to 26.0 σ_θ down to 26.4 to 26.6 σ_θ, respectively. These ventilation times, determined from wind stress, geostrophic flow, and subduction rates as discussed above, are much slower than those implied by the penetration of CFCs (this work and Warner et al. 1996), and tritium (Michel and Suess 1975, Fine et al. 1981, Van Scoy et al. 1991) into the subtropical North Pacific thermocline. On shallower isopycnals that outcrop within the subtropical gyre the slower subduction rates may be due to Huang and Qiu's use of the Hellerman and Rosenstein wind stress data reduced by a factor of 0.8. Huang and Qiu chose this factor to assure that the total amount of Ekman pumping would equal the total horizontal divergence of geostrophic flow (using a reference level of 2000m) below the Ekman layer. Also, subduction rates computed from climatology data are likely underestimated due to poor spatial resolution across fronts and within the western boundary current in the original temperature and salinity data compiled by Levitus (1982), and because smaller-scale and episodic mixing events are missing from this data set. Finally, Huang and Qiu point out that maximum mixed layer depths may be underestimated using the Levitus data, thus underestimating the mass flux into the ventilated thermocline.

Oxygen utilization rates

The meridional cross section of oxygen along 152°W (Fig. 2.9) exhibits many of the same ventilation features evident in the CFC section (Fig. 2.3). Oxygen concentrations increase northwards at the surface and on all isopycnals shallower than 27.0 σ_θ within the North Pacific, with the strongest subsurface meridional gradients between 10°N and 20°N. The major

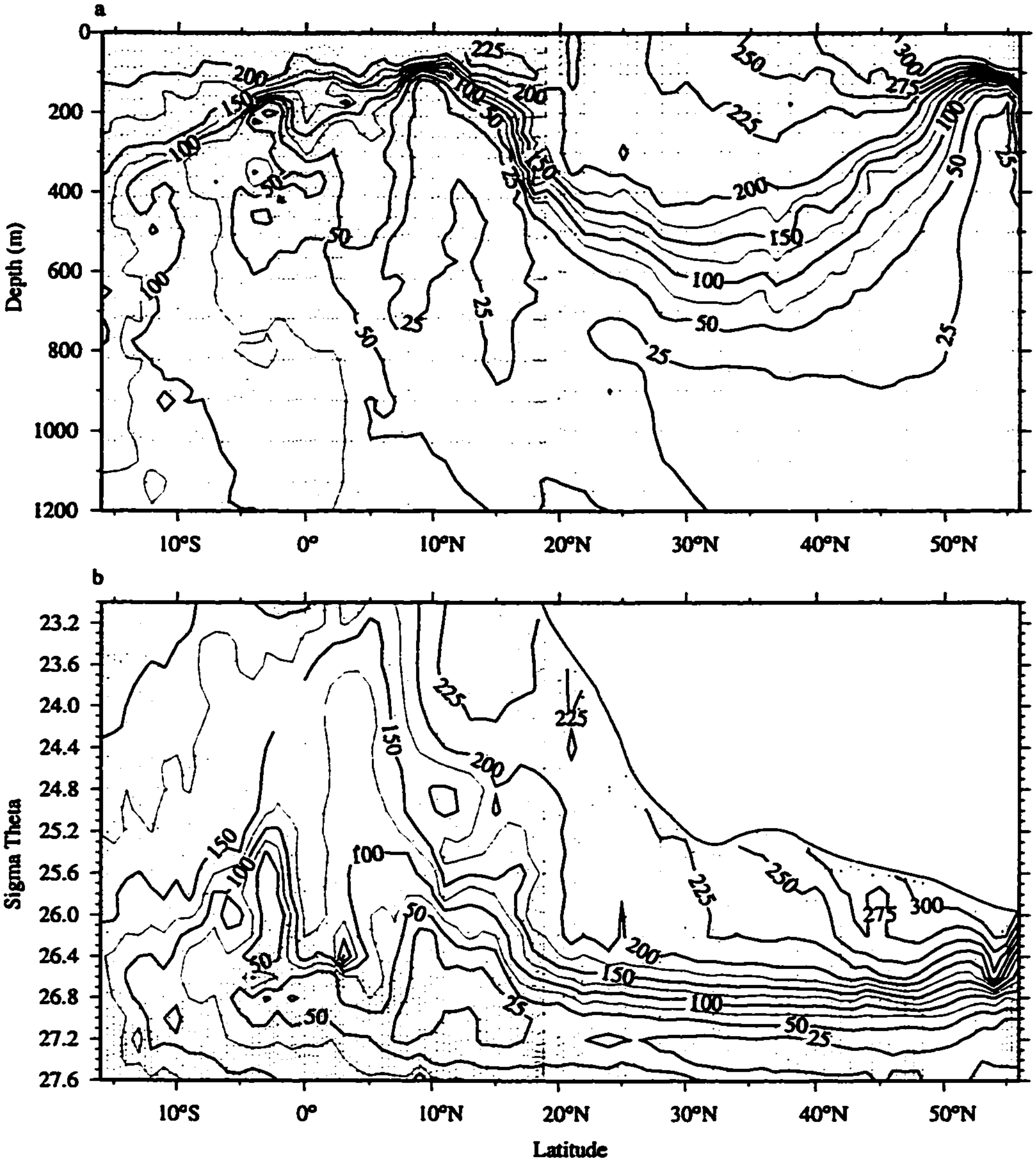

Figure 2.9. The depth (a) and density (b) distributions of oxygen (μmol kg^{-1}) along 152°W measured from bottles during WOCE P16 (February and March, 1991 north of 18°N and September 1991 south of 18°N) in the North Pacific Ocean.

subsurface maximum between 25.5 and 26.2 σ_θ between 20°N and 40°N seen in the CFC section is absent in the oxygen section. The absence of this feature is consistent with remineralization of organic matter at depth consuming ~1 to ~10 μmol oxygen kg^{-1} yr^{-1} based on the water ages reported above. In-situ oxygen utilization rates on the four thermocline isopycnals can be estimated by applying the advective-diffusive scheme to the measured oxygen fields.

$$\frac{dO_2}{dt} = -v\frac{dO_2}{dx} + K\frac{d^2O_2}{dx^2} - J \qquad (2.3)$$

Here O_2 represents oxygen concentration, $-v$ and K are the along-isopycnal southward velocity and diffusivity, respectively, and J represents the in-situ oxygen utilization rate. A crucial assumption inherent in this approach is that, like the CFCs, zonal gradients and vertical mixing are negligible compared to meridional transport of oxygen. The former assumption is only true north of the North Equatorial Current (around 18°N for the isopycnals of interest), so we shall confine this discussion to the subtropical oxygen distributions only.

We use the CFC-calibrated advection and diffusion rates (Table 2.2), and assign oxygen concentrations observed during P16 (February and March 1991 along 152°W) at the outcrop and at the southern extent of the subtropics (18°N) for each isopycnal. We assume that the oxygen distributions are at steady state and on each layer prescribe the average OUR to minimize a reduced chi-squared fit to the subtropical oxygen distributions (Fig. 2.10). The OURs, which are primarily dependent on the meridional gradients in oxygen, decrease weakly with depth from 6.6 to 3.2 μmol kg^{-1} yr^{-1} between 25.5 and

26.6 σ_θ (Fig. 2.11). The low OUR values on 26.2 to 26.4 σ_θ and 26.4 to 26.6 σ_θ reflect the almost negligible meridional gradient in oxygen concentrations north of 20°N measured on these isopycnals along 152°W (Figs. 2.9 and 2.10). The uncertainties in the OURs (Fig. 2.11) primarily reflect the sensitivity of the reduced chi-squared fit to the uncertainties in the model advection and diffusion terms (Table 2.2).

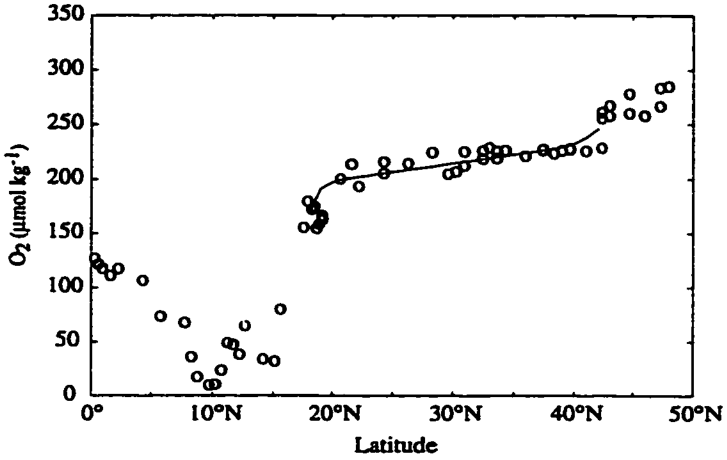

Figure 2.10. The meridional advection-diffusion model oxygen simulation (line) for 26.2 to 26.4 σ_θ, using an in-situ oxygen utilization rate of 3.5 μmol kg^{-1} yr^{-1} and the CFC-calibrated transport terms (Table 2.2) compared to observations (o) made during P16 in 1991 along 152°W.

Calculating OURs in this fashion relies on the assumption that zonal transport of oxygen is not significant relative to the calculated meridional transport. Based on the Levitus (1982) data, between 25.5 and 26.6 σ_θ zonal gradients in oxygen are much smaller than meridional gradients throughout the central subtropical North Pacific (160°E to 130°W, 15°N to 45°N). The largest zonal gradients within this region are found on 25.5 to 26.0 σ_θ between

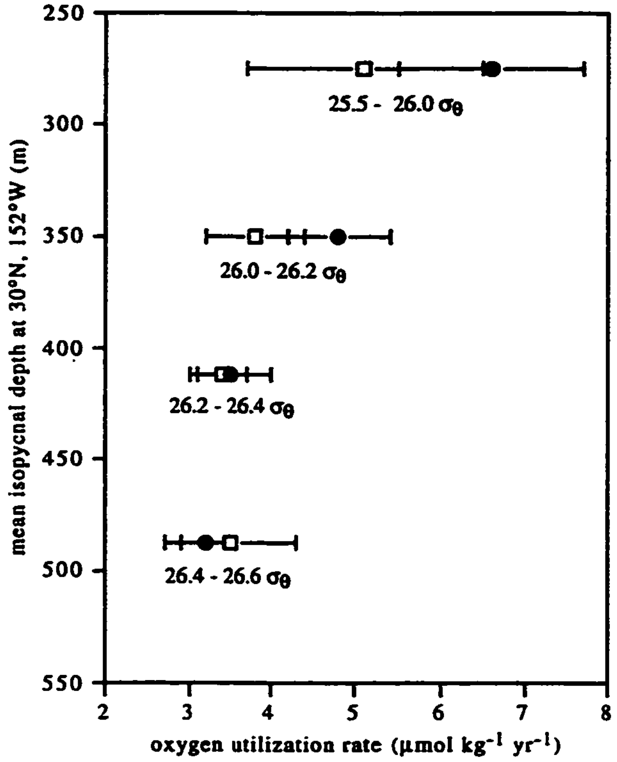

Figure 2.11. In-situ oxygen utilization rates (OURs) calculated from the meridional oxygen distributions and the advection-diffusion model mixing rates (●). Error bars represent the uncertainty (± 1 sd) of the best fit OURs due to uncertainty in the models' mixing and advection terms. OURs calculated by dividing apparent oxygen utilization (AOU) by CFC-11 concentration ages, for samples from 20°N to 30°N, are included for comparison (□). Error bars in these estimates reflect ± 1 sd of mean AOU/CFC-age ratio determinations between 20°N and 30°N.

30°N and 35°N where the zonal trend is still only 5 per cent of the meridional trend. The eastward flow of lower oxygen waters may cause the model to overestimate the actual in-situ OUR in this region. However, the eastward flow also brings in lower CFC-11 waters from the West which would cause the CFC-calibrated transports, and thus the OURs, to be underestimated in this region as discussed above. These two processes may offset each other somewhat and are small relative to the meridional transports.

The OURs computed with the advective-diffusive scheme compare well with those calculated by dividing each sample's apparent oxygen utilization (AOU) by its CFC-11 concentration age (Fig. 2.11), as expected from the generally good agreement between CFC ages and ideal tracer ages (Fig. 2.8). As in the advective-diffusive model, for the AOU and CFC-11 age calculation we assign the average saturation levels observed for both CFC-11 and oxygen at each isopycnal's southernmost outcrop during P16N (Table 2.1). An example of the meridional trend in CFC-11 age, AOU and OUR results on 26.2 to 26.4 σ_θ is presented in Fig. 2.12. The oxygen utilization rate calculated by AOU versus CFC-11 age on this isopycnal is fairly constant around 2 to 4 μmol kg^{-1} yr^{-1} throughout the subtropical gyre. The maximum in CFC-11 age, AOU, and OUR around 10°N likely reflects westward advection of relatively isolated waters of the eastern equatorial Pacific shadow zone predicted by Luyten et al. (1983). The higher OURs between 5°N and 15°N could be due to several contributing factors: 1) higher productivity rates in the tropical versus subtropical Pacific (Chavez and Barber 1987), 2) shoaling of this isopycnal with correspondingly higher oxygen utilization rates at shallower depth. A similar OUR trend is observed north of 35°N where the isopycnals shoal. 3) Underestimating the CFC-11 ages for waters older than 20 years (in 1991) due to non-linear mixing effects, as discussed above. In this situation, i.e., south of ~ 15°N on this isopycnal, oxygen utilization rates derived from AOU and CFC-11 ages would be overestimated (Doney and Bullister 1992). 4) Finally, the calculated OUR integrates the oxygen consumed over the pathway of the water parcel since leaving the mixed layer

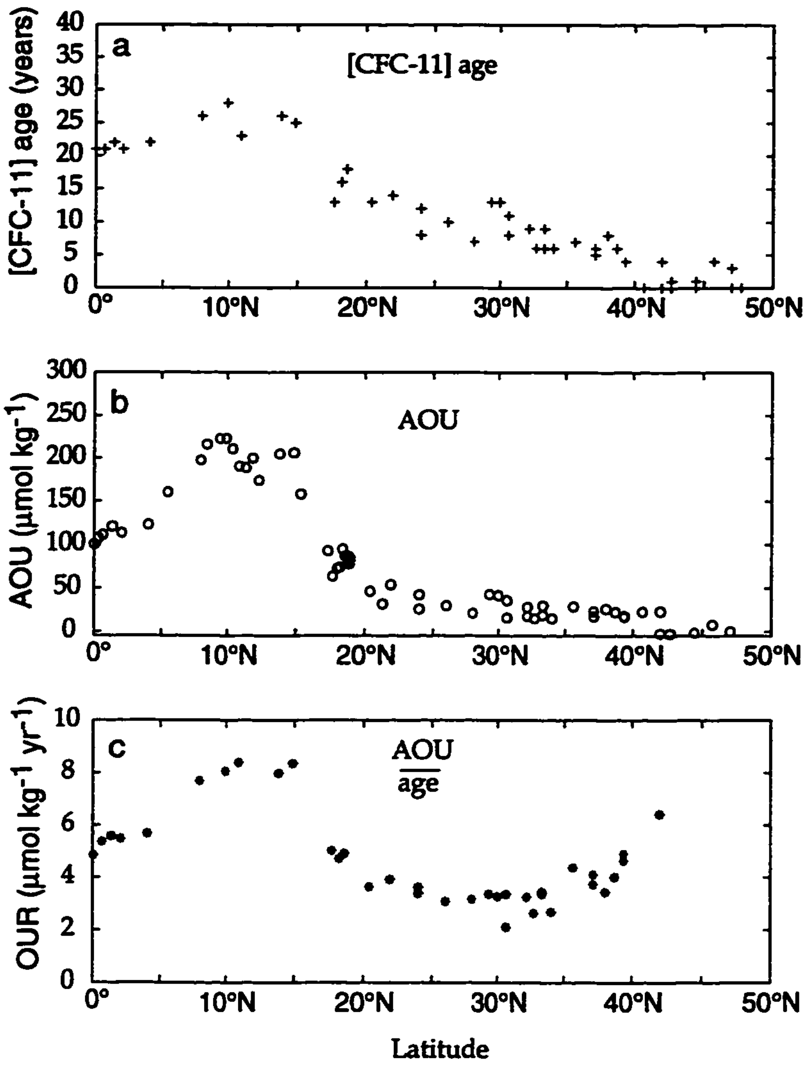

Figure 2.12. The meridional trends in CFC-11 concentration ages (a), apparent oxygen utilization (b), and oxygen utilization rates (c) on 26.2 and 26.4 σ_θ using data collected during WOCE P16 along 152°W in 1991.

and does not reflect only oxygen utilization rates at the location where the water sample was collected. Thus the high OUR values south of 15°N may primarily reflect the westward input of older, isolated, CFC-free water with high AOU levels from the eastern tropical Pacific that causes a CFC minimum (Fig. 2.4) and an AOU maximum (Fig. 2.12) and thus overestimated oxygen utilization rates as discussed above.

Integrating the in-situ oxygen utilization rates calculated from the advective-diffusive scheme from 25.5 to 26.6 σ_θ (~ 250 to ~ 500 meters), assuming an O_2/C ratio of 1.45 (Anderson and Sarmiento 1994), yields a carbon remineralization rate of 1 ± 0.1 moles C m^{-2} yr^{-1} between 20°N and 30°N. The uncertainty in this value is derived from the OUR uncertainties (Fig. 2.11) only and not from the depth integration or uncertainty in the O_2/C ratio. Since this integrated OUR includes remineralization rates from deeper than 250 meters only, the portion of the organic carbon rain remineralized immediately below the euphotic zone (~100 to 250 m) is not included, and thus the 1 ± 0.1 mole C m^{-2} yr^{-1} value must be considered a minimum.

We can estimate the contribution of remineralization above 25.5 σ_θ by extrapolating to the base of the euphotic zone using a normalized power function fit through the remineralization rate data (Fig. 2.11) as reported by Martin et al. (1987):

$$R_Z = R_{100}\left(\frac{Z}{100}\right)^b \tag{2.4}$$

Here R_{100} represents the remineralization rate at the base of the euphotic zone (nominally 100 meters), b represents the slope of the log-log relationship, and Z is depth in meters. Fitting equation (2.4) to the OURs calculated for the four isopycnal horizons (Fig. 2.11), using average isopycnal depths at 30°N, 152°W during P16, and the C/O_2 ratio above, yielded values for b and R_{100} of -1.3 ± 0.3 and 17 ± 2 µmol C kg^{-1} yr^{-1}, respectively. Integrating this relationship from 500 to 100 meters, i.e., ~ 26.6 σ_θ to the base of the euphotic zone, implies a carbon export rate of 2.2 ± 0.5 moles C m^{-2} yr^{-1} from the overlying euphotic zone. The uncertainties reported reflect the log-log fit's sensitivity to the uncertainties in the model-derived OURs (Fig. 2.11) only. This result can be compared to organic carbon export rates of 2.7 ± 1.7 moles C m^{-2} yr^{-1}, 1.6 ± 0.9 moles C m^{-2} yr^{-1}, and 2.0 ± 0.9 moles C m^{-2} yr^{-1} based on annual mass-balance calculations of oxygen, DIC and δ^{13}C-DIC, and organic carbon, respectively, in the upper 100 meters at station ALOHA (22° 45'N, 158°W, Emerson et al. 1997). Integrating the model's OUR versus depth relationship from 500 to 150 meters implies a carbon export rate of 1.5 ± 0.3 moles C m^{-2} yr^{-1} from overlying waters. This result can be compared to sediment trap particulate organic carbon fluxes of 1.1 ± 0.35 moles C m^{-2} yr^{-1} measured at 150 meters at station ALOHA (Karl et al. 1995).

Radiocarbon in the meridional model

The meridional distribution of radiocarbon (^{14}C) was measured during WOCE P13N along 165°E (NOSAMS 1995), P16 along 135°W and 152°W (NOSAMS 1994a, 1996) and P17C along 135°W (NOSAMS 1994b) in 1991-1992 and during GEOSECS in 1973-1974 (Östlund and Stuiver 1980). A discussion of the WOCE ^{14}C sampling, extraction and analytical procedures can be found in McNichol and Jones (1991), McNichol et al. (1994) and Jones et al. (1994), respectively. The meridional ^{14}C distributions on isopycnals within the main thermocline of the North Pacific differ from the CFC distributions in two significant ways (Fig. 2.13). First, subtropical ^{14}C concentrations are higher than in the subpolar gyre. In the subpolar gyre, unlike the subtropical gyre,

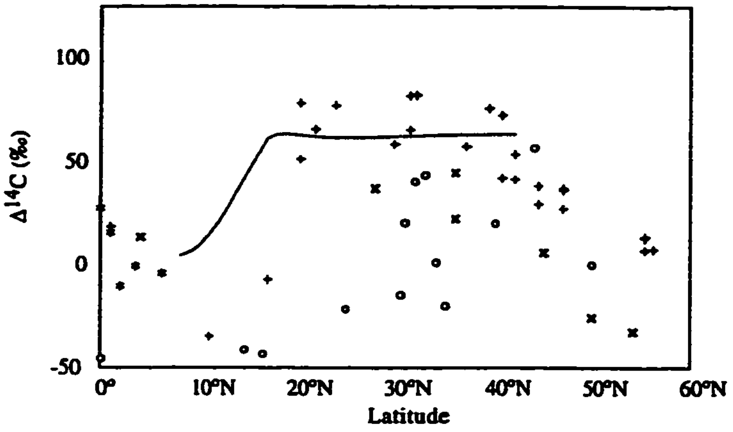

Figure 2.13. The meridional trend in $\Delta^{14}C$ measured in the North Pacific Ocean during WOCE P13N (x, 165°E in 1992), P16 (+, 152°W in 1991), P17C (*, 135°W in 1991) and GEOSECS (o, 127°W to 152°E 1973-1974) between 26.2 and 26.4 σ_θ. The solid line represents the predicted meridional trend in $\Delta^{14}C$ in 1991 south of 42°N using the CFC-11 calibrated model mixing rates (see text for discussion).

there is no clear evidence that either the levels or the meridional gradients in ^{14}C have changed much since the 1970s. The evolution of the meridional ^{14}C distributions since the 1970s shows that although along isopycnal transport from the subpolar outcrops may have been supplying radiocarbon to the subtropics at the time of GEOSECS, this is no longer true by the 1990s (Fig. 2.13). Second, zonal gradients of radiocarbon are comparable to, if not larger than, meridional gradients within the subtropical gyre based on a comparison of data from WOCE P13N (165°E) to P16 (135°W and 152°W), and in the subpolar gyre ^{14}C levels are higher in the East rather than in the West. The subtropical ^{14}C distributions have apparently, with the data available, homogenized meridionally (but not zonally) since the 1970s (Figs. 2.13 and 2.14). In fact, the scatter observed between 30-35°N during GEOSECS reflects

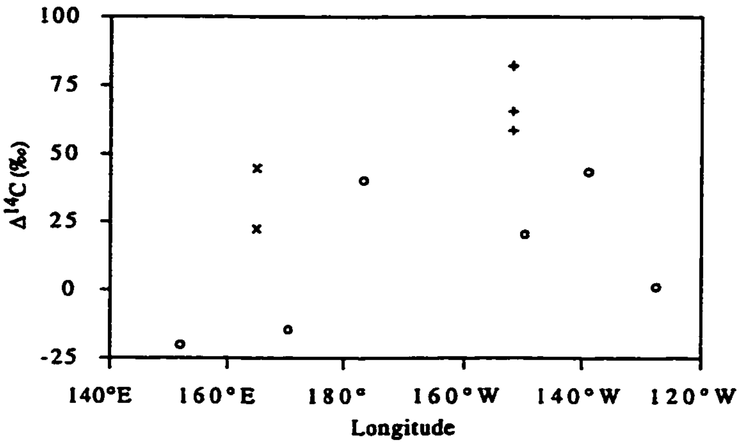

Figure 2.14. The zonal trend in Δ^{14}C on 26.2 to 26.4 σ_θ across the subtropical North Pacific (30°N to 36°N) during GEOSECS (o) in 1973-1974 and WOCE (x,+) in 1991-1992.

primarily the zonal trend of Δ^{14}C on this isopycnal in 1973-1974, with highest values in the central gyre and the lowest values to the West (Fig. 2.14). The zonal trend in ^{14}C in the subpolar region (Fig. 2.13), combined with southward flow in the eastern rather than the western subtropical gyre (Fig. 2.5) may maintain the zonal trend in ^{14}C observed on isopycnals within the subtropics (Fig. 2.14). In contrast, for CFCs the opposite subpolar zonal trend (higher in the West) coupled with likely slower southward ventilation in the West rather than the East may help establish the zonally uniform CFC distributions on isopycnals in the subtropical gyre (Fig. 4).

We can evaluate the importance of zonal processes by testing the one-dimensional meridional advection-diffusion model's simulation of bomb ^{14}C uptake in the subtropics. Because of the much slower mixed layer air-sea equilibration time for $^{14}CO_2$ (~10 years) versus CFCs (~ 1 month), the outcropping boundary conditions for $\Delta^{14}C$ were set equal to surface water $\Delta^{14}C$ values observed in the central Pacific (170°E to 135°W) within 2.5° latitude of the outcrop as a function of time using data from Linick (1978) for 1957 through 1970, GEOSECS for 1973 and 1974 (Östlund and Stuiver 1980), two NOAA cruises in 1982 and 1983 (Paul Quay, unpublished data), and WOCE measurements in 1991 (NOSAMS 1994a,b, 1996) as shown for example in Fig. 2.15. We initialize each isopycnal using an estimate of pre-nuclear $\Delta^{14}C$ distributions based on silica concentrations (Broecker et al. 1995), and step the model through time from 1950 to 1991 using the outcropping boundary condition defined as above. The uncertainty in the ^{14}C time history at the outcrops is the largest source of uncertainty in our radiocarbon simulations.

For all of the isopycnals considered in this analysis, the 1991 model-predicted meridional distribution of $\Delta^{14}C$ in the subtropics (20°N to 40°N) falls within the range of the measurements, however, $\Delta^{14}C$ values south of 20°N are overestimated (Fig. 2.13). Correctly simulating the $\Delta^{14}C$ distributions south of 20°N would require smaller along-isopycnal diffusivities of 2000 $m^2 s^{-1}$ for 25.5 to 26.0 σ_θ, 650 $m^2 s^{-1}$ for 26.0 to 26.2 σ_θ, and 500 $m^2 s^{-1}$ for the two deepest isopycnals. These values are 55 to 75 percent of the values determined by fitting the CFC distribution, as discussed above. This suggests that westward advection of waters from the eastern tropical Pacific may have a greater effect on the radiocarbon minimum at 10°N than on the CFC minimum. The model predictions for ^{14}C, however, are more poorly constrained than for CFCs because of the uncertainties in the ^{14}C outcropping boundary conditions as discussed above. Since the subtropical

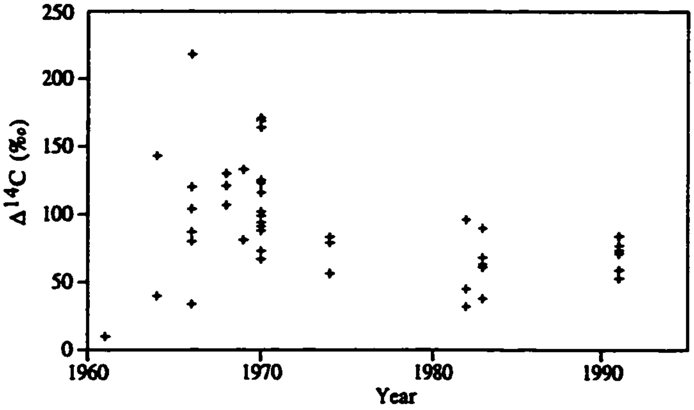

Figure 2.15. Surface water radiocarbon measurements in the North Pacific between 170°E and 135°W and 40°N to 45°N from cruises occurring between 1960 and 1971 (Linick 1978), GEOSECS in 1973-1974 (Östlund and Stuiver 1980), 1982-1983 (Paul Quay, unpublished data), and WOCE P16N (NOSAMS 1994a).

gyre on 25.5 to 26.6 σ_θ ventilates on time-scales less than 25 years (Fig. 2.8), the models' tropical ^{14}C values strongly depend on the temporal trend of $\Delta^{14}C$ in the subpolar outcrops during the decade after the maximum atmospheric ^{14}C levels, 1965-1975. During this time period surface ^{14}C values show considerable scatter (Fig. 2.15). Also, applying mean surface values at the outcrop sites likely overestimates the outcrops' ^{14}C values in winter when the mixed layer is deepest. For example, although the WOCE subtropical ^{14}C distributions predicted by the advective-diffusive models are reasonable (Fig. 2.13), the predicted ^{14}C levels at the time of GEOSECS (1973), just after the peak in subpolar mixed-layer ^{14}C values (Fig. 2.15), are overestimated. At this time, given the current uncertainties in the isopycnals' outcropping boundary conditions for radiocarbon, the bomb ^{14}C distribution does not add a quantitative constraint of the advective-diffusive models' transport terms.

That is to say, within the uncertainties in the subpolar surface ^{14}C time history (Fig. 2.15), a suitable fit to both the 1973 and 1991 Δ^{14}C distributions can be achieved using the CFC-calibrated transport terms. However the occurrence of zonal ^{14}C gradients, in contrast to the zonally homogeneous CFCs, may potentially yield useful constraints, when coupled with CFCs, on the meridional versus zonal components of thermocline ventilation in the subtropical North Pacific.

Salinity in the meridional model

Despite the general northward decrease in salinity on thermocline isopycnals in the North Pacific, within the subtropics salinity, like oxygen and radiocarbon, is relatively constant (Fig. 2.16). Salinity, like radiocarbon, exhibits zonal gradients that are comparable to meridional gradients between 30°N and 40°N (Fig. 2.16), so the assumption that zonal mixing has a negligible effect on the meridional distribution likely does not hold. To assess the effect of zonal mixing and advection we used the CFC calibrated meridional advection-diffusion scheme to simulate salinity at steady state by fixing the subpolar and tropical (18°N) end-members. In the subtropics, the model's salinity distribution is dominated by the southward advection of low-salinity subpolar waters. As a result, the model consistently underestimates salinities in the subtropics.

Eastward advection of higher salinity waters, especially between 30°N and 40°N (Fig. 2.16), is a source of salt to the eastern subtropical gyre that the one-dimensional model neglects. To balance the influx of low-salinity waters predicted by the CFC-calibrated meridional mixing rates, eastward advection

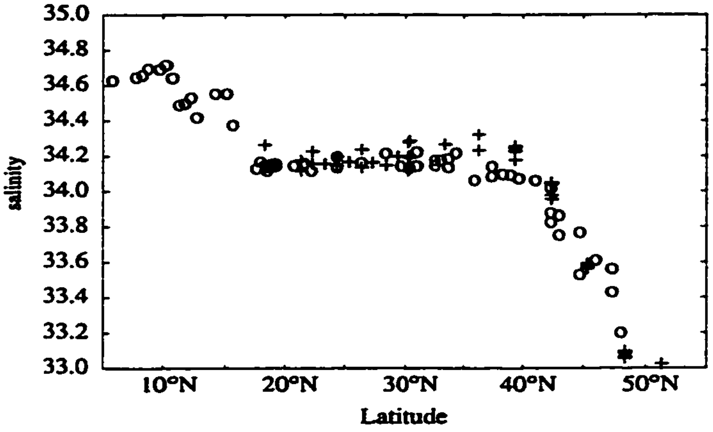

Figure 2.16. Meridional trends in salinity along 170°W (+) (Reid 1969) and 152°W (o) (WOCE P16, 1991) on the isopycnal layer between 26.2 and 26.4 σ_θ in the North Pacific Ocean.

rates on the order of 3 cm s^{-1} (from 25.5 down to 26.6 σ_θ) would be required, using the zonal salinity gradients measured between 170°W and 152°W. These velocities are two to three times larger than the zonal advection rates reported by Coats (1981) at 35°N, 155°W and the geostrophic estimates reported by Roemmich and McCallister (1989) across 152°W for this density range.

Vertical (cross-isopycnal) mixing supplies salt downward because of the steep vertical gradient between 25.5 and 26.6 σ_θ in the subtropics (Fig. 2.2). To test the sensitivity of the predicted salinity fields to vertical mixing we have added three layers each above and below 25.5 and 26.6 σ_θ, and added a constant cross-isopycnal turbulent mixing term, $Kz(d^2C/dZ^2)$ to equations (2.1) and (2.2). To calculate cross-isopycnal tracer fluxes, we used annual average isopycnal depths along 152°W calculated from the Levitus (1982) data set and marched all layers together forward in time as in the 1-D simulations. The model, as constructed, neglects cross-isopycnal advection which must accompany cross-isopycnal turbulent diffusion if the density field is to remain steady (Walin 1982). The cross-isopycnal advection associated with a *Kz* value of 0.1 $cm^2 s^{-1}$ is small (< 1.5 m yr^{-1}) and implies 1991 CFC fluxes generally 20 % of the cross-isopycnal mixing CFC fluxes and < 5 % of the along-isopycnal advective CFC fluxes. The implied vertical advective CFC flux is small relative to the overall uncertainties in our 2-D modeling approach.

With cross-isopycnal mixing included, the along-isopycnal advection and diffusion rates were refitted to the 1991 CFC-11 observations. On isopycnals within the subsurface CFC maximum in the subtropical North Pacific (Fig. 2.3), vertical mixing acts as a local sink for CFCs. Therefore, between 25.5 to 26.0 σ_θ and 26.2 to 26.4 σ_θ the best fit CFC-derived along-isopycnal advection rates are generally larger by < 15 % when compared to rates determined without vertical mixing terms. On 26.4 to 26.6 σ_θ, the best-fit along-isopycnal velocity decreases by < 5 % when vertical mixing terms are included. Applying the re-calibrated advection and mixing rates to the salinity distributions, we find that, due to the intensity of vertical salinity gradients in the subtropical thermocline, a cross-isopycnal mixing term no larger than 0.3 $cm^2 s^{-1}$ and generally around 0.1 $cm^2 s^{-1}$ is required to allow the model to satisfy the subtropical salinity, ^{14}C and CFC distributions simultaneously. These vertical mixing terms are consistent with *Kz* values of about 0.2 $cm^2 s^{-1}$ derived from microstructure measurements in the abyssal ocean (Toole et al. 1994) and 0.11 $cm^2 s^{-1}$ determined from tracer release experiments conducted in the subtropical Atlantic thermocline (Ledwell et al. 1993). Although the above results indicate that a small cross-isopycnal mixing term allows the model to satisfy the salinity distribution in the subtropics, we are reluctant to use salinity as a quantitative constraint on the model's CFC-derived meridional transport terms because of the potentially significant contribution of zonal transport to the salinity distribution along 152°W.

We have recalculated the steady-state OURs using the cross-isopycnal mixing rates and re-calibrated along-isopycnal transports discussed above. The 2-D OUR calculations generally agree (within errors) with those calculated from the 1-D transports. On 25.5 to 26.0 σ_θ and 26.0 to 26.2 σ_θ, the slightly larger along-isopycnal velocities in the subtropics lead to ~ 5 % larger calculated OURs for a vertical mixing term of 0.1 $cm^2\,s^{-1}$. On 26.2 to 26.4 σ_θ and 26.4 to 26.6 σ_θ, vertical mixing acts as a net oxygen sink, so the calculated OURs are 10-20 % smaller when a vertical mixing term of 0.1 $cm^2\,s^{-1}$ is included. Depth-integrating the 2-D OURs from 500 m to 250 m (~ 26.6 to 25.5 σ_θ) yields the same net carbon remineralization rate from the overlying euphotic zone as calculated from the 1-D model, i.e., 1 mole C $m^{-2}\,yr^{-1}$. However, the 2-D OURs describe a slightly steeper remineralization rate versus depth profile than do the 1-D results. Integrating Martin et al.'s (1987) power function fit through the 2-D OUR results for Kz=0.1 $cm^2\,s^{-1}$ from 100 m to 500 m implies a somewhat larger carbon export estimate than that derived from the 1-D results (2.8 versus 2.2 moles C $m^{-2}\,yr^{-1}$, respectively).

Summary

We determined the along isopycnal advection and diffusion rates required to yield the meridional CFC-11 distribution measured along 152°W during WOCE P16 (1991) in the North Pacific thermocline. In the along-isopycnal models, calculated southward advection rates ranged from 1.03 to 0.56 cm s^{-1}, and along-isopycnal mixing rates ranged from 2750 to 700 $m^2 s^{-1}$ between 25.5 and 26.6 σ_θ, respectively. Ventilation times between northern outcrops and 15°N to 20°N (along 152°W) were calculated by incorporating an ideal-age tracer into the model mixing scheme and ranged from 10 to 27 years from 25.5 to 26.6 σ_θ, respectively. From 25.5 to 26.4 σ_θ, the model-derived ages were in excellent agreement with CFC-11 concentration ages, suggesting that the CFC-11 ages are little affected by mixing when waters are less than 20 years old in 1991. On the deepest isopycnal, 26.4 to 26.6 σ_θ, the mean model-derived ages were slightly older than CFC-11 concentration ages.

Applying the model-derived mixing scheme to the measured oxygen distributions, we found that in-situ oxygen utilization rates decreased with depth from 6.6 to 3.2 μmol kg^{-1} yr^{-1} from 25.5 to 26.6 σ_θ. Vertically integrating the OURs from 250 to 500 meters implied an overlying organic carbon export rate of 1 ± 0.1 mole carbon m^{-2} yr^{-1} in the central subtropical gyre. When the OUR versus depth trend at 30°N, 152°W was extrapolated to the base of the euphotic zone using the normalized power function reported by Martin et al. (1987), an organic carbon export rate of 2.2 ± 0.5 mole carbon m^{-2} yr^{-1} was determined. This rate is in good agreement with estimates of organic carbon export rates from the euphotic zone of the subtropical North Pacific.

Incorporation of bomb ^{14}C and salinity into the meridional advective-diffusive model indicated that zonal transport and cross-isopycnal mixing are important for these tracers. Neither radiocarbon nor salinity is conserved in the one-dimensional meridional model scheme. Testing the meridional advective-diffusive 1-D model against ^{14}C and salinity measurements, we found that both zonal and vertical mixing are important in explaining the subtropical distributions of these tracers. A cross-isopycnal diffusivity on the order of 0.1 to 0.3 $cm^2 s^{-1}$ was sufficient to allow the meridional model to satisfy the time evolution of subtropical CFC and ^{14}C distributions and the steady-state salinity distribution simultaneously.

The model's along-isopycnal transports of oxygen and CFCs are affected only slightly by the vertical (cross-isopycnal) mixing terms estimated from the salinity distribution. The substantial subsurface maximum in CFCs and the lack of zonal gradients in oxygen and CFCs implies that southward along-isopycnal advection and diffusion must be the dominant mechanism ventilating these gases into the main thermocline of the subtropical gyre in the North Pacific. Thus, although the 1-D model is very simple, the predominance of meridional gradients in CFCs and oxygen affords fairly robust estimates of the meridional along-isopycnal transport terms and in-situ oxygen utilization rates within the subtropical gyre.

Chapter 3 : Reconstructing the oceanic ^{13}C Suess effect using preformed ^{13}C[Ψ]

Introduction

The addition of anthropogenic CO_2 has caused a decrease in the $^{13}C/^{12}C$ ratio of atmospheric CO_2, the so-called "^{13}C Suess effect", because fossil fuels are relatively depleted in ^{13}C (Friedli et al., 1986; Keeling et al., 1989). The observation that the $^{13}C/^{12}C$ ratio of the oceanic dissolved inorganic carbon (DIC) pool is also decreasing (the oceanic ^{13}C Suess effect) has provided a means for estimating oceanic uptake of anthropogenic CO_2. Quay et al. (1992) calculated the ocean's uptake of fossil-fuel CO_2 based on observed changes in the $\delta^{13}C$ of oceanic DIC between the early 1970s and 1990s and a mass-balance of $^{12}CO_2$ and $^{13}CO_2$ in the atmosphere, ocean and terrestrial biosphere. This approach required measurements of the depth-integrated oceanic ^{13}C Suess effect, which was determined from a comparison of $\delta^{13}C$ of DIC depth profiles measured at seven sites in the Pacific Ocean in the 1970s and 1990s. Quay et al. (1992) used the observed correlation between depth-integrated ^{13}C changes and bomb ^{14}C inventories determined during GEOSECS to calculate a net oceanic uptake rate of 2.1 ± 0.8 Gt. C yr^{-1} (1 Gt. = 1 gigaton = 10^{12} kg).

Tans et al. (1993) also used a $^{12}CO_2$ and $^{13}CO_2$ mass balance in the atmosphere, terrestrial biosphere and ocean to calculate oceanic CO_2 uptake. Their approach depended on estimating the gross air-sea CO_2 exchange flux

---

[Ψ] This chapter will be published by R. E. Sonnerup, P. D. Quay, T. A. Westby, H. L. Anderson, A. P. McNichol and J. L. Bullister in *Global Biogeochemical Cycles* (in press).

and determining the isotopic disequilibrium between the atmosphere and the ocean. Their best estimate of the global average air-sea $\delta^{13}C$ disequilibrium implied almost no net oceanic uptake, i.e., 0.2 Gt. C yr^{-1}. However, Tans et al. (1993) pointed out that the calculated CO_2 uptake rate is highly sensitive to the magnitude of the average air-sea ^{13}C disequilibrium, which has been difficult to determine. Heimann and Maier Reimer (1996) estimated the uncertainty in this CO_2 uptake estimate to be $\pm \sim 1.7$ Gt. C yr^{-1}.

Heimann and Maier-Reimer (1996) proposed a method for calculating oceanic CO_2 uptake from ^{13}C that relied on the observation that the time histories of the atmospheric CO_2 increase and $\delta^{13}C$ of CO_2 decrease are roughly the same, so the oceanic penetration depths of both perturbations should be similar. Incorporating their approach and the budgets of Quay et al. (1992) and Tans et al. (1993) into a "total inversion" calculation, they constructed a global carbon cycle scenario which is consistent with all three methods and implies an oceanic CO_2 uptake rate of 2.1 ± 0.9 Gt. C yr^{-1}. Heimann and Maier-Reimer's sensitivity analysis demonstrated that uncertainty in the oceanic ^{13}C Suess effect accounted for 73 % and 78 % of the uncertainty of oceanic CO_2 uptake rates determined by Quay et al.'s and their approach, respectively.

Bacastow et al. (1996) introduced another method for estimating oceanic CO_2 uptake rates from oceanic $\delta^{13}C$ data. They used the measured surface ocean $\delta^{13}C$ decrease from 1984 through 1993, based on time-series observations near Bermuda, and an ocean general circulation model (OGCM) to relate this local $\delta^{13}C$ change to the global mean Suess effect. They found that the intensity of meridional gradients in the simulated surface ocean ^{13}C

Suess effect near Bermuda led to considerable uncertainty in relating the change observed at Bermuda to the global average surface ocean Suess effect. However they showed, using a box-diffusion model (Oeschger et al., 1975), that a superior estimate of the surface ocean ^{13}C Suess effect could be used as a strong constraint on oceanic CO_2 uptake rates.

All of these methods, with the exception of the Tans et al. (1993) budget, are limited by the substantial uncertainty in the magnitude of the oceanic ^{13}C Suess effect. Previous estimates of the Suess effect were based on comparisons of synoptic measurements taken ~ 20 years apart (Quay et al., 1992), a time series of surface water $\delta^{13}C$ of DIC (Bacastow et al., 1996), or analyses of $\delta^{13}C$ in aragonite incorporated into a sclerosponge (Druffel and Benavides, 1986). The information derived from synoptic comparisons has been limited primarily by the lack of high quality data collected prior to 1980 and, to a lesser extent, suffers from aliasing of seasonal and inter-annual variability in surface water $\delta^{13}C$ (Bacastow et al., 1996). $\delta^{13}C$ data from time series stations provide direct evidence of the oceanic ^{13}C Suess effect, but are presently limited to only two stations, one at Bermuda (Bacastow et al., 1996), and one near Hawaii (Paul Quay, unpublished data). Measurements of the ^{13}C Suess effect in corals or sponges are relatively scarce and limited to tropical waters. Extrapolation of these local results to the global ocean introduces considerable uncertainty because spatial variability in the surface ocean Suess effect is substantial (Quay et al., 1992).

In this paper we improve estimates of both the surface and depth-integrated oceanic ^{13}C Suess effect. Our approach makes use of extensive synoptic $\delta^{13}C$ data collected during WOCE and NOAA cruises in the late 1980s and early 1990s, and does not depend on past data. We estimate the Suess effect from recent surveys by reconstructing "preformed" $\delta^{13}C$ of DIC distributions on isopycnal surfaces (Kroopnick, 1985) and determine the rate of change of preformed $\delta^{13}C$ using water ages calculated from concurrent CFC measurements (Doney and Bullister, 1992). We calculate the ^{13}C Suess effect in the North Atlantic, South Indian, and Pacific Oceans and estimate the global surface and depth-integrated ^{13}C Suess effect from these local calculations. We apply our global estimate of the depth-integrated oceanic ^{13}C decrease to the atmospheric $^{12}CO_2$ and $^{13}CO_2$ mass balance (Quay et al., 1992) and calculate an oceanic CO_2 uptake rate of 2.0 ± 0.9 Gt. C yr^{-1} over the time period 1970-1990.

Reconstructing anthropogenic ^{13}C changes in the ocean

A number of researchers have sought to quantify the ocean's anthropogenic CO_2 content using calculations of "preformed" DIC, that is, DIC° (Brewer, 1978; Chen and Pytkowicz, 1979; Chen and Millero, 1979; Chen, 1982). The primary limitation of these methods is uncertainty due to mixing among water masses with different DIC° properties (Shiller, 1981; Chen et al., 1982), and in the C/O_2 ratio of organic matter remineralization (Brewer et al., 1997). Recently, Gruber (1996, 1998) attempted to eliminate mixing effects by subtracting a sample's DIC value which would be in equilibrium with the pre-industrial atmosphere (fCO_2=280 μatm) and applying a two end-member mixing model. Assuming the ocean-atmosphere DIC disequilibrium has been constant over time, the anthropogenic CO_2 content is estimated by subtracting out today's ocean-atmosphere DIC disequilibrium for each component of the mixture on that isopycnal. We use a similar approach to determine trends in preformed $^{13}C/^{12}C$ of DIC along isopycnals. The assumption that the $\delta^{13}C$ air-sea disequilibrium has been constant in time, however, is less certain than for CO_2 because of the much longer equilibration time for the $^{13}C/^{12}C$ than the concentration of DIC. Instead, we deal with mixing biases by analyzing preformed ^{13}C trends along isopycnals in regions where mixing can be neglected.

Preformed DIC (DIC°) is defined as the measured DIC content of a sea water sample, minus the proportion of that DIC that has been added from remineralization of organic matter and dissolution of carbonate shells at depth:

$$DIC^{o} = DIC - \left\{ AOU \cdot \left(\frac{C}{O_2} \right)_{org} \right\} - \frac{1}{2} \left\{ \Delta ALK_{spl-sfc} + AOU \cdot \left(\frac{N}{O_2} \right)_{org} \right\} \tag{3.1}$$

The DIC contribution from organic matter remineralization is calculated from the sample's apparent oxygen utilization (AOU) and the "Redfield" carbon to oxygen ratio $(C/O_2)_{org}$. The extent of $CaCO_3$ dissolution at depth is usually estimated from the alkalinity difference between the subsurface sample and surface waters in the water mass' outcropping area $(\Delta ALK_{spl\text{-}sfc})$, and the proton flux associated with organic matter remineralization is estimated from AOU and the "Redfield" nitrogen to oxygen ratio $(N/O_2)_{org}$. DIC° represents an estimate of the DIC content of a water parcel at the time it was subducted from the mixed layer.

Preformed ^{13}C ($\delta^{13}C^{o}$) is the analogous calculation for the $^{13}C/^{12}C$ ratio of the DIC in the subsurface sample (Kroopnick, 1985):

$$\delta^{13}C^{o} = \frac{DIC \cdot \delta^{13}C - \left\{ AOU \cdot \left(\frac{C}{O_2} \right)_{org} \cdot \delta^{13}C_{org} \right\} - \frac{1}{2} \left\{ \left(\Delta ALK_{spl-sfc} + AOU \cdot \left(\frac{N}{O_2} \right)_{org} \right) \cdot \delta^{13}C_{CaCO_3} \right\}}{DIC - \left\{ AOU \cdot \left(\frac{C}{O_2} \right)_{org} \right\} - \frac{1}{2} \left\{ \Delta ALK_{spl-sfc} + AOU \cdot \left(\frac{N}{O_2} \right)_{org} \right\}} \tag{3.2}$$

Here $\delta^{13}C$ is the $\delta^{13}C$ of DIC in the water sample, $\delta^{13}C_{org}$ represents the $\delta^{13}C$ of oceanic organic matter, typically -21 ‰ over most of the world ocean (Goericke and Fry, 1994), and $\delta^{13}C_{CaCO_3}$ represents the $\delta^{13}C$ of calcium carbonate shells, which is typically within ± 1 ‰ of the $\delta^{13}C$ of surface water DIC (Bonneau et al., 1980). If the "Redfield" ratios, $\delta^{13}C_{org}$ and $\delta^{13}C_{CaCO_3}$ were constant, DIC^{o} and $\delta^{13}C^{o}$ would behave as nearly conservative tracers below the mixed layer. In the absence of an anthropogenic disturbance, the distributions of DIC^{o} and $\delta^{13}C^{o}$ could be used like "NO" (Broecker, 1974) or salinity as tracers of water masses and mixing in the ocean interior. Conversely, the magnitude of the anthropogenic disturbance must be evaluated in regions where the DIC^{o} and $\delta^{13}C^{o}$ distributions are not affected by mixing or where mixing effects can be quantified using conservative tracers such as "NO" or salinity, as discussed below.

In the absence of $CaCO_3$ dissolution, DIC^{o} and $\delta^{13}C^{o}$ can be calculated using only measurements from one water sample. Calculating the contribution from carbonate dissolution is more difficult because it requires an estimate of the sample's preformed alkalinity, i.e., its alkalinity at the time it was subducted, which cannot be calculated directly from the one sample. Since the ratio of $CaCO_3$ dissolution to organic matter remineralization may be as much as 1:4 (Broecker and Peng, 1982) the inorganic contribution is important in establishing DIC distributions. In contrast, formation and dissolution of $CaCO_3$ has little effect on the $\delta^{13}C$ of DIC because the $\delta^{13}C$ of $CaCO_3$ is within ± 1 ‰ of the $\delta^{13}C$ of DIC (Bonneau et al., 1980). Fortunately, therefore, the $CaCO_3$ dissolution terms can be neglected with little impact on the calculated $\delta^{13}C^{o}$ distributions and estimates of the preformed alkalinity are not required.

The value chosen for the $\delta^{13}C$ of organic matter (Fig. 3.1) has a substantial impact on the $\delta^{13}C^{o}$ calculation. Between 40°N and 40°S $\delta^{13}C$ of particulate organic carbon ($\delta^{13}C_{POC}$) values compiled by Goericke and Fry (1994) varied between -18.5 and -22 ‰, with a mean of -20.3 ‰. In cold Arctic waters, $\delta^{13}C_{POC}$ values were somewhat lower, averaging ~ -23.4 ‰, and in the high-latitude southern ocean $\delta^{13}C_{POC}$ varied between -24 ‰ and -36‰. For our $\delta^{13}C^{o}$ reconstructions on high latitude southern ocean isopycnals, instead of using a constant $\delta^{13}C_{org}$ value (equation 2), we calculated the organic contribution by assuming that the meridional isopycnal trend in AOU was caused entirely by remineralization of POC raining down from overlying waters with its associated $\delta^{13}C_{POC}$ (see Table 3.1).

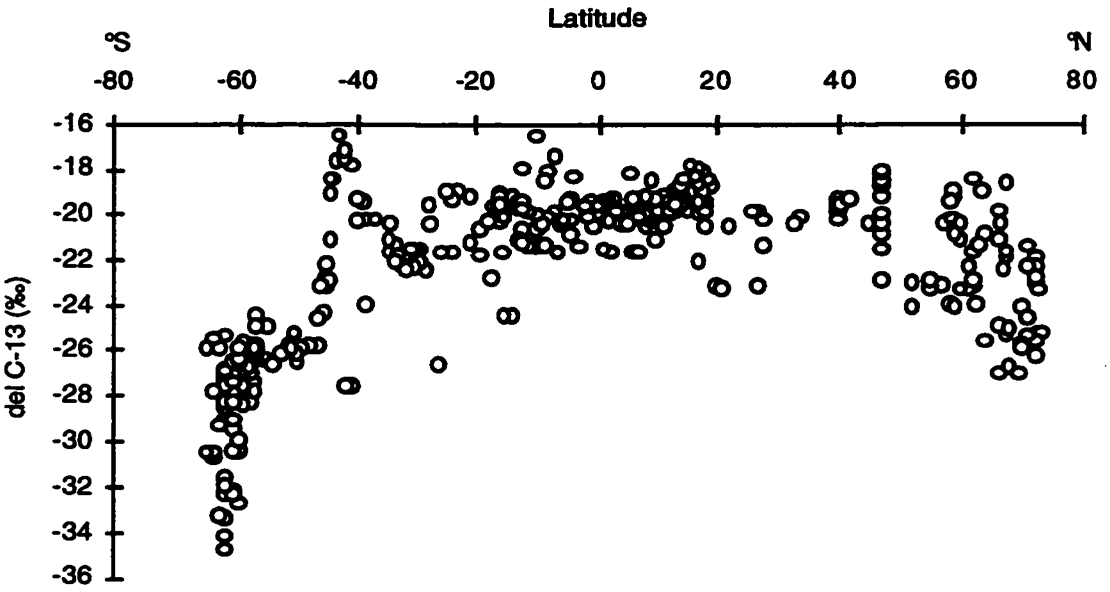

Figure 3.1. The $\delta^{13}C$ of particulate organic matter and plankton from the surface ocean mixed layer, compiled by Goericke and Fry (1994), and used to estimate $\delta^{13}C_{org}$.

Uncertainties in the $\delta^{13}C°$ calculations

The uncertainty in $\delta^{13}C°$ was evaluated by propagating the $\pm$ 1 σ uncertainty in each term in equation 3.2 using a Monte-Carlo approach. The uncertainties in each term (Table 3.2) were assumed to be normally distributed and uncorrelated. The uncertainty in our manometric DIC measurements was $\pm$ 5 μmol kg^{-1} based on a comparison with concurrent coulometric DIC determinations. The error in the $\delta^{13}C$ of DIC was $\pm$ 0.03 ‰ based on analyses of replicate samples and standards. The uncertainty in the $\delta^{13}C$ of organic matter, derived from the scatter in the observations

Table 3.1. The $\delta^{13}C$ of particulate organic matter used when calculating preformed $\delta^{13}C$ of DIC (equations 2-3) along isopycnals from changes in AOU. The $\delta^{13}C_{POC}$ data were compiled by Goericke and Fry (1994), and the uncertainties reported represent ± 1 σ of the scatter in the observations (Fig. 3.1).

Latitude band of AOU change	$\delta^{13}C_{POC}$ assumed
south of 60°S	-29 ± 2.5 ‰
60°S to 50°S	-26.4 ± 1 ‰
50°S to 40°S	-22 ± 3.5 ‰
40°S to equator	-20.6 ± 1.6 ‰
equator to 20°N	-19.8 ± 0.9 ‰
20°N to 65°N	-21.1 ± 1.8 ‰

(Goericke and Fry, 1994), was typically < 2 ‰ in the temperate and tropical oceans (Fig. 3.1). The $\delta^{13}C$ of $CaCO_3$ was assumed to be 1.5 ± 0.5 ‰ (Bonneau et al., 1980). Although the uncertainty in oxygen measurements is typically ~ 1 μmol kg^{-1}, surface water oxygen values probably varied within ± 4 μmol kg^{-1} of saturation with respect to the atmosphere (Gruber et al., 1996) and dominated the error in AOU.

Throughout this study we adopted the N/O_2 and C/O_2 ratios of remineralization determined from nutrient trends along neutral surfaces (Anderson and Sarmiento, 1994). Due to the presence of anthropogenic CO_2 on many of these surfaces, the C/O_2 ratio could not be determined with the same confidence as the other "Redfield" ratios using this technique. An O_2/C ratio between 1.3 and 1.6 was estimated based on the likely compositions of planktonic organic matter (Laws, 1991; Anderson and Sarmiento, 1994;

Takahashi et al., 1985). The ± 0.15 uncertainty in the O_2/C ratio of 1.45 reported by Anderson and Sarmiento (1994), and adopted here, represented the possible range for this ratio, and not the ± 1 σ error. The DIC input due to $CaCO_3$ remineralization was assumed to be 25 % of the input from organic matter remineralization (Broecker and Peng, 1982).

The overall uncertainty (± 1 σ) in $\delta^{13}C^{\circ}$ was most sensitive to AOU and increased from ± 0.04 ‰ at AOU=0 μmol kg^{-1} to ± 0.08 ‰ at AOU=100 μmol kg^{-1} (Table 3.2), where the latter value represents the maximum AOU sample used in this study. At AOU=0 μmol kg^{-1}, the uncertainty in $\delta^{13}C^{\circ}$ was equally derived from the errors in the assumption of O_2 saturation at the surface outcrop and in the $\delta^{13}C$ measurement (Table 3.2). When AOU was > 75 μmol kg^{-1}, uncertainties in the C/O_2 ratio and $\delta^{13}C_{org}$ dominated (Table 3.2). Uncertainties in the measurement of DIC and in the $\delta^{13}C$ value of dissolving $CaCO_3$ shells (Table 3.2) made a negligible contribution to the error in $\delta^{13}C^{\circ}$.

When the alkalinity terms in equation 2 were neglected, the calculated $\delta^{13}C^{\circ}$ values were < 0.005 ‰ higher at AOU = 100 μmol kg^{-1}. Although the trend in $\delta^{13}C^{\circ}$ versus AOU was slightly steeper when $CaCO_3$ terms were neglected, this offset was very small (< 2 %) relative to the ± 1 σ errors resulting from the remaining terms in equation 2 (Table 3.2). Therefore, in the remainder of this study we report trends for $\delta^{13}C^{\circ}$ values calculated

Table 3.2. The uncertainty (± 1 σ) in $\delta^{13}C°$ calculated as a function of AOU, and the percent contribution to that error from individual terms in the $\delta^{13}C°$ calculation (equation 2). Uncertainties (± 1 σ) in the terms used for the $\delta^{13}C°$ calculations are outlined in the column headings.

AOU (µmol kg^{-1})	$\delta^{13}C°$ error (‰)	O_2/C (± 0.15) percent	AOU (± 4.1 µmol kg^{-1}) percent	$\delta^{13}C$ (± 0.03 ‰) percent	$\delta^{13}C_{org}$ (± 1.5 ‰) percent	$\delta^{13}C_{CaCO3}$ (± 0.5 ‰) percent	DIC (± 5 µmol kg^{-1}) percent
0	0.04	0	51	49	0	0	0.0
25	0.05	9	43	42	7	0	0.0
50	0.06	22	27	31	20	0.1	0.0
75	0.07	34	18	20	28	0.2	0.0
100	0.08	40	13	15	32	0.2	0.0
150	0.12	47	6	7	40	0.3	0.0
200	0.15	49	4	5	42	0.3	0.0

using the following simplified equation:

$$\delta^{13}C^{o} = \frac{DIC \cdot \delta^{13}C - \left\{ AOU \cdot \left(\frac{C}{O_2} \right)_{org} \cdot \delta^{13}C_{org} \right\}}{DIC - \left\{ AOU \cdot \left(\frac{C}{O_2} \right)_{org} \right\}} \tag{3.3}$$

Sample isopycnal $\delta^{13}C^{\circ}$ distribution along 105°W

In addition to the random errors in $\delta^{13}C^{\circ}$ reported in Table 3.2, there are systematic errors due to mixing in the ocean interior which can bias the $\delta^{13}C^{\circ}$ trends observed on isopycnals, as discussed by Shiller (1981) for calculated DIC° distributions. We minimized the uncertainty due to mixing by estimating the ^{13}C Suess effect on isopycnals where only one end-member water mass was evident based on "NO" and salinity distributions. To illustrate such a situation, we show the ^{13}C Suess effect calculation from the South Pacific Ocean along 105°W within the 27.0 to 27.1 σ_θ density interval (Fig. 3.2) which represents the core of the Subantarctic Mode Water described by McCartney (1982). This water mass is formed by wintertime deep convection at around 55°S along this section (McCartney, 1982), and reaches a maximum depth interval of ~ 600 to ~ 800 m within eastern arm of the South Pacific subtropical gyre. The flow along this section is generally northwards to around 25°S.

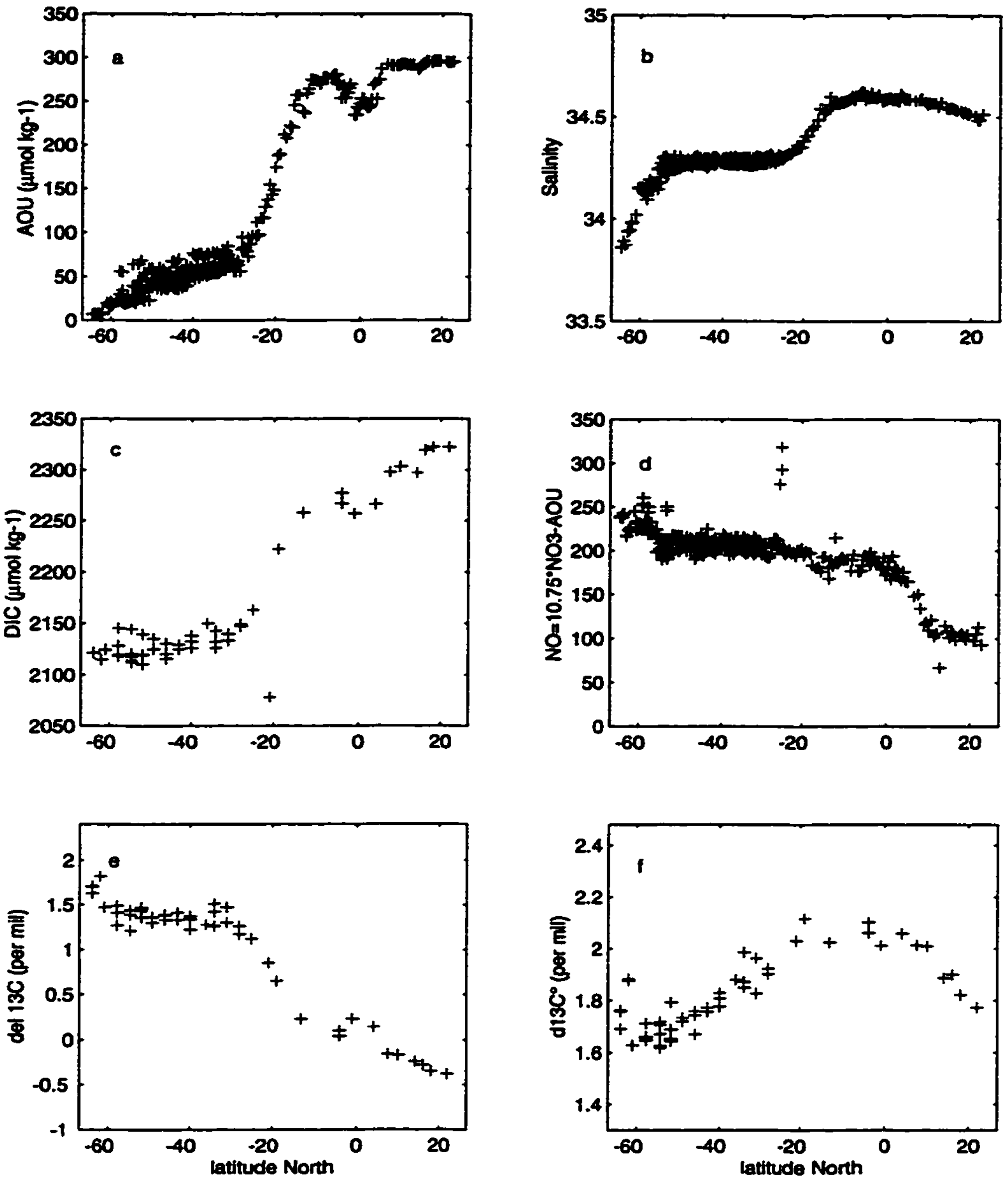

Figure 3.2. Distributions of A) AOU, B) salinity, C) dissolved inorganic carbon (DIC), D) "NO", E) $\delta^{13}C$ of DIC and F) preformed $\delta^{13}C$ ($\delta^{13}C°$) within the isopycnal horizon 27.0-27.1 σ_θ along 105°W and 110°W measured during the Climate and Global Change 1994 (WOCE P18) cruise in the Pacific Ocean in 1994.

AOU values reached zero south of the wintertime outcrop in late summer on this isopycnal (Fig. 3.2). AOU and DIC increased and $\delta^{13}C$ decreased north of this region due to in-situ remineralization of isotopically depleted organic matter. Salinity and "NO" were constant between the outcrop region (55°S) and 27°S. North of 27°S, however, the increase in salinity and decrease in "NO" indicate that mixing with another water mass, with distinct preformed properties, occurs. North of 5°N DIC increased and $\delta^{13}C$ and $\delta^{13}C^{\circ}$ decreased without a corresponding increase in AOU. This situation illustrates the effect of de-nitrification (Codispoti and Richards, 1973) on $\delta^{13}C^{\circ}$ and DIC° distributions.

$\delta^{13}C^{\circ}$ increased northward in the uniform water mass region between 55°S and ~ 27°S. The $\delta^{13}C^{\circ}$ values were lowest in the most recently ventilated waters and highest in older waters (Fig. 3.2). Because waters in this region had preserved the salinity and "NO" characteristics imparted at the outcrop, the lower $\delta^{13}C^{\circ}$ in younger waters indicated that the $\delta^{13}C^{\circ}$ of the winter mixed layer in the outcropping region has decreased during the time period of ventilation of the subtropical gyre on this isopycnal. This $\delta^{13}C$ decrease results from oceanic uptake of relatively ^{13}C depleted anthropogenic CO_2.

Dating the changes in $\delta^{13}C^{\circ}$

The time rate of change of the anthropogenic ^{13}C signal was calculated using CFC ages. The meridional trend in CFC-11 on 27.0 to 27.1 σ_{θ} along 105°W (P18) shows near atmospheric saturation levels south of 60°S and a decrease northward reaching the detection limit at ~ 20°S (Fig. 3.3). We estimated a subduction date, i.e., the time when the water left the surface, by assuming that the surface water was saturated with respect to atmospheric CFCs when it was subducted and comparing each subsurface sample's CFC-11 concentration with a reconstruction of the atmospheric CFC-11 history (Walker et al., 1995). CFC ages were < 10 years south of 50°S and reached 25-30 years at 27°S (Fig. 3.3). Atmospheric CFC-11 levels increased in a roughly linear fashion between 1968 and 1991. To minimize the impact of water mass mixing on CFC-11 derived water ages, samples with CFC-11 ages between 3 and 26 years in 1994 only were used to estimate the time rate of change of $\delta^{13}C°$. The slope of the $\delta^{13}C°$ versus [CFC-11] age trend yields a $\delta^{13}C°$ change rate of -0.15 ± 0.02 ‰ decade^{-1} on the 27.0 to 27.1 σ_θ isopycnal (Fig. 3.4).

The assumption that waters were 100 % saturated when they were subducted results in a systematic bias of CFC-derived formation dates. Assuming instead that waters were only 86 % saturated when they were subducted, i.e., the saturation level observed in the 55°S outcrop region of 27.0 to 27.1 σ_θ during P18, yielded significantly younger ages (3-4 years) near the outcrop, while the older dates were affected less (Fig. 3.3). The reason is that the percentage annual change of CFCs has been decreasing over time, so the change in saturation level assumed translated into a larger age change in modern samples. Recalculating the $\delta^{13}C°$ versus age relationship using the observed saturation level of 86 % yielded only a slightly smaller $\delta^{13}C°$ versus age trend of -0.13 ± 0.02 ‰ decade^{-1}. Since water masses formed in deep winter mixed layers are often undersaturated with respect to atmospheric CFCs when formed (Wallace and Lazier, 1988), in the remainder of this study we used the saturation levels observed in each isopycnal's outcropping

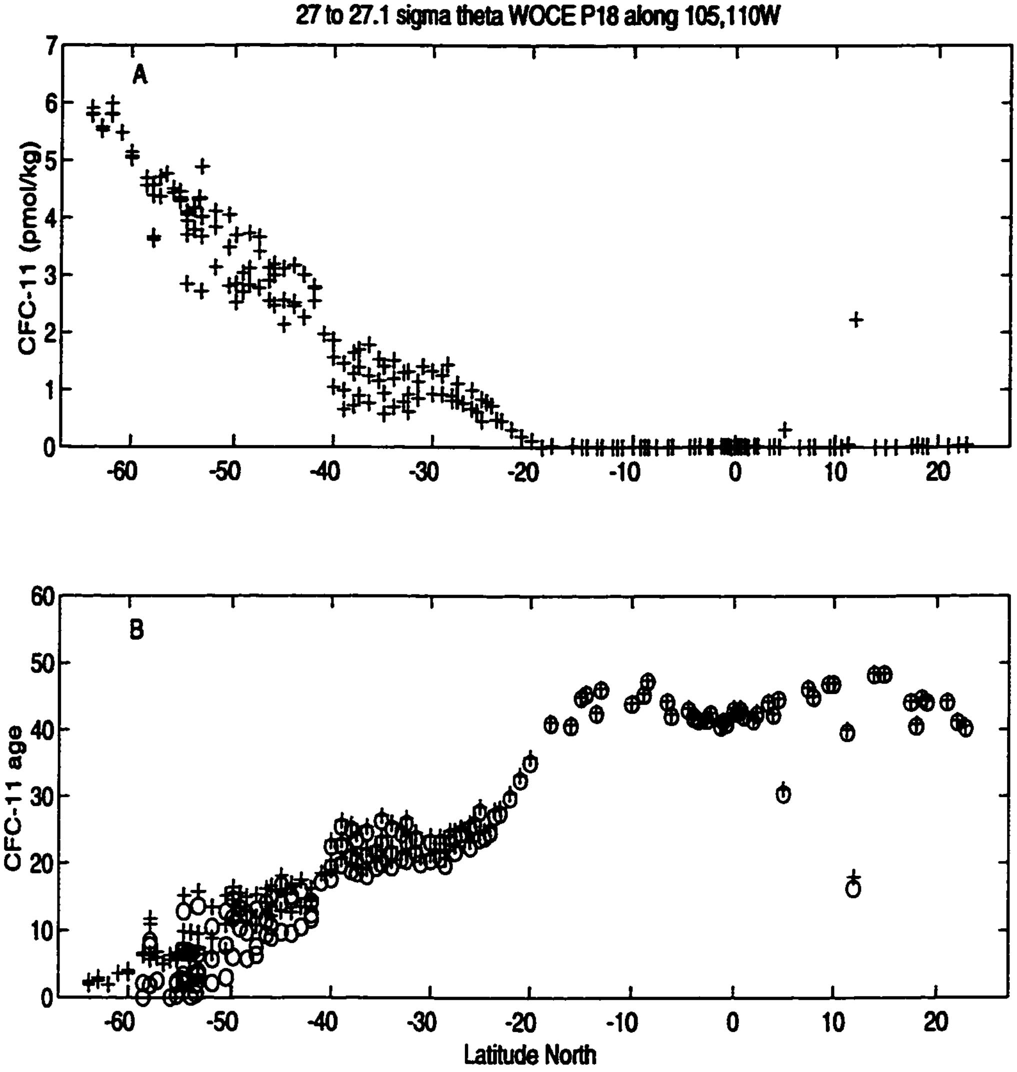

Figure 3.3. A) Distribution of CFC-11 within the isopycnal horizon 27.0-27.1 σ_θ measured during P18 along 105°W and 110°W in the Pacific Ocean in 1994. B) Ventilation ages calculated from CFC-11 concentrations and a reconstruction of the atmospheric CFC-11 history (Fig. 1.4, Walker et al., 1995) assuming that waters were either 100 % (+) or 86 % (o) saturated with respect to atmospheric CFC-11 during subduction.

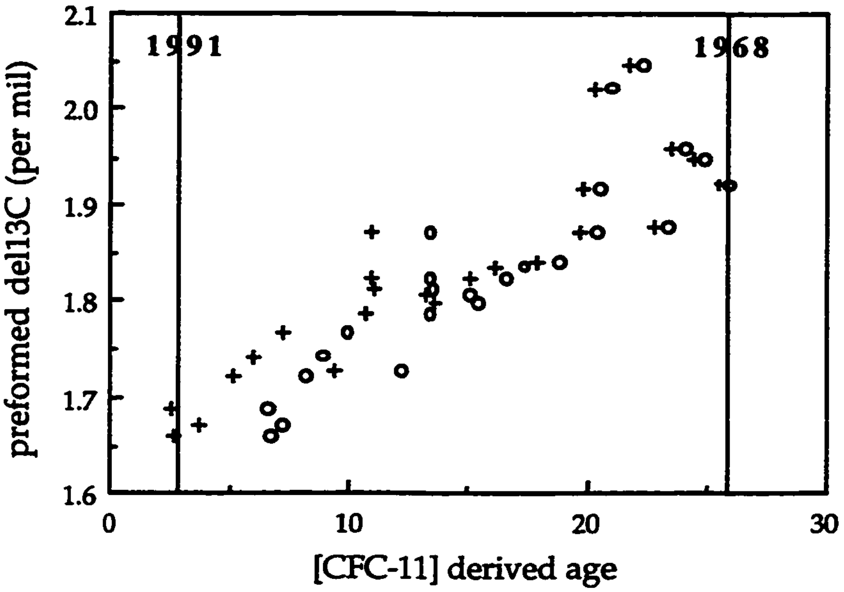

Figure 3.4. The trend in preformed $\delta^{13}C$ ($\delta^{13}C^{o}$) versus ages calculated from concurrent CFC-11 concentrations assuming either 100 % (o) or 86 % (+) CFC saturation during subduction on 27.0 to 27.1 σ_θ between 55°S and 27°S along 105°W using data collected during P18 in the Pacific Ocean. The $\delta^{13}C^{o}$ time rates of change between 1968-1991 are -0.15 ± 0.02 ‰ decade^{-1} and -0.13 ± 0.02 ‰ decade^{-1}, assuming 100 % and 86 % CFC saturation at the outcrop, respectively. The uncertainty reported is the standard error (± 1 σ) of the regression-derived slope.

region. The $\delta^{13}C^{o}$ versus age trends reported in this paper represent the average of the $\delta^{13}C^{o}$ versus CFC-11 age and CFC-12 age trends.

CFC ages are also susceptible to biases due to mixing. For mixing between waters outcropped between 1968 and 1991, when the CFC-11 and CFC-12 versus time trends in the atmosphere were roughly linear (Fig. 1.4), these effects are likely small (see chapter two). The nonlinear trend in atmospheric CFC-11 prior to 1968, however, causes the CFC-11 ages of mixtures of waters to be biased younger (Doney and Bullister, 1992), and would lead to an overestimate of the rate of the anthropogenic $\delta^{13}C^{\circ}$ changes. To avoid this bias, water samples with CFC derived formation dates prior to 1968 or after 1991 were generally, with three exceptions noted below, excluded from our analyses of the ^{13}C Suess effect.

Uncertainty in the time rate of $\delta^{13}C^{\circ}$ change

The uncertainty reported for the trend in $\delta^{13}C^{\circ}$ versus CFC age (Table 3.4) reflects the standard error ($\pm 1\ \sigma$) of the regression-derived slope of that trend. An alternate error analysis would calculate a distribution of regression-derived slopes based on a population of data sets randomly generated (bootstrapped) from the mean and $\pm 1\ \sigma$ uncertainty of each $\delta^{13}C$ and CFC age point. For example, the data shown in Fig. 3.4 coupled with the uncertainties listed in Table 3.2 and an assumed ± 2 year uncertainty in CFC-11 ages yield a $\delta^{13}C^{\circ}$ versus age trend calculated in this fashion of -0.13 ± 0.02 ‰ decade^{-1}. This error was the same as the regression derived error in the slope. In this study we report uncertainties calculated from the regression statistics because this error pertains to the likelihood that there is a $\delta^{13}C$ versus water age trend. The numerical bootstrap procedure, on the other hand, yields an uncertainty that depends primarily on AOU values (Table 3.2), and not on the scatter in the $\delta^{13}C$ versus age trend.

Additional uncertainties and assumptions

In the illustrative example calculation on 27.0 to 27.1 σ_θ along 105°W in the South Pacific Ocean (Fig. 3.2), we calculated $\delta^{13}C^{o}$ by integrating the relationship between the latitudinal trend of AOU on isopycnals and that of $\delta^{13}C_{POC}$ in the overlying surface waters. In doing so, we assumed that all of the in-situ oxygen consumption observed at depth was due to oxidation of particulate organic carbon raining down from overlying surface waters. Hansell and Waterhouse (1997) showed, based on dissolved organic carbon measurements along this section (P18), that the maximum amount of DOC consumed along this isopycnal between 55°S and 27°S was ≤ 5 µmol kg^{-1}. This DOC consumption represents 10 % of the total organic carbon remineralization and supported our assumption that the AOU observed was due to remineralization of particulate organic carbon from above. The assumption of *all* particulate remineralization leads to a slight (< 0.1 %) underestimate of the ^{13}C trends in this example. Also, we assumed that meridional gradients in AOU greatly exceed zonal gradients. The two-dimensional distribution of AOU on this isopycnal (Levitus and Boyer, 1994b) confirmed that zonal AOU gradients are much smaller than meridional gradients in this region on this isopycnal, and on the reconstructions we performed in the South Pacific and South Indian Oceans (Table 3.4).

The meridional distribution of alkalinity on 27.0 to 27.1 σ_θ measured during WOCE P18 along 105, 110°W showed no significant change in alkalinity from the outcrop (55°S) to 27°S (Fig. 3.5). The AOU change over the same area was about 65 µmol kg^{-1}, so the C added from $CaCO_3$ dissolution, which was not visible as an increase in alkalinity because this increase was titrated by the proton flux due to organic matter remineralization, can be calculated as $\frac{1}{2} \cdot AOU \cdot \left(\frac{N}{O_2}\right)_{org} \approx 3$ μmol kg^{-1} (equation 2). This compared to a calculated organic carbon addition of $AOU \cdot \left(\frac{C}{O_2}\right)_{org} \approx 45$ μmol kg^{-1}. The fact that $^{13}C/^{12}C$ fractionation and total C fluxes due to $CaCO_3$ dissolution were both very small in the relatively shallow waters considered in this study meant that the $CaCO_3$ dissolution C flux had very little impact on the $\delta^{13}C$ distributions. In other words, the trend in $\delta^{13}C^{\circ}$ versus CFC-11 age (Fig. 3.4) was not changed appreciably when $CaCO_3$ remineralization was included in the $\delta^{13}C^{\circ}$ calculations.

In regions where $\delta^{13}C^{\circ}$ changes along isopycnals, but salinity and "NO" do not, as in this example, $\delta^{13}C^{\circ}$ trends can be related to water ages based on transient tracer concentrations in a straight-forward fashion, as discussed above. However, uniform salinity and "NO" distributions are not always present on isopycnals. In these situations, biases due to mixing with waters with different $\delta^{13}C^{\circ}$ signatures must be considered. In a two or three end-member mixing scheme, one is tempted to use salinity and "NO" data to determine the influence of mixing on the calculated $\delta^{13}C^{\circ}$. A problem with this approach is that the temporal history of $\delta^{13}C^{\circ}$ in the end-members is usually unknown. This does not present a significant problem on deeper isopycnals, as these older water masses have usually experienced little anthropogenic disturbance, as evidenced by a lack of CFCs. However, for isopycnals where CFCs are present, i.e., ventilated within the last ~ 30 years, mixing among anthropogenically perturbed end-members likely occurs.

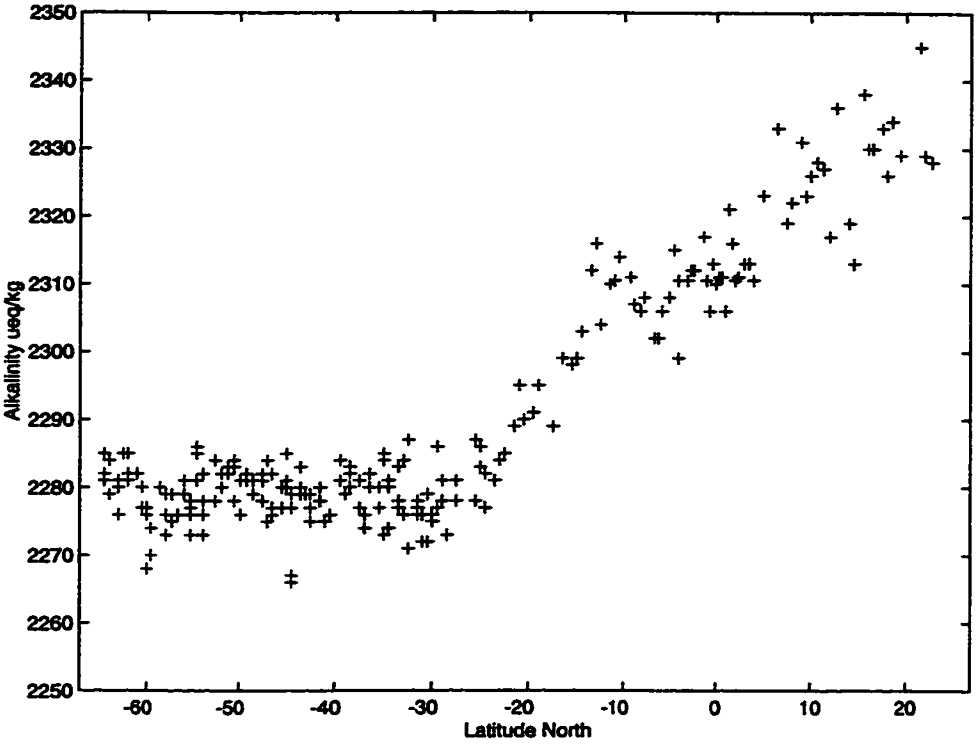

Figure 3.5. The meridional distribution of titration alkalinity on the isopycnal horizon 27.0-27.1 σ_θ measured during P18 along 105°W and 110°W in the Pacific Ocean.

Since we use CFCs to quantify the time rate of the ^{13}C changes, all of the Suess effect calculations presented in this paper are from isopycnal regions where salinity and "NO" were constant, e.g., between 27.0-27.1 σ_θ along P18 between 55°S and 27°S (Fig. 3.2), and no mixing corrections were applied. Many isopycnals were analyzed where anthropogenic ^{13}C signals were expected, based on detectable levels of CFCs, but could not be resolved from mixing effects. These situations are not included in the present analysis, although they likely bear a ^{13}C Suess effect.

In all of our calculations we assumed that ventilation of the permanent subtropical thermocline occurs predominantly in late winter (Stommel, 1979) by along-isopycnal processes. This assumption was supported by observations of major subsurface CFC maxima that were deeper than the local maximum winter mixed layer depth in the subtropical gyres of the North Pacific (Warner et al., 1996), North Atlantic (Doney and Bullister, 1992), South Indian and South Pacific (John Bullister, unpublished data) Oceans. Furthermore, we assumed that an isopycnal's outcrop exhibits no zonal trend in $\delta^{13}C$. We tested this by evaluating the $\delta^{13}C$ data from two meridional sections typically separated by 30° to 65° of longitude in the Indian and Pacific Oceans (e.g., WOCE P18 and P15 along 105°W and 170°W, respectively, in the South Pacific Ocean). Similar checks were not possible in the Atlantic Ocean. Finally, we assumed that "Redfield" ratios of remineralization and $\delta^{13}C_{org}$ values (Table 3.1) are independent of depth. Both Anderson and Sarmiento's (1994) and Shaffer et al.'s (1998) analysis of nutrient trends along neutral surfaces indicated little significant variability in the C/O_2 remineralization ratio with depth. Druffel et al. (1992) showed that in the open ocean the $\delta^{13}C$ of POC was independent of depth within the $\pm \sim 1.5$ ‰ uncertainties in $\delta^{13}C_{org}$ (Table 3.2).

Data

We analyzed the $\delta^{13}C$ of DIC and CFC measurements from three meridional sections each in the Pacific and Indian Oceans, and from one meridional section in the Atlantic Ocean (Fig. 3.6). The Pacific Ocean sections were occupied during the time period 1991-1994 as part of NOAA's Climate and Global Change (CGC) program. Along 105°W in the South Pacific we also used $\delta^{13}C$ of DIC and CFC data collected on 26.8 to 26.9 σ_θ during 1989 as part of NOAA's Radiatively Important Trace Species (RITS) program. The Atlantic and Indian Ocean sections were occupied during 1993-1996 as part of NOAA's Ocean Atmosphere Carbon Exchange Study (OACES) program. Five of these cruises were part of the WOCE hydrographic program (P13, P16N, P18, I8N and I8S/I9S). The cruise locations and dates are found in Table 3.3.

$\delta^{13}C$ of DIC were measured at the University of Washington's Stable Isotope Lab (UW) for the P13, P18, N. Atlantic 1993, I8N and I8S (Sept. 1995) cruises, and at the National Ocean Sciences AMS facility (NOSAMS) for the P16N, I8S (Dec. 1994) and I9S cruises. Sample collection and preparation procedures generally followed those described by Quay et al. (1992) with slight differences between labs. At the University of Washington, Helium was used as a stripping gas followed by $\delta^{13}C$ determination of the extracted CO_2 on a Finnigan MAT 251 isotope-ratio mass spectrometer (Quay et al., 1992). At NOSAMS the DIC samples were stripped of CO_2 in the original sample bottle using N_2 carrier gas. A split of the extracted CO_2 gas was either transferred directly to an isotope ratio mass spectrometer or stored in a flame-sealed tube for later stable isotope analysis (McNichol et al., 1994). NOSAMS $\delta^{13}C$ values were measured on three different instruments--a VG Prism in the Earth and Planetary Science Department at Harvard University, and on a VG Prism and a VG Optima at NOSAMS. Both laboratories report a measurement precision of ± 0.03 ‰ (1 σ) based on analyses of duplicate samples and standards. Based on 135 $\delta^{13}C$ measurements made at both the UW and NOSAMS labs of CO_2 gas extracted at UW the mean offset between the two labs was 0.01 ‰. Based on an informal exchange of DIC standards between the two labs, the $\delta^{13}C$

Table 3.3. Locations and dates of the cruise sections used in this study (see also Fig. 3.6).

Cruise Section	Location	Season and Year
N. Atlantic OACES/CO_2 (N. Atlantic '93)	5°S, 25°W to 63°N, 20°W	July-September 1993
NOAA Radiatively Important Trace Species 1989 (RITS '89)	14°N, 105°W to 61°S, 110°W	February-March 1989
Climate and Global Change '94 (CGC-94/WOCE P18)	67°S, 105°W to 23°N, 110°W	February-April 1994
CGC-92 (WOCE P13)	54°N, 162°E to 17°S, 163°E	August-September 1992
CGC-91 (WOCE P16N)	29°N, 155°W to 152°W, 53.5°N	February-April 1991
WOCE I8S	30°S, 95°E to 63°S, 82°E 43°S, 92°E to 33°S, 92°E	December 1994 September 1995
WOCE I9S	64°S, 111°E to 35°S, 115°E	January 1995
WOCE I8N	33°S, 80°E to 5°N, 80°E	October 1995

offset was 0.012 ± 0.012 ‰ (n=6). No offset correction was applied to the Atlantic and Pacific Ocean data because the $\delta^{13}C$ data were analyzed for spatial trends on individual cruise sections where all of the analyses were performed at one laboratory, so an inter-laboratory offset would have no effect on the calculated Suess effect. In the Indian Ocean, no significant (± 0.01 ‰) offset

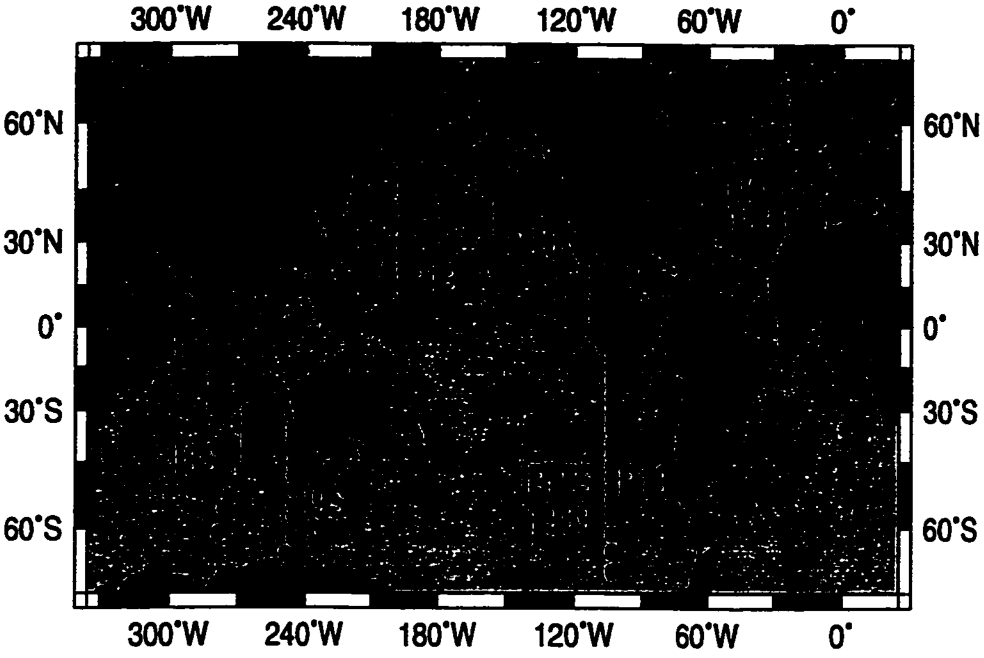

Figure 3.6. Map of the station locations where depth profiles of $\delta^{13}C$ of DIC were measured during the cruise sections (see Table 3.3).

was observed between a depth profile of $\delta^{13}C$ collected from one station (33°S, 95°E) analyzed at the University of Washington (sampled along I8S in Sept. 1995) and a previous occupation (I8S in Dec. 1994) analyzed at the National Ocean Sciences AMS facility. The accuracy of the $\delta^{13}C$ of DIC measurement was checked by comparing Na_2CO_3 solution standards to direct acidification of the solid Na_2CO_3: there was no significant offset (i.e., $< 0.01 \pm 0.05$ ‰, n=62) between the two values.

DIC concentrations from both manometric and coulometric determinations were used. At UW, the yields of the DIC extraction procedure averaged 99.47 ± 0.33 % based on a comparison of manometric measurements of the CO_2 extracted to the amount expected based on gravimetric measurement of Na_2CO_3 standards. The UW manometric DIC analyses exhibited a systematic offset from concurrent coulometric DIC measurements on all of the cruise sections included in this study. A constant DIC correction of 13.9, 10.1, 7.2 and 3.7 μmol kg^{-1} was added to the UW manometric DIC data from the N. Atlantic 1993, WOCE P13, P18 and I8S,N cruise sections, respectively. Although this correction increased each sample's DIC value, it had a negligible effect on $\delta^{13}C°$ versus age trends (< 0.001 ‰ $decade^{-1}$). The offset-corrected manometric DIC values agree within ± 5 μmol kg^{-1} (1 σ) with concurrent coulometric DIC determinations. When $\delta^{13}C$ of DIC values were determined at the NOSAMS facility, i.e., I8S (Dec. 1994), I9S and P16N we used the coulometric DIC values measured on these cruises by NOAA/PMEL (P16N, Slansky et al., 1997) and the U. S. Department of Energy (I8S (Dec. 1994) and I9S, Douglas Wallace, personal communication).

The shipboard dissolved CFC measurements were made by the group at NOAA/PMEL (John Bullister, personal communication), and generally had a detection limit of 0.005 to 0.01 pmol kg^{-1} for CFC-11 and 0.005 pmol kg^{-1} for CFC-12. The precision of the CFC-11 and CFC-12 measurements, based on analyses of replicate samples, was estimated to be 0.01 pmol kg^{-1} or 1 % of CFC concentration, whichever was greater. A full discussion of the CFC analytical techniques can be found in Bullister and Weiss (1988). All CFC values were adjusted to the SIO 1993 scale as outlined in Cunnold et al. (1994). The CFC saturation levels were calculated from gas solubility (Warner and Weiss, 1985) and time trends of atmospheric CFC concentrations supplied by Walker et al. (1995). In this reconstruction, the post-1981 atmospheric values were based on direct measurements, while the pre-1981 values were based on CFC production and emission estimates applied in a two-box model of the atmosphere (Walker et al., 1995). They estimated an uncertainty of < 3 % (1 σ)

in atmospheric CFC-11 and CFC-12 values reconstructed during the time period 1960-1981 which translated into an age uncertainty of < 0.5 years.

The oxygen values determined during the N. Atlantic 1993 cruise were systematically lower by 7.5 μmol kg^{-1} for the entire cruise compared to the same section occupied in 1988 (Oceanus 202, Tsuchiya and Talley, 1992). This systematic offset in O_2 has been observed on previous NOAA/AOML cruises (Castle et al., 1998), so the N. Atlantic 1993 oxygen data were adjusted by adding 7.5 μmol kg^{-1} to all values. No corrections were applied to the oxygen data from any other cruises.

Surface ocean ^{13}C Suess effect

Reconstructions of the δ^{13}C changes were made, using the approach described above, on four isopycnals in the North Pacific and North Atlantic Oceans, on five isopycnals in the South Pacific Ocean, and on three isopycnals in the South Indian Ocean (Table 3.4). The Suess effect from these sections were reconstructed on isopycnals which exhibited the following three characteristics: 1) a uniform water mass structure, diagnosed from "NO" (Broecker, 1974) and salinity, over an extensive meridional range. 2) CFC concentrations corresponding to atmospheric values between 1968 and 1991, except for three deeper isopycnals which maximize our spatial coverage and exhibited CFC ages as old as 1960 (Table 3.4). On these isopycnals, the time rate of change may be overestimated slightly due to non-linear mixing of CFC ages, as discussed above. 3) at least four δ^{13}C measurements within the region constrained by criteria 1 and 2.

Overall the reconstructed $\delta^{13}C$ Suess effect ranged from -0.07 to -0.23 ‰ decade^{-1} and averaged -0.15 ± 0.04 ‰ decade^{-1} (Table 3.4). Generally, the reconstructed $\delta^{13}C$ change was fastest on shallower isopycnals outcropping in subtropical regions and slowest on deeper isopycnals outcropping at higher latitudes. In the North Atlantic between 45° and ~60°N the time rate of change of $\delta^{13}C°$ ranged from -0.23 ± 0.06 ‰ decade^{-1} from ~800 - 1000 m down to -0.11 ± 0.04 ‰ decade^{-1} from ~1700 - 2200 m. The shallowest isopycnal layer, 27.2 to 27.4 σ_θ (~600 - 800 m), was just below the maximum depth of wintertime convection in this region (Levitus and Boyer, 1994a; Levitus et al., 1994) and showed a Suess effect of -0.18 ± 0.02 ‰ decade^{-1}. Since the deepest isopycnal reconstruction, on 36.9 to 37.0 σ_2, included only CFC dates from 1960-1978 the time rate of change may be overestimated on this surface due to nonlinear mixing of CFC ages, as discussed above. In the North Pacific, the along-isopycnal $\delta^{13}C°$ changes ranged from -0.17 to -0.21 ‰ decade^{-1} through the main thermocline between ~250 m (25.5 σ_θ) and ~650 m (26.8 σ_θ) with no significant depth variability and a typical uncertainty of ± 0.05 ‰ decade^{-1}. These $\delta^{13}C°$ rates of change were comparable to those in the N. Atlantic on isopycnals at < 1000 m depth.

In the South Pacific the isopycnal ^{13}C Suess effect was smaller than in the N. Atlantic and N. Pacific at equivalent depths. The $\delta^{13}C°$ time rate of change decreased from -0.15 ± 0.04 ‰ decade^{-1} on 26.8 to 26.9 σ_θ (~400 - 450 m depth along 105°W) to -0.07 ± 0.04 ‰ decade^{-1} on 27.2 to 27.4 σ_θ (~1000 - 1300 m). In the South Indian Ocean the $\delta^{13}C°$ time rates of change were comparable to those for the South Pacific, and decreased from -0.18 ± 0.07 ‰

decade^{-1} on 26.6 to 26.8 σ_θ (~350 - 600 m depth along 85°E) to -0.12 ± 0.03 ‰ decade^{-1} on 27.0 to 27.2 σ_θ (~800 - 1000 m).

The reconstructed $\delta^{13}C$ changes represent the time rate of change of $\delta^{13}C$ in the mixed layer at the isopycnals' outcropping regions because the calculations were performed in regions where only one water mass was evident in the salinity and "NO" distributions (Table 3.4). Since waters are subducted out of the mixed layer into the permanent thermocline in late winter only (Stommel, 1979), the isopycnal reconstructions represent the time history of surface $\delta^{13}C$ at the wintertime outcrop region. Thus the depth trend in the $\delta^{13}C$ time rate of change essentially translates into the meridional trend in the surface ocean Suess effect during wintertime.

The reconstructed surface ^{13}C Suess effect in each basin is slower at high latitudes (Fig. 3.7). In the Pacific Ocean these reconstructed $\delta^{13}C$ changes compared well to direct estimates of the Suess effect derived from the difference between two synoptic meridional sections of $\delta^{13}C$ in surface water measured in 1970 and 1993 (Figs. 3.7 and 3.8). In the North Pacific, the reconstructed changes also agree with direct measurements of the time rate of change of $\delta^{13}C$ of -0.2 ± 0.02 ‰ decade^{-1} (Paul Quay, unpublished data) at the HOT time series station near Hawaii (22°45' N, 158°W). The reconstructed meridional trend in the surface water $\delta^{13}C$ Suess effect in the South Indian

Table 4. The along-isopycnal $\delta^{13}C^{\circ}$ Suess effect for the North Atlantic, Pacific, and South Indian Oceans. The error reported represents $\pm 1\ \sigma$ of the regression of $\delta^{13}C^{\circ}$ versus CFC age, see text for discussion. The depth, temperature and salinity values reported for each potential density surface are the mean along the cruise section within the latitude ranges over which the Suess effect was evaluated. The latitude band represents the region of uniform "NO" and salinity, see text for discussion.

Density Interval	Depth (m)	T (°C)	S	Latitude Band	Number of $\delta^{13}C$ Samples	CFC Saturation at Outcrop (%)	Age Range Observed	Suess Effect (‰ decade^{-1})
North Atlantic Ocean (N. Atlantic 1993)								
27.2-27.4 σ_θ	600-800	10.3	35.51	25°N - 37°N	4	100	1969-1979	-0.18 ± 0.02
27.4-27.6 σ_θ	800-1000	7.1	35.12	45°N - 60°N	10	90	1973-1990	-0.23 ± 0.06
36.5-36.8 σ_2	1000-1400	5.7	35.06	45°N - 62°N	27	85	1973-1991	-0.13 ± 0.03
36.9-37.0 σ_2	1700-2200	4.2	34.98	45°N - 67°N	9	70	1960-1978	-0.11 ± 0.04
North Pacific Ocean (WOCE P13, P16N)								
25.5-26.0 σ_θ	250-350	14.6	34.60	16°N - 34.5°N	19	97	1978-1989	-0.20 ± 0.05
26.0-26.2 σ_θ	350-425	13.3	34.50	18°N - 38°N	8	95	1978-1988	-0.19 ± 0.04
26.2-26.6 σ_θ	425-575	9.2	34.17	20°N - 40°N	11	95	1973-1986	-0.21 ± 0.03
26.6-26.8 σ_θ	575-675	8.4	34.14	20°N - 40°N	5	89	1970-1976	-0.18 ± 0.07
South Pacific Ocean (RITS '89, WOCE P18)								
26.8-26.9 σ_θ	400-450	7.2	34.31	25°S - 45°S	4	90	1981-1989	-0.15 ± 0.04
26.9-27.0 σ_θ	450-500	6.4	34.31	30°S - 50°S	13	86	1975-1989	-0.14 ± 0.02
27.0-27.1 σ_θ	500-800	5.5	34.28	28°S - 55°S	23	86	1969-1991	-0.13 ± 0.02
27.1-27.2 σ_θ	800-1000	5.1	34.28	28°S - 57°S	10	81	1964-1979	-0.10 ± 0.02
27.2-27.4 σ_θ	1000-1300	3.6	34.33	30°S - 60°S	11	90	1960-1979	-0.07 ± 0.04
South Indian Ocean (WOCE I8S, I9S, I8N)								
26.6-26.8 σ_θ	350-600	11.2	35.0	35°S - 12°S	14	100	1984-1991	-0.18 ± 0.07
26.8-27.0 σ_θ	600-800	8.5	34.62	38°S - 15°S	16	100	1971-1989	-0.16 ± 0.03
27.0-27.2 σ_θ	800-1000	5.5	34.38	48°S - 30°S	12	90	1968-1982	-0.12 ± 0.03

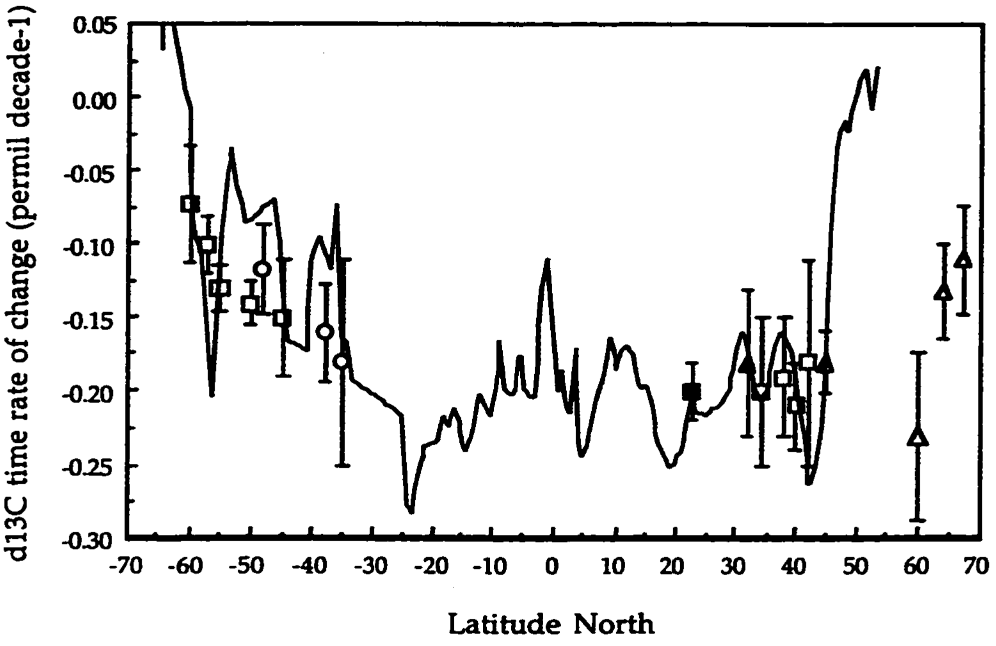

Figure 3.7. The reconstructed $\delta^{13}C$ Suess effect on thermocline isopycnals from the Pacific (□), Indian (o) and Atlantic (Δ) Oceans plotted against the latitude of the isopycnal's outcrop (see Fig. 3.6). The deepest isopycnals in the North Pacific and North Atlantic, which outcrop north of the cruise sections' northernmost stations, are plotted against their southernmost (wintertime) outcrop location estimated from sea surface σ_θ (Levitus et al., 1994, Levitus and Boyer, 1994a). Included for comparison are ^{13}C Suess effect estimates from time series of surface water $\delta^{13}C$ of DIC near Hawaii (■) (22°45' N, 158°W, Paul Quay, unpublished data) and near Bermuda (▲) (32°N, 64°30'W, Bacastow et al., 1996) and from the difference in surface water $\delta^{13}C$ values between two meridional sections occupied in April-June 1970 (Kroopnick et al., 1977) and again in March-April 1993 in the central Pacific Ocean (solid line; see Fig. 3.8).

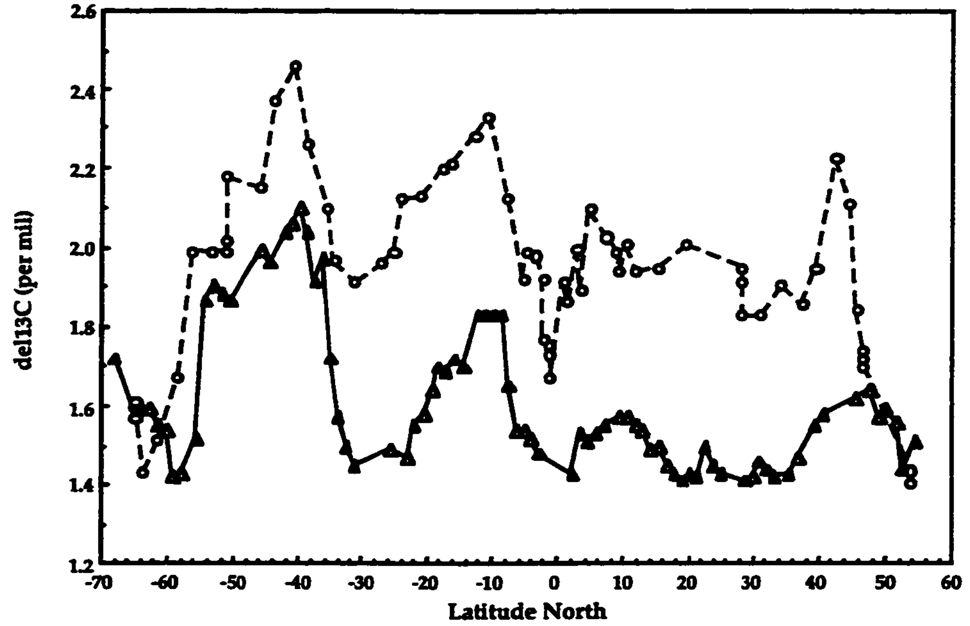

Figure 3.8. $\delta^{13}C$ of surface water DIC values measured along 150°W in April-June 1970 (o, Kroopnick et al., 1977) and along 140°W in March-April 1993 (Δ, Paul Quay, unpublished data).

Ocean is similar to that directly observed and reconstructed in the South Pacific Ocean. In the North Atlantic, the only available direct estimate for the surface ocean Suess effect after 1970 is the value of -0.18 ± 0.05 ‰ decade^{-1} measured at Bermuda (32°N, 64°30'W, Bacastow et al., 1996). Although our reconstructed surface $\delta^{13}C$ changes are from farther north (and east), the southernmost value agrees well with the trend at Bermuda (Fig. 3.7).

The magnitude and meridional trend in the reconstructed surface ocean $\delta^{13}C$ Suess effect was compared to an ocean general circulation model's predictions (Fig. 3.9). The Hamburg model predictions of $\delta^{13}C$ change (Bacastow et al., 1996, Fig. 9a) reproduce the observed meridional trend in $\delta^{13}C$ changes, i.e., higher in the subtropics than in subpolar regions. The model slightly overestimates the magnitude of the change in the southern hemisphere and slightly underestimates the changes in the northern hemisphere, however.

A closer examination of the Hamburg model predictions along 150°W (Bacastow et al., 1996, Fig. 9a) in the Pacific Ocean indicate fairly good agreement with the $\delta^{13}C$ changes determined from the difference between the surface water $\delta^{13}C$ measurements in 1970 and 1993 (Fig. 3.8). The average model-predicted change along 150°W between 65°S and 54°N was -0.18 ‰ decade^{-1}, which was larger than the average $\delta^{13}C$ change based on the section difference, -0.16 ‰ decade^{-1}. We use the results of this model versus observation comparison to globally extrapolate the observed $\delta^{13}C$ changes in the Pacific Ocean. The Hamburg model predicts a global surface ocean average $\delta^{13}C$ rate of change of -0.171 ‰ decade^{-1} between 1983 and 1995 (Bacastow et al., 1996). We estimate a global average surface ocean Suess effect between 1970 and 1993 of -0.15 ‰ decade^{-1} by scaling our observed surface $\delta^{13}C$ changes along 150°W by the factor -0.171/-0.18.

Based on the preformed $\delta^{13}C$ reconstructions (Table 3.4), the area-weighted mean surface ocean Suess effect from 47°S to 33°S and from 62°S to 42°S in the South Indian and South Pacific Oceans, respectively, and from

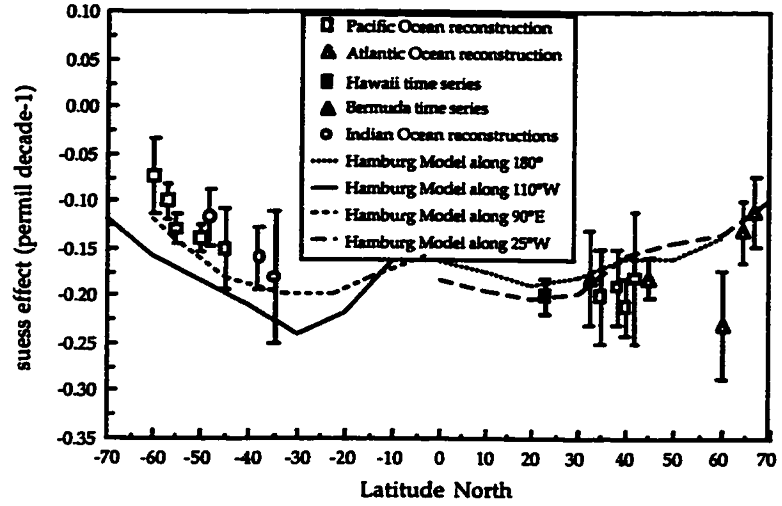

Figure 3.9. The reconstructed ^{13}C Suess effect from the Pacific (□), Indian (o) and Atlantic (Δ) Oceans plotted against the latitude of the isopycnal's outcrop on the cruise section where the reconstructions were performed (see Fig. 3.6) compared to that predicted along the same cruise sections (solid lines) during 1983-1993 using a Hamburg model simulation of the ocean carbon cycle (Bacastow et al., 1996, Fig. 9a).

34°N to 43°N and from 35°N to 70°N in the North Pacific and North Atlantic Oceans, respectively, was -0.15 ± 0.04 ‰ decade^{-1}. The Hamburg model simulation yielded a larger mean surface ocean Suess effect of -0.17 ‰ decade^{-1} over the same area (Bacastow et al., 1996, Fig. 9a), which equals the predicted global average change between 1983 and 1995. Because the areal and global mean model predicted $\delta^{13}C$ rates of change are the same, we estimate a global mean surface ocean Suess effect of -0.15 ± 0.04 ‰ decade^{-1} based on our reconstructions. In comparison, the measured $\delta^{13}C$ of atmospheric CO_2 decreased by 0.23 ‰ $decade^{-1}$ during the time period 1978-1988 (Keeling et al., 1989). The box-diffusion model simulation results of Bacastow et al. (1996) indicate that a global ocean $\delta^{13}C$ Suess effect of -0.15 ± 0.04 ‰ $decade^{-1}$ implies an ocean uptake rate of CO_2 of 2.5 ± 1.4 Gt. C yr^{-1} over the time period 1984-1993.

Depth-integrated ^{13}C Suess effect

Calculations of oceanic uptake of fossil-fuel CO_2 using Quay et al.'s (1992) atmospheric CO_2 and $^{13}CO_2$ budget approach and Heimann and Maier-Reimer's (1996) "dynamic constraint" method depend primarily on an accurate estimate of the global depth-integrated oceanic $\delta^{13}C$ change, or $\int\Delta\delta^{13}C$. Quay et al. (1992) used the correlation between observed $\int\Delta\delta^{13}C$ and bomb ^{14}C inventories ($\int\Delta\Delta^{14}C$) at the seven Pacific Ocean stations available at the time to extrapolate to a global $\int\Delta\delta^{13}C$ value. Heimann and Maier-Reimer (1996), however, have shown that the bomb ^{14}C perturbation in the 1970s and the ^{13}C perturbations between 1970 and 1990 are not well correlated in OGCM simulations. The lack of direct station comparisons and, to a lesser degree, possible calibration offsets and seasonal aliasing of the $\delta^{13}C$ change, limit the potential of this approach.

To increase the oceanic coverage of the depth-integrated $\delta^{13}C$ change, we integrated the isopycnal $\delta^{13}C$ Suess effect reconstructions (Table 3.4) with respect to depth and compared them to previous station-to-station depth profile comparisons (Fig. 3.10). On all isopycnals, the reconstructed time rate of change of $\delta^{13}C$ was assumed to be zonally homogeneous and integrated basinwide. In the North Pacific, $\delta^{13}C^{\circ}$ reconstructions were performed within the density range 25.5 to 26.8 σ_θ between 20°N and 40°N (Table 3.4). To estimate the total depth-integrated change, we assumed the surface water $\delta^{13}C$ Suess effect of 0.2 ± 0.02 ‰ decade^{-1} observed at the time-series site near Hawaii (22°45'N, 158°W, Paul Quay, unpublished data) applied within the subtropical latitudes from the surface down to 25.5 σ_θ, i.e., from the surface to a maximum of 250 m. This assumption had no significant effect on the depth-integrated $\delta^{13}C^{\circ}$ change because the shallowest reconstruction in the North Pacific agrees well with the directly measured change near Hawaii. The underlying isopycnal reconstructions were integrated by isopycnal volumes down to 26.8 σ_θ (maximum depth ~ 800 m). In the North Atlantic the ^{13}C Suess effect was depth-integrated in two regions. Between 25°N and 35°N the time rate of $\delta^{13}C$ change of 0.18 ± 0.05 ‰ decade^{-1} observed at Bermuda (Bacastow et al., 1996) was assumed to apply from the mixed layer down to 27.2 σ_θ (~600 m), as discussed above, and the four isopycnal reconstructions were integrated below. For the surface layer between 45°N and 50°N we used the Suess effect reconstructed at individual isopycnal outcrops along 25°W and integrated the isopycnal $\delta^{13}C^{\circ}$ versus age trends below.

In the South Pacific and South Indian Oceans, we depth-integrated the ^{13}C Suess effect from 40°S to 50°S and from 35°S to 45°S, respectively. For the surface layer we used the Suess effect reconstructed at individual isopycnal outcrops along 105°W in the Pacific Ocean and along 95°E and 115°E in the Indian Ocean (Figs. 3.6 and 3.7). The $\delta^{13}C^{\circ}$ changes on individual isopycnals were integrated down to 27.4 σ_θ (~1300 m) in the South Pacific Ocean and 27.2 σ_θ (~1000 m) in the South Indian Ocean. In all basins there were detectable levels of CFCs observed deeper than the deepest isopycnal $\delta^{13}C$ reconstructions. These waters likely bore Suess effects which were not reconstructed here because either we could not isolate the Suess effect from mixing's effects on $\delta^{13}C^{\circ}$ distributions, or the CFC content was too low for the waters to be confidently dated. Thus, our depth-integrations likely represent an underestimate of the total change in $\delta^{13}C$.

In the Pacific Ocean, the reconstructed depth-integrated $\delta^{13}C$ change generally agreed well with the station-to-station "snapshot" comparisons made previously (Quay et al., 1992) at similar latitudes (Fig. 3.10). In the South Indian and North Atlantic Oceans the depth-integrated $\delta^{13}C^{\circ}$ and bomb ^{14}C changes were higher than in the Pacific Ocean, with the greatest integrated changes occurring in the North Atlantic (Fig. 3.10). If we weight the basinwide integrated reconstructions equally with the single station comparisons (reoccupations), then a regression-derived trend of $\Delta\delta^{13}C$ (‰ m decade^{-1}) = -8.8 - 11.0 $\Delta\Delta^{14}C$ (10^9 atoms cm^{-2}) is determined, where $\Delta\Delta^{14}C$ represents the bomb ^{14}C inventory determined during GEOSECS (Broecker et al., 1985). The slope is slightly steeper than that based on the seven station reoccupations only ($\Delta^{13}C$ (‰ m decade^{-1}) = -27.9 - 9.1 $\Delta\Delta^{14}C$ (10^9 atoms cm^{-2}), Quay et al., 1992), primarily due to the inclusion of the North Atlantic reconstructions.

A global ocean average depth-integrated $\delta^{13}C$ Suess effect of -10.2 ± 2.6 ‰ m yr^{-1} is determined by applying the ocean wide average bomb ^{14}C

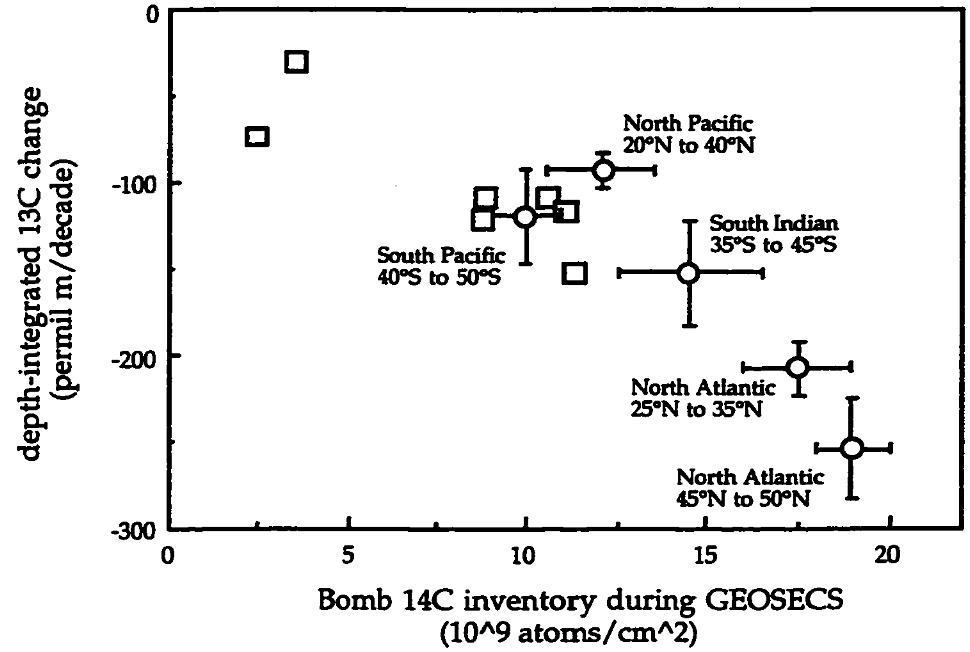

Figure 3.10. Depth integrated $\delta^{13}C$ change (‰ m decade^{-1}) between ~1970 and 1990 versus integrated bomb ^{14}C inventory measured during GEOSECS (Broecker et al., 1985) for station-to-station comparisons in the Pacific Ocean (□, Quay et al., 1992), and from depth-integrating the isopcynal $\delta^{13}C$ changes reconstructed from $\delta^{13}C°$ versus CFC age trends (o). The uncertainties (± 1 sd) in the reconstructed changes represent the depth-integrated errors in the Suess effect (Table 3.4) and the scatter in the bomb ^{14}C inventories over the integration areas outlined in the text.

inventory of 8.4 x 10^9 atoms cm^{-2} measured during GEOSECS (Broecker et al., 1985) to the regression relationship above. Quay et al. (1992) derived a similar rate of -10.4 ± 2.3 ‰ m yr^{-1} when only the 7 stations from the Pacific Ocean were used. The errors reported reflect uncertainties in the regression only.

Table 3.5. Global carbon cycle parameters used to derive an oceanic CO_2 uptake rate from atmospheric $^{13}CO_2$ and $^{12}CO_2$ budgets following the approach of Quay et al. (1992). All values, except our estimated depth-integrated oceanic $\delta^{13}CO_2$ change, are from Heimann and Maier-Reimer (1996).

Carbon Cycle Parameter 1970-1990	Value
Atmospheric CO_2 inventory	715 ± 7 Gt. C
Change in atmospheric CO_2 inventory	60 ± 6 Gt. C
$\delta^{13}C$ of atmospheric CO_2	-7.55 ± 0.1 ‰
Change in $\delta^{13}C$ of atmospheric CO_2	-0.4 ± 0.2 ‰
$\delta^{13}C$ of anthropogenic CO_2 source	-28.1± 0.5 ‰
$\delta^{13}C$ of oceanic dissolved inorganic carbon (DIC)	1.8 ± 0.5 ‰
Depth-integrated change of oceanic $\delta^{13}C$ of DIC	-204 ± 52 ‰ m
Suess effect in the terrestrial biosphere	-18 ± 12 Gt. C ‰ yr^{-1}

To determine an oceanic CO_2 uptake rate we used our estimate of the depth-integrated oceanic ^{13}C Suess effect in the atmosphere-ocean-terrestrial biosphere budgets of $^{12}CO_2$ and $^{13}CO_2$ developed by Quay et al. (1992). Using the carbon cycle parameters (Table 3.5) of Heimann and Maier-Reimer (1996), this implies an oceanic CO_2 uptake rate of 2.0 ± 0.9 Gt. C yr^{-1} during the time period ~1970 - 1990, very similar to the rate of 2.1 ± 0.8 Gt. C yr^{-1} derived by Quay et al. (1992), and the IPCC estimate of 2.0 ± 0.8 Gt. C yr^{-1} (Houghton et al., 1995), and slightly larger than Keeling et al.'s (1996) estimate of 1.7 ± 0.9 Gt. C yr^{-1} based on secular changes in atmospheric O_2 concentrations during 1991-1994. A slightly greater oceanic CO_2 uptake rate of ~ 2.7 ± 1 Gt. C yr^{-1} is calculated using our integrated time rate of change of $\delta^{13}C$ and Heimann and Maier-Reimer's (1996) "dynamic constraint" method.

Discussion

Reconstructed surface $\delta^{13}C$ changes based on the calculated preformed $\delta^{13}C$ distributions agree well with direct measurements of the $\delta^{13}C$ change in the Pacific. The agreement provides support for both methods which rely on considerable, but unrelated, assumptions with corresponding uncertainties. Furthermore, the agreement provides confidence in both the surface and depth-integrated ^{13}C reconstructions made for the Atlantic and Indian Oceans, where there were no direct measurements of the oceanic ^{13}C Suess effect. The reconstructed depth-integrated $\delta^{13}C$ change in the Atlantic, Indian and Pacific Oceans support the global $\int\Delta\delta^{13}C$ value determined by Quay et al. (1992) using only a handful of Pacific Ocean station comparisons.

Based on our reconstructed ^{13}C changes, the global mean penetration depth of the ^{13}C perturbation, defined as the depth-integrated ^{13}C change divided by the average surface change, was 680 ± 250 m. Although our estimate is deeper than the 520 ± 110 m reported by Quay et al. (1992), the uncertainties in both estimates are substantial. Broecker and Peng (1983) estimated a ^{13}C perturbation penetration depth of 570 m by adjusting the global mean GEOSECS bomb ^{14}C penetration depth of 360 m (Broecker et al., 1985) for the longer time history of the atmospheric ^{13}C perturbation. Using Broecker et al.'s (1995) redetermination of the average GEOSECS bomb ^{14}C penetration depth, 391 m, results in an estimated ^{13}C perturbation penetration depth of 620 m, in rough agreement with our estimate.

Most of the uncertainty (69 %) in the fossil-fuel CO_2 uptake rate of 2.0 ± 0.9 Gt. C yr^{-1} calculated from the oceanic $\delta^{13}C$ change stems from the ± 26 % uncertainty in the global $\int\Delta\delta^{13}C$ value (Table 3.5). The primary source of uncertainty in the global $\int\Delta\delta^{13}C$ value, in turn, stems from uncertainty in the global ocean's $\int\Delta\delta^{13}C$ versus $\int\Delta\Delta^{14}C$ relationship (Fig. 3.10). The correlation between anthropogenic ^{13}C and ^{14}C changes determined using WOCE instead of GEOSECS ^{14}C measurements would likely improve the situation because the time-scale of bomb-^{14}C penetration into the ocean in the 1990s is close to the time constant of the evolution of the ^{13}C signal in the atmosphere, i.e., ~ 30 years. An improved determination of the $\int\Delta\delta^{13}C$ versus $\int\Delta\Delta^{14}C$ relationship, therefore, awaits a redetermination of the global ocean $\int\Delta\Delta^{14}C$ using WOCE ^{14}C data.

The best estimate of depth-integrated oceanic ^{13}C changes will likely be derived from global coverage of the $\delta^{13}C$ changes alone and won't rely on an oceanic $\int\Delta\delta^{13}C$ to $\int\Delta\Delta^{14}C$ relationship. Since high quality $\delta^{13}C$ data from the past is limited, in many regions the only available estimates of the ^{13}C change are reconstructions like those presented in this paper. However, these reconstructions are currently limited geographically due to their sensitivity to mixing biases and have not, for example, been attempted in tropical waters. As a result, the reconstructed depth-integrated ^{13}C changes derived to date are biased towards the subtropical regions which exhibit higher than average depth-integrated ^{13}C (and ^{14}C) changes (Broecker et al., 1985). Therefore, we still rely on the observed $\int\Delta\Delta^{14}C$ to obtain the best global $\int\Delta\delta^{13}C$ estimate. Combining our $\delta^{13}C°$ reconstructions with analogous reconstructions of changes in preformed DIC (Gruber, 1998) and bomb ^{14}C inventories (Broecker et al., 1995), both along isopycnals and depth integrated over specific oceanic regions, will yield estimates of the relations among the anthropogenic $^{13}CO_2$, $^{14}CO_2$ and $^{12}CO_2$ oceanic perturbations. These relations potentially provide useful information on surface-to-deep ocean exchange times, gas-exchange equilibration rates, terrestrial biota turnover times (Keir et al., 1998), and powerful constraints on model based simulations of oceanic CO_2 uptake.

Chapter 4 : The Indian Ocean ^{13}C Suess effect

Introduction

The oceanic ^{13}C Suess effect, defined as the decrease in the $\delta^{13}C$ of oceanic dissolved inorganic carbon (DIC) due to addition of relatively ^{13}C depleted anthropogenic CO_2 (Broecker and Peng, 1982), has recently attracted interest because it provides a means for estimating the ocean's uptake rate of fossil-fuel CO_2 (Quay et al., 1992; Heimann and Maier-Reimer, 1996; Bacastow et al., 1996). In addition, the oceanic ^{13}C Suess effect is potentially a constraint on the magnitude of gross carbon exchange fluxes between the atmosphere and terrestrial biosphere (Broecker and Peng, 1993; Keir et al., 1998). However, determination of oceanic $\delta^{13}C$ changes has been difficult due to scarcity of oceanic $\delta^{13}C$ data from the past (Quay et al., 1992).

The most direct means of determining the oceanic ^{13}C Suess effect is from time series' of $\delta^{13}C$ of DIC, which have been available at two locations. The $\delta^{13}C$ time series at Bermuda (32°N, 64°30'N) shows considerable (~ 0.2 ‰) seasonal variability and a time rate of change of surface water $\delta^{13}C$ of DIC over ten years (1983-1993) of -0.22 ± 0.02 ‰ decade^{-1} (Bacastow et al., 1996). The Bermuda data also showed some interannual variability in temperature that biased the $\delta^{13}C$ time rate of change calculation above. Bacastow et al. (1996) removed the effects of this variability using $\delta^{13}C$ correlations with temperature to derive a Suess effect estimate of -0.18 ± 0.05 ‰ decade^{-1} over the time period 1983-1993. Quay (unpublished data) found a similar time rate of change of surface water $\delta^{13}C$ at the HOT time series station ALOHA (24°45'N, 158°W), -0.2 ± 0.02 ‰ decade^{-1} during 1991-1998. Analyses of the $\delta^{13}C$ of aragonite incorporated into a sclerosponge at Jamaica (18°N, 78°W in the Caribbean) imply that local surface water $\delta^{13}C$ of DIC values decreased by 0.4 to 0.5 ‰ during ~1910-1970 (Druffel and Benavides, 1986; Böhm et al., 1996), and that the $\delta^{13}C$ decrease rate during 1970-1990 was about -0.18 ‰ decade^{-1} (Böhm et al., 1996).

Another way to estimate the oceanic ^{13}C Suess effect is to compare $\delta^{13}C$ of DIC data from cruises sufficiently far apart in time to resolve relatively small long-term $\delta^{13}C$ changes (the Suess effect) from seasonal and interannual variability. This approach has afforded rough estimates of the ^{13}C Suess effect in the Pacific (Quay et al., 1992; chapter three) and Indian (P. Quay, unpublished data) Oceans. However, the approach potentially suffers due to aliasing of seasonal, spatial and interannual variability in $\delta^{13}C$, and is sensitive to long-term changes in circulation and biological remineralization rates. Nevertheless, it provides greater geographical coverage than do time series data, and thus has provided information on the meridional and depth distribution of the oceanic ^{13}C Suess effect (e.g., Quay et al., 1992). Because there were analytical problems with the GEOSECS Atlantic and Pacific Ocean $\delta^{13}C$ of DIC data (Kroopnick, 1985), this approach is currently limited to comparisons of modern day $\delta^{13}C$ data to the 1978 GEOSECS Indian Ocean $\delta^{13}C$ data (Kroopnick, 1985), and to a few early 1970s cruises in the Pacific Ocean, e.g., HUDSON 1970 (Kroopnick et al., 1977) and ANTIPODES, SCAN and TOW in 1970-1971 (Kroopnick et al., 1974).

In chapter three we attempted to reconstruct the oceanic ^{13}C Suess effect by calculating preformed $\delta^{13}C$ ($\delta^{13}C$ corrected for biological cycling) trends in modern $\delta^{13}C$ data. We quantified temporal changes in $\delta^{13}C$ along isopycnals using water ages calculated from concurrent chlorofluorocarbon (CFC) measurements. The calculated along isopycnal $\delta^{13}C$ changes are not sensitive to seasonal cycles in surface ocean $\delta^{13}C$. Because this method accounts for organic matter remineralization at depth using AOU, it is not sensitive to possible long term changes in in-situ metabolic rates. Since the temporal changes are calculated from in-situ CFC measurements, changes in oceanic circulation rates are implicitly accounted for. Most importantly, the preformed method does not rely on data from the past, so it was possible to estimate the Suess effect in the North Atlantic and South Indian Oceans as well as in the Pacific Ocean. However, uncertainties due to mixing biases and reliance on CFC or other (^{3}H-^{3}He) dating techniques limit the geographic, depth and time range over which this approach can be reliably applied (see chapter three).

In this chapter we assess the $\delta^{13}C$ Suess effect in the Indian Ocean using a time-series multiparameter linear regression (MLR) approach that is analogous to that used previously to calculate the magnitude of the oceanic DIC change (Wallace, 1995; Slansky et al., 1997). The approach involves comparing $\delta^{13}C$ of DIC data from stations reoccupied 15-20 years apart in time. It uses $\delta^{13}C$ correlations with steady-state nutrient and hydrographic data at one time to predict, based on later nutrient and hydrographic data, $\delta^{13}C$ of DIC values at a later time. To estimate the temporal $\delta^{13}C$ change, these predictions are then compared to analogous predictions based only on later

$\delta^{13}C$ measurements and nutrient and hydrographic data. The MLR approach accounts for biases due to spatial variability of $\delta^{13}C$ and due to temporal (seasonal and interannual) variability in water mass ventilation and biological metabolic rates to the extent that such variability is reflected in differences in the nutrient and hydrographic data sets.

Our application of the MLR approach assumes that oceanic uptake of anthropogenic CO_2 is an abiotic process which affects only the DIC content and the $\delta^{13}C$ of DIC in seawater, while the overall temperature, salinity, oxygen, nutrient and alkalinity distributions in the ocean have not changed. The several steps in the approach are described as follows: 1) We derive an empirical equation, using multiple linear regression, that relates the $\delta^{13}C$ content of waters measured during GEOSECS to the nutrient and hydrographic parameters measured in those same samples:

$$\delta^{13}C = f\{\theta, S, O_2, PO_4, NO_3, NO_2, SiO_3, AOU, ALK\} + \mathrm{E} \tag{4.1}$$

Here the error in the MLR fit to the data is expressed as a residual, E, for each value. 2. A second MLR relationship is derived that fits a modern-day (e.g., WOCE in the 1990s) $\delta^{13}C$, hydrographic and nutrient data set. 3. The GEOSECS-era MLR equation is used to calculate, based on the WOCE (1990s) hydrographic and nutrient data, a hypothetical $\delta^{13}C$ distribution that would have been measured in the 1990s in the absence of any anthropogenic disturbance. 4. Finally, the magnitude of the anthropogenic $\delta^{13}C$ change (the Suess effect) is calculated from the difference between the $\delta^{13}C$ distributions predicted by the GEOSECS MLR equation and the WOCE MLR equation when both are using WOCE hydrographic and nutrient data in the right hand side of equation (4.1). We use this approach to determine the surface and depth-integrated $\delta^{13}C$ Suess effect in the Indian Ocean, and compare our results with direct station-to-station $\delta^{13}C$ difference calculations, as described above, with preformed $\delta^{13}C$ versus CFC age reconstructions, and with an ocean general circulation model's predictions. Finally, using existing modeling (Bacastow et al., 1996) and budgeting (Quay et al., 1992; Heimann and Maier-Reimer, 1996) approaches, we use our Suess effect estimates to calculate the global ocean's CO_2 uptake rate.

Data

In this study, we apply the MLR approach to $\delta^{13}C$ of DIC data collected in the Indian Ocean during the 1994-1995 WOCE legs I8N along 80°E, I8S along 80°E to 90°E and I9S along 115°E and to GEOSECS $\delta^{13}C$ of DIC data collected in the Indian Ocean during 1978 (Kroopnick, 1985; Fig. 4.1). For the predictive variables (right hand side of equation 4.1), we used potential temperature, salinity, oxygen and phosphate data collected from the same bottles. Possible calibration offsets between GEOSECS and WOCE in the $\delta^{13}C$ and predictive variables data were corrected by subtracting an overall offset between the residuals from the GEOSECS and WOCE MLR predictions in deep waters where no Suess effect was expected based on unmeasurable levels of CFCs, as discussed below. We also make a few direct (station-to-station) comparisons of the $\delta^{13}C$ change between GEOSECS and WOCE. For these comparisons we included $\delta^{13}C$ of DIC data collected during the WOCE I7N repeat section collected along 55°E during March-April 1995 (Fig. 4.1).

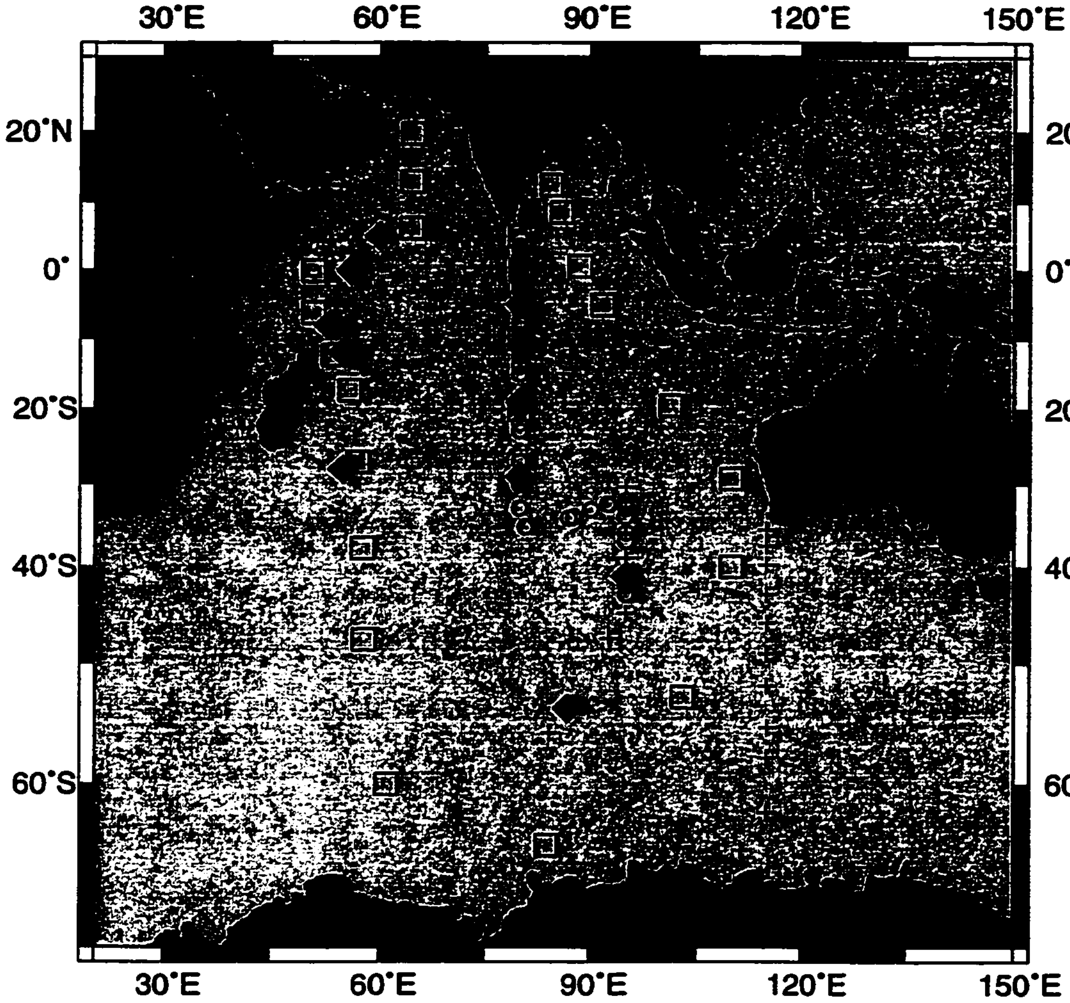

Figure 4.1. Locations where $\delta^{13}C$ of DIC with corresponding θ, S, O_2, PO_4 and AOU measurements were collected during the 1978 GEOSECS expedition (□), the WOCE I8S (Sept. 1995) and I8N sections (o) and the I8S (Dec. 1994) and I9S (+) sections during 1994-1995. Locations where depth profiles of $\delta^{13}C$ of DIC collected during WOCE I7N (along 50°E to 60°E) and WOCE I8N/S (along 80°E and 115°E) were compared to the closest GEOSECS depth profiles of $\delta^{13}C$ of DIC are included (◆).

The GEOSECS $\delta^{13}C$ of DIC data set has been described by Kroopnick (1985). $\delta^{13}C$ of DIC were measured at the University of Washington's Stable Isotope Lab (UW) for the I8N, I8S (Sept. 1995) and I7N cruises, and at the National Ocean Sciences AMS facility (NOSAMS) for the I8S (Dec. 1994) and I9S cruises. Sample collection and preparation procedures generally followed those described by Quay et al. (1992) with slight differences between labs. At the University of Washington, Helium was used as a stripping gas followed by $\delta^{13}C$ determination of the extracted CO_2 on a Finnigan MAT 251 isotope-ratio mass spectrometer (Quay et al., 1992). At NOSAMS the DIC samples were stripped of CO_2 in the original sample bottle using N_2 carrier gas. A split of the extracted CO_2 gas was either transferred directly to an isotope ratio mass spectrometer or stored in a flame-sealed tube for later stable isotope analysis (McNichol et al., 1994). NOSAMS $\delta^{13}C$ values were measured on two different instruments--a VG Prism and a VG Optima at NOSAMS. Both laboratories report a measurement precision of ± 0.03 ‰ (1 σ) based on analyses of duplicate samples and standards. Based on 135 $\delta^{13}C$ measurements made at both the UW and NOSAMS labs of CO_2 gas extracted at UW the mean offset between the two labs was 0.01 ‰. Based on an informal exchange of DIC standards between the two labs, the $\delta^{13}C$ offset was 0.012 ± 0.012 ‰ (n=6). In the Indian Ocean, however, no significant (± 0.01 ‰) offset was observed between a depth profile of $\delta^{13}C$ collected from one station (33°S, 95°E) analyzed at the University of Washington (sampled along I8S in Sept. 1995) and a previous occupation (I8S in Dec. 1994) analyzed at the National Ocean Sciences AMS facility.

Deriving the predictive equation

Our first task was to find the combination of hydrographic and nutrient data that, when included as predictive variables in the MLR, provided the most accurate predictions of the $\delta^{13}C$ distributions, as defined by minimizing the ± 1 σ scatter in the residual terms, i.e., E in equation 4.1. To accomplish this, we tested all random combinations of variables in any number selecting from among θ, S, O_2, NO_3, NO_2, PO_4, SiO_3, ALK and AOU. For the GEOSECS and WOCE $\delta^{13}C$ distributions, the variable set that provided the most accurate predictions and where each variable contributed significantly to the $\delta^{13}C$ prediction, as discussed below, was θ, S, O_2, PO_4 and AOU:

$$\delta^{13}C = \beta + m_1 \cdot \theta + m_2 \cdot S + m_3 \cdot O_2 + m_4 \cdot PO_4 + m_5 \cdot AOU + \mathrm{E} \tag{4.2}$$

where β represents the intercept term, m_1 through m_5 represent the regression coefficients for each predictive variable, and E represents the regression's residual or error terms, defined as the measured minus predicted value for each data point. Using the GEOSECS Indian Ocean nutrient and hydrographic data, equation 2 predicted the GEOSECS $\delta^{13}C$ distribution, on average, to within ± 0.07 ‰ (Fig. 4.2), about twice the measurement precision. DIC slightly improved the MLR equation's predictive ability, but was not included as a predictive variable because oceanic DIC concentrations have likely changed since GEOSECS.

Coefficients of partial determination, calculated as the fractional increase in the sum of the squares of the residual terms when a predictive variable is omitted, indicated that AOU, O_2 and θ provided the most predictive power, while inclusion of PO_4 and S contributed the least predictive power (Table 4.1). However, calculated partial F-ratios (Frees, 1996; Slansky et al., 1997) of determination indicated that inclusion PO_4 and S caused a significant improvement in the GEOSECS and WOCE predictions. Thus we used all five variables θ, S, O_2, PO_4 and AOU as predictive variables. The predictive variables, however, are not independent. O_2, AOU and PO_4, for example, covary strongly.

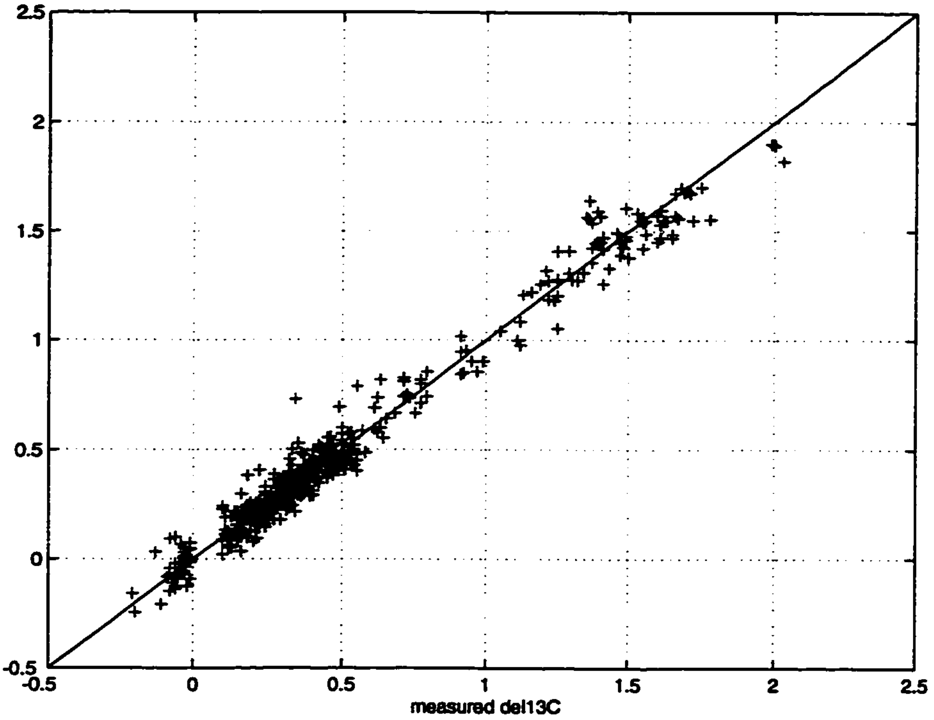

Figure 4.2. $\delta^{13}C$ (‰) predicted from the MLR equation using GEOSECS θ, S, O_2, PO_4 and AOU plotted against concurrent GEOSECS $\delta^{13}C$ measurements. The predicted data's 1 σ scatter about the 1:1 correlation line is ± 0.07 ‰.

Table 4.1. Least squares coefficients of $\delta^{13}C$ versus hydrographic and nutrient data determined from the 1978 GEOSECS and the 1994-1995 WOCE I8N, I8S and I9S cruises in the Indian Ocean. The a-priori coefficients represent calculations of $\delta^{13}C$'s dependence on equilibrium gas-exchange temperature dependence for θ and O_2, and on organic matter cycling for PO_4, O_2 and AOU (see text for discussion). The individual regression results represent coefficients from regressions of individual predictive variables alone against $\delta^{13}C$.

Predictive Variable	A-Priori Slope	GEOSECS individual regression slope	GEOSECS MLR slope $1\sigma=0.0709$ intercept=12.65 $r^2 = 0.98$	GEOSECS coefficient of partial determination	WOCE Individual Regression Slope	WOCE MLR slope $1\sigma=0.1137$ intercept=9.978 $r^2 = 0.94$	WOCE coefficient of partial determination
AOU	-0.0062 ‰ $\mu mol^{-1}\ kg^{-1}$	-0.0069	-0.0282	0.76	-0.0058	-0.0243	0.5765
O_2	0.0062 to 0.0191 ‰ $\mu mol^{-1}\ kg^{-1}$	0.0041	-0.0199	0.69	0.0056	-0.0162	0.467
θ	-0.105 ‰ °C^{-1}	0.037	-0.0926	0.57	0.034	-0.0713	0.3055
S	--	-0.14	-0.1351	0.12	0.264	-0.1036	0.02
PO_4	-1.05 ‰ $\mu mol^{-1}\ kg^{-1}$	-0.27	0.2231	0.09	-0.53	0.3281	0.06

Applying the MLR approach to the GEOSECS and WOCE $\delta^{13}C$ data yielded coefficients for the variables θ, S, O_2, PO_4 and AOU (m_1-m_5 in equation 2) that differed from coefficients calculated from individual linear regressions of each predictive variable against $\delta^{13}C$, and often differed from coefficients predicted a-priori (Table 4.1). For example, the temperature dependence of $\delta^{13}C$ of DIC in gas exchange equilibrium with the atmosphere has been determined to be $\delta^{13}C_{eq} = \delta^{13}C_{atm} + 10.51 - 0.105\ \theta$ (Zhang et al., 1995). Regressing $\delta^{13}C$ versus θ alone yielded a positive θ coefficient, indicating that other processes, e.g., circulation and organic matter cycling, must dominate $\delta^{13}C$ distributions. However, when more variables, e.g., AOU, O_2 and PO_4, were included in the model, the MLR θ coefficient was close to the equilibrium gas exchange value of -0.105 ‰ $°C^{-1}$, suggesting that the remaining variables may have accounted for much of the $\delta^{13}C$ variability caused by circulation and organic matter cycling.

In the individual linear regression, the $\delta^{13}C$ versus AOU coefficient was similar to that calculated a-priori from cycling of organic matter whose $\delta^{13}C_{org}$ = -21 ‰ (Goericke and Fry, 1994) using the remineralization ratios $P/N/C_{org}/\text{-}O_2$ of 1/16/117/170 (Anderson and Sarmiento, 1994; Table 4.1). However, when O_2 was included in the MLR, the AOU coefficient was much larger. The fact that O_2 contributed any predictive power at all in combinations including AOU, θ and S was surprising because O_2 is a function of AOU, θ and S. A-priori O_2 coefficients of 0.0062 ‰ $\mu mol^{-1}\ kg^{-1}$ and 0.0191 ‰ $\mu mol^{-1}\ kg^{-1}$ were calculated due to organic matter cycling, and due to the θ dependence of O_2 solubility (Weiss, 1970) and equilibrium gas exchange $\delta^{13}C$

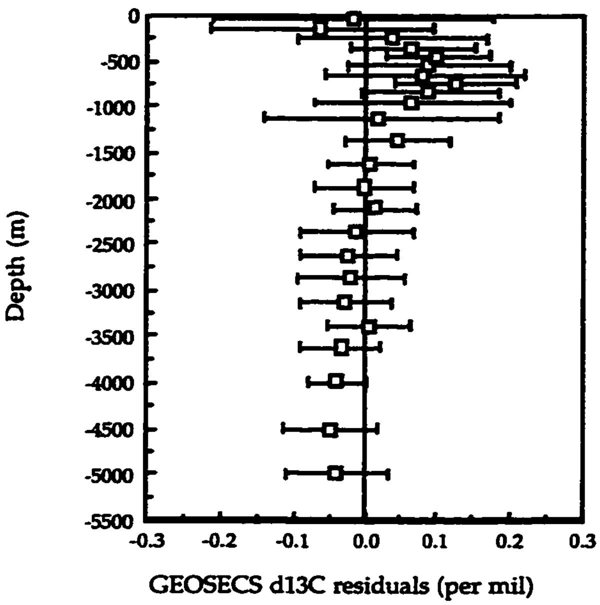

Figure 4.3. Residuals ($\delta^{13}C$ measured - $\delta^{13}C$ predicted) from the GEOSECS $\delta^{13}C$ versus θ, S, PO_4 and AOU multiple linear regression binned into 100 m intervals shallower than 1000 m, 250 m intervals from 1000 m - 3750 m, and 500 m intervals deeper than 3750 m. Error bars represent the scatter (1 σ) in the residuals within each depth interval.

fractionation, as discussed above, respectively. The MLR O_2 coefficients were opposite in sign (Table 4.1) from these a-priori values, which indicates that O_2 was likely contributing predictive power as a water mass tracer or as a tracer of processes other than Redfield type organic matter cycling or temperature dependent equilibrium $\delta^{13}C$ gas exchange fractionation. When O_2 was omitted as a predictive variable, the residuals were strongly biased in the depth range 400-1000 m (Fig. 4.3). This depth range coincides with the strong O_2 minimum zone in the North Indian Ocean (Fig. 4.4), where denitrification

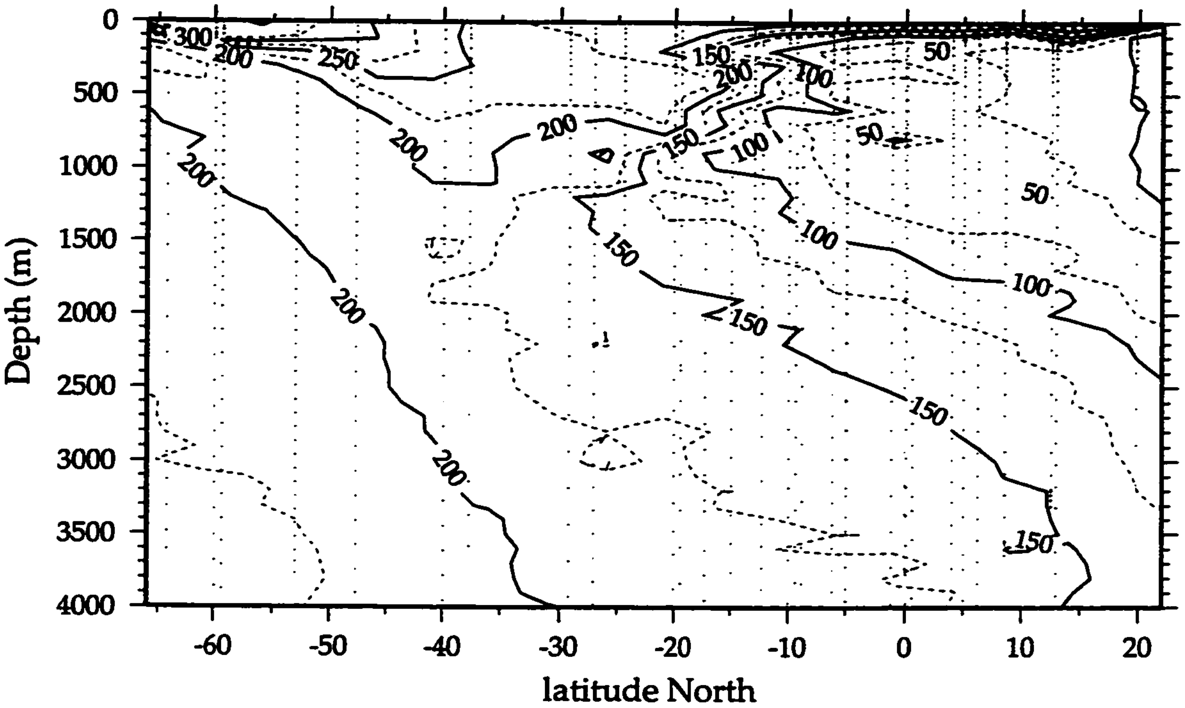

Figure 4.4. Oxygen (μmol kg^{-1}) measured along ~ 60°E and ~ 100°E in 1978 during the GEOSECS expedition in the Indian Ocean.

occurs (Brandes, 1996). Under denitrification conditions, AOU distributions are a function of θ and S only and the uniformly zero O_2 distribution becomes independent of AOU, θ and S. When we tuned the MLR to the WOCE I8S/I9S $\delta^{13}C$, θ, S, O_2, PO_4 and AOU data only, i.e., using data from south of 30°S only, oxygen contributed no significant predictive power. In addition, the MLR AOU coefficient was -0.0055, close to the value predicted a-priori due to organic matter cycling, as discussed above. Thus we conclude that when combined with AOU, θ and S in the predictive variable set, O_2 is contributing as a tracer of waters, with their associated $\delta^{13}C$, from the Arabian Sea oxygen minimum zone. Similarly, the PO_4 and S coefficients likely reflected

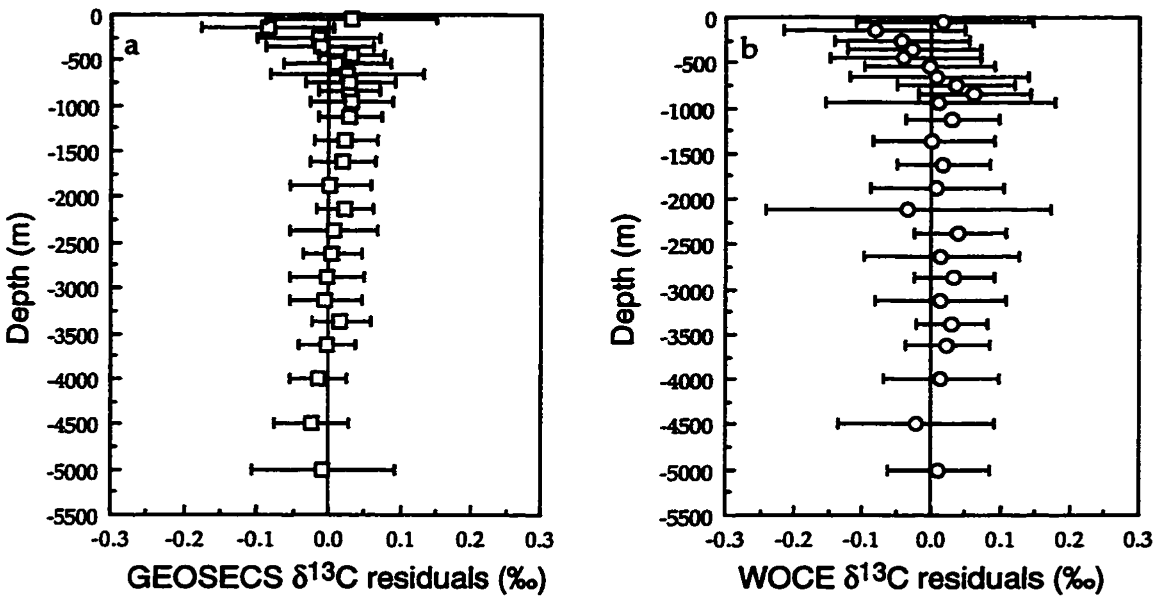

Figure 4.5. Residuals ($\delta^{13}C$ measured - $\delta^{13}C$ predicted) from the a) GEOSECS and b) WOCE $\delta^{13}C$ versus θ, S, O_2, PO_4 and AOU multiple linear regression binned into 100 m intervals shallower than 1000 m, 250 m intervals from 1000 m - 3750 m, and 500 m intervals deeper than 3750 m. Error bars represent the scatter (1 σ) in the residuals within each depth interval.

sensitivity to water mass driven variability of $\delta^{13}C$ in the Indian Ocean (Kroopnick et al., 1985).

The magnitude of the $\delta^{13}C$ residuals for the GEOSECS dataset using θ, S, O_2, PO_4 and AOU generally decreased with increasing depth (Fig. 4.5). The typical uncertainty in the top 100 m was ± 0.12 ‰, and decreased to about ± 0.06 ‰ by 500 m depth. Typical deep water (1000 - 4000 m) uncertainties were on the order of ± 0.05 ‰. Overall, the MLR equation provided an accurate

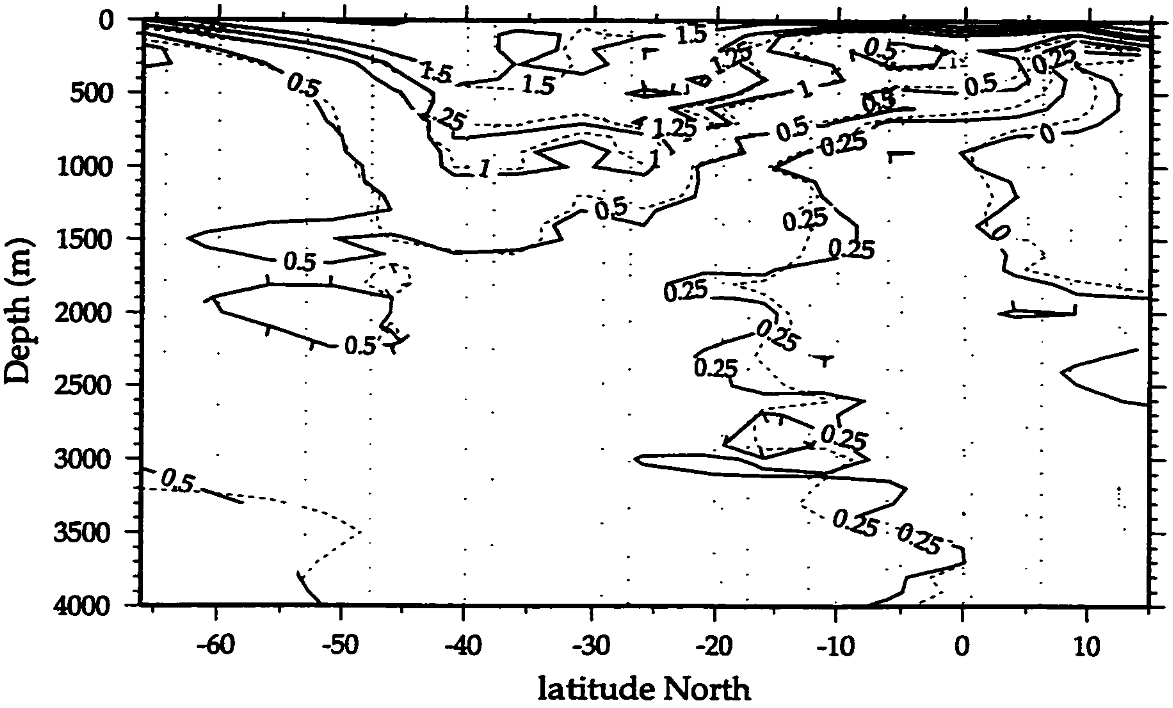

Figure 4.6. GEOSECS $\delta^{13}C$ values measured during 1978 in the Indian Ocean (solid line) and predicted using the MLR equation tuned to GEOSECS $\delta^{13}C$ and θ, S, O_2, PO_4 and AOU data (dashed line).

estimate of the large scale $\delta^{13}C$ distribution observed during GEOSECS (Fig. 4.6).

When the $\delta^{13}C$ distribution measured during WOCE was regressed against WOCE θ, S, O_2, PO_4 and AOU data, the MLR predicted $\delta^{13}C$ agrees, on average, to within ± 0.11 ‰ overall. The depth dependence of the WOCE residuals was similar to GEOSECS (Fig. 4.5), and decreased with increasing depth from about ± 0.12 ‰ in the top 500 m to about ± 0.08 ‰ by 1000m. The deep water (1000 - 4000 m) residuals were on the order of ± 0.05 to ± 0.09 ‰. Based on the residuals in the GEOSECS and WOCE regressions, we calculated an average error in determining the $\delta^{13}C$ difference between GEOSECS and WOCE on the order of ± 0.13 ‰ in the top 1500 m, i.e., where we expect to find a $\delta^{13}C$ change. However, this uncertainty was strongly latitude dependent, as discussed below, and was smaller (± 0.1 ‰) north of 40°S. For comparison, surface ocean Suess effect reconstructions along 80°E and 110°E using preformed $\delta^{13}C$ values (chapter three) indicated a 1978 - 1995 $\delta^{13}C$ change of -0.2 to -0.3 ‰ between 55°S and 35°S, respectively. Thus, the surface water signal-to-noise ratio in calculating the GEOSECS to WOCE $\delta^{13}C$ change in the Indian Ocean was ~ 1 to ~ 3, depending on latitude, using the MLR approach.

The relatively large uncertainties in the difference calculations is the primary limitation of the time-series MLR approach. These uncertainties are caused in part by errors in the $\delta^{13}C$ measurements, but uncertainties in the predictive variables contribute as well. For example, the primary source of uncertainty among our predictive variables was AOU which, at best, was determined to within ± 4.1 μmol kg^{-1} (Gruber et al., 1996). This uncertainty, coupled with the MLR AOU parameters (Table 4.1), resulted in ~ ± 0.1 ‰ and ~ ± 0.05 ‰ uncertainties in the $\delta^{13}C$ predictions in surface and deep (AOU ≈ 100 μmol kg^{-1}) waters, respectively. Also, uncertainties in composite calibration offsets between cruises may contribute some systematic error. Finally, uncertainties in predicted $\delta^{13}C$ values may also result from variability in seawater $\delta^{13}C$ that is not reflected in the predictive variable distributions. For example, the substantial variability in carbon isotopic fractionation during photosynthetic uptake of CO_2 in the Southern Ocean (Goericke and Fry, 1994) complicates the relationship between oceanic $\delta^{13}C$ and oxygen and nutrient data. The variability in the $\delta^{13}C$ of organic matter observed from 40°S to the equator is about ± 1.6 ‰ (Table 3.1), which combined with a representative AOU (~100 μmol kg^{-1}) in this region along the I8N and I8S/I9S sections, causes about ± 0.04 ‰ of variability in $\delta^{13}C$ that is not accounted for by tracers of organic matter cycling such as PO_4, O_2 and AOU. In addition the surface ocean gas exchange boundary condition for $\delta^{13}C$ is considerably more complex than for any readily available steady-state predictive variables (Lynch-Stieglitz et al., 1995).

Indian Ocean ^{13}C change

To calculate the $\delta^{13}C$ Suess effect, we used the MLR coefficients derived from GEOSECS data (Table 4.1) with the predictive variables θ, S, O_2, PO_4 and AOU measured during WOCE, to calculate the 1995 $\delta^{13}C$ distribution expected if there had been no anthropogenic $\delta^{13}C$ change since GEOSECS. Comparing the residuals (measured - predicted) in the WOCE predictions resulting from use of the GEOSECS tuned versus the WOCE tuned MLR equations revealed a systematic deviation towards negative values in the top 1000 m in the GEOSECS derived residuals (Fig. 4.7). In other words, near-surface $\delta^{13}C$ values measured during WOCE were lower than predicted from the GEOSECS $\delta^{13}C$ versus θ, S, O_2, PO_4 and AOU MLR relationship. The decrease in WOCE versus GEOSECS $\delta^{13}C$ values results from oceanic uptake of relatively ^{13}C depleted anthropogenic CO_2 (Druffel and Benavides, 1986).

The average $\delta^{13}C$ change between GEOSECS and WOCE along the WOCE sections decreased almost linearly with depth from a maximum of -

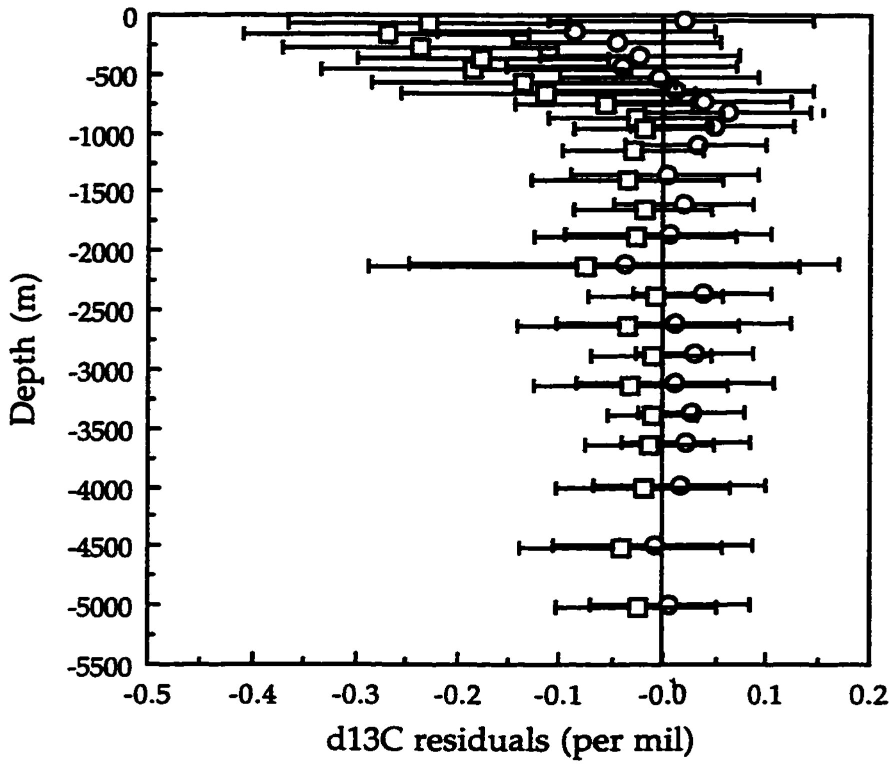

Figure 4.7. Residuals ($\delta^{13}C$ measured - $\delta^{13}C$ predicted) from the WOCE $\delta^{13}C$ versus θ, S, O_2, PO_4 and AOU multiple linear regression binned into 100 m intervals shallower than 1000 m, 250 m intervals from 1000 m - 3750 m, and 500 m intervals deeper than 3750 m (o). Overlain are residuals ($\delta^{13}C$ measured during WOCE - $\delta^{13}C$ predicted) from predicting the WOCE $\delta^{13}C$ data set by applying the GEOSECS tuned multiple linear regression equation to the WOCE θ, S, O_2, PO_4 and AOU data set (□). The two data sets are offset by ± 15 m to aid in distinguishing the overlapping error bars.

0.25 ‰ in the top 100 m, to being indistinguishable from 0 ‰ at depths deeper than 1000 m (Fig. 4.7). Deeper than 2000 m, there was a systematic offset between the two predictions which was likely not attributable to a Suess effect because CFCs have not penetrated this deep over much of the section (Fig. 4.8). The offset could be due in part to calibration offsets between the GEOSECS and WOCE data sets. Also, because the WOCE residuals are predominantly negative in the upper 750 m (Fig. 4.5), the MLR coefficients determined during WOCE (Table 4.1) predict relatively higher residuals at depth in order to yield a mean residual of zero in the overall cruise prediction. The tendency towards negative values in the upper ocean is not as pronounced in the GEOSECS residuals (Fig. 4.5), so the deep residuals are, on average, closer to zero. We determined a net offset deeper than 2000 m between the WOCE predicted and GEOSECS predicted $\delta^{13}C$ values when both predictions used WOCE θ, S, O_2, PO_4 and AOU data of -0.038 ‰ for all CFC-free waters north of 40°S.

The use of CFC measurements as a guide to identifying waters unlikely to reflect any anthropogenic $\delta^{13}C$ perturbation could cause some systematic bias in our Suess effect calculation. Analyses of the $\delta^{13}C$ of aragonite in a sclerosponge at Jamaica (18°N, 78°W in the Caribbean) indicate that local surface ocean $\delta^{13}C$ values had decreased by as much as 0.05 ‰ during 1920-1940 (Böhm et al., 1996), prior to the introduction of significant levels of CFCs into the atmosphere (Walker et al., 1995). Thus part of the -0.038 ‰ offset between the WOCE and GEOSECS predictions in deep waters where CFC levels were below the detection limit may have been due to the Suess effect in waters ventilated prior to the 1940s. However, the deep water offset was due primarily to differences in the depth-dependent trends in the MLR residuals between the GEOSECS and WOCE cruises, as discussed above. When we tuned the GEOSECS and WOCE MLR equations to deep waters (Z > 2000 m) north of 40°S and compared the GEOSECS tuned to the WOCE tuned

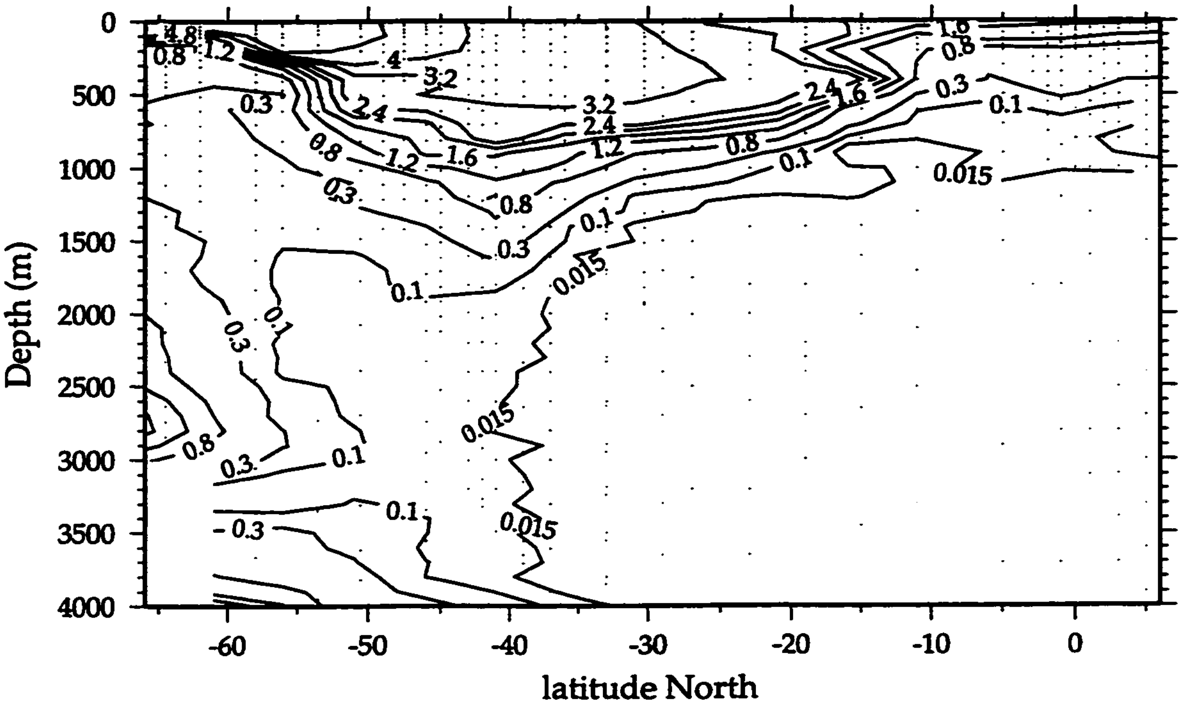

Figure 4.8. CFC-11 (pmol kg^{-1}) measured along 80°E to 115°E in 1995 during WOCE I8N, I8S and I9S in the Indian Ocean (J. Bullister, personal communication).

predictions when WOCE predictive variables alone were used, the deep prediction offset was 0.025 ‰, i.e., the opposite sign. Thus we find no evidence based on the deep MLR $\delta^{13}C$ predictions or on the penetration of CFCs (Fig. 4.8) that the deepwater offsets we calculated for the entire sections above were due to anthropogenic $\delta^{13}C$ changes in the deep Indian Ocean north of 40°S. Because carbon tetrachloride (CCl_4) was introduced into the atmosphere about 25 years before the CFCs (chapter five), an Indian ocean section of CCl_4 measurements would provide a more useful analog than CFCs for the pre- 1960 Suess effect.

Some of the scatter in the residuals (Fig. 4.7) results from systematic (Fig. 4.6) rather than random errors, i.e., the overall errors, as indicated by the magnitude of the residuals in the $\delta^{13}C$ predictions, were depth and latitude dependent. In our Suess effect calculations we compared predictions based on the GEOSECS tuned and the WOCE tuned MLR equations (Table 4.1) when both were applied to WOCE hydrographic and nutrient data. By comparing the $\delta^{13}C$ predictions, we canceled any systematic covariations of the WOCE and GEOSECS residuals (Fig. 4.5). To determine the distribution of the uncertainty in the $\delta^{13}C$ change between WOCE and GEOSECS, we determined the 1 σ variability in the subtraction of the WOCE residuals from the GEOSECS residuals (Fig. 4.5). Since the WOCE and GEOSECS sample locations do not coincide, the residuals from the MLR predictions of the $\delta^{13}C$ distribution from GEOSECS and WOCE (Fig. 4.5), were interpolated onto a 100 m depth by 5° latitude grid between 66°S and 5°N (Smith and Wessel, 1990). The gridded WOCE residuals were then subtracted from the gridded GEOSECS residuals, thus canceling systematic co-variations of the GEOSECS and WOCE residuals. In general, the WOCE and GEOSECS residuals (Fig. 4.5) were not well correlated, so overall the calculated error in the predicted Suess effect did not change much from the error estimates discussed above.

The scatter in the gridded difference residuals decreased with depth from a maximum ± 0.12 ‰ at the surface to ~ ± 0.06 ‰ at depths > 1200 m. This depth trend was similar to the trend for the individual GEOSECS and WOCE residuals (Figs. 4.5 and 4.9). The scatter in the residuals also was strongly latitude dependent (Fig. 4.9). The 1 σ scatter in the vertical profiles decreased from a maximum of ± 0.16 ‰ at 65°S to around ± 0.06 ‰ north of

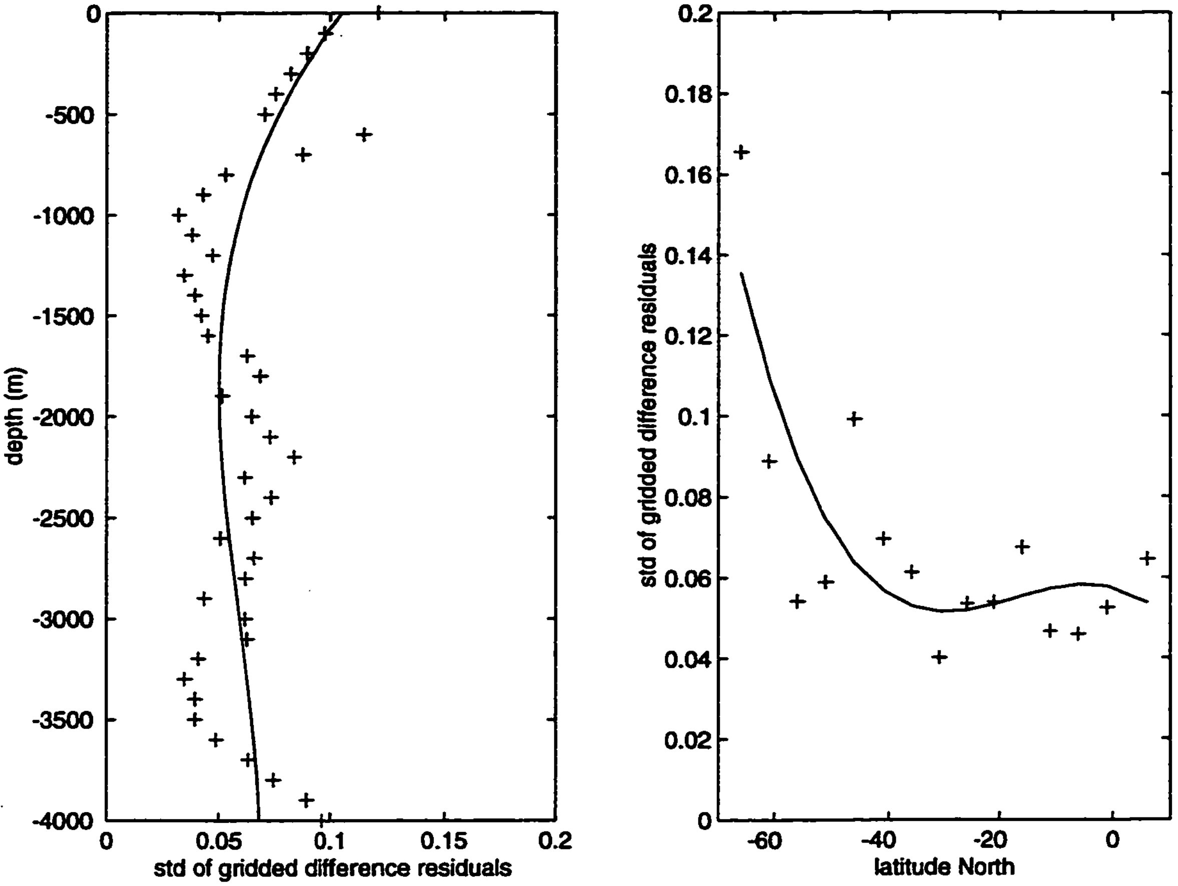

Figure 4.9. The ± 1 σ scatter in the GEOSECS - WOCE gridded difference residuals for each (a) 100 m and (b) 5° latitude grid interval. The solid lines are the least-squares fit of cubic polynomials to the 1 σ versus (a) depth and (b) latitude trends. See text for discussion.

42°S. In other words, the error in the calculated GEOSECS-WOCE $\delta^{13}C$ difference was, on average, two to three times smaller north of 42°S.

We used cubic spline fits to the depth and latitude trends in the gridded difference residuals to calculate the error in the MLR derived $\delta^{13}C$ change at an individual station (Fig. 4.9). Thus, for each station we shifted the depth profile of the 1 σ error of the residual difference (Fig. 4.9a) to yield the mean difference residual scatter for the station's latitude (Fig. 4.9b). As a result of accounting for the depth and latitude trends in the difference residuals, errors in the calculated $\delta^{13}C$ change between GEOSECS and WOCE in surface waters decreased from ± 0.16 ‰ at 65°S to a relatively uniform value of ± 0.1 ‰ north of 42°S. The minimum uncertainties occurred between 1000 m and 3000 m depth (Fig. 4.9), and decreased from ± 0.12 ‰ at 65°S to values ranging from ± 0.05 to ± 0.06 ‰ at stations north of 42°S.

The meridional and depth distribution of the $\delta^{13}C$ Suess effect in the Indian Ocean (Fig. 4.10) determined by the MLR method was consistent with the penetration of CFCs measured on this section (Fig. 4.8) despite the significant uncertainties in the $\delta^{13}C$ change calculation. The maximum $\delta^{13}C$ decrease of -0.25 to -0.3 ‰ occurred within and above the main subtropical (20°S to 40°S) thermocline (shallower than 300 m). The -0.05 ‰ contour, which we take as the minimum significant calculated $\delta^{13}C$ change, penetrated to a maximum depth of about 1200 m at 40°S along this section. A slightly lower $\delta^{13}C$ change of -0.2 to -0.1 ‰ was determined for the subtropical thermocline between 500 m and 1000 m depth.

Surface ocean ^{13}C change

The surface water time rate of change of $\delta^{13}C$ increased northwards from ~ -0.1 ‰ decade^{-1} at 55°S to a maximum of ~ -0.18 ‰ decade^{-1} from 35°S to 20°S, and then decreased to ~ -0.13 ‰ decade^{-1} at the equator (Fig. 4.11). The average uncertainties in the surface water $\delta^{13}C$ change rates were

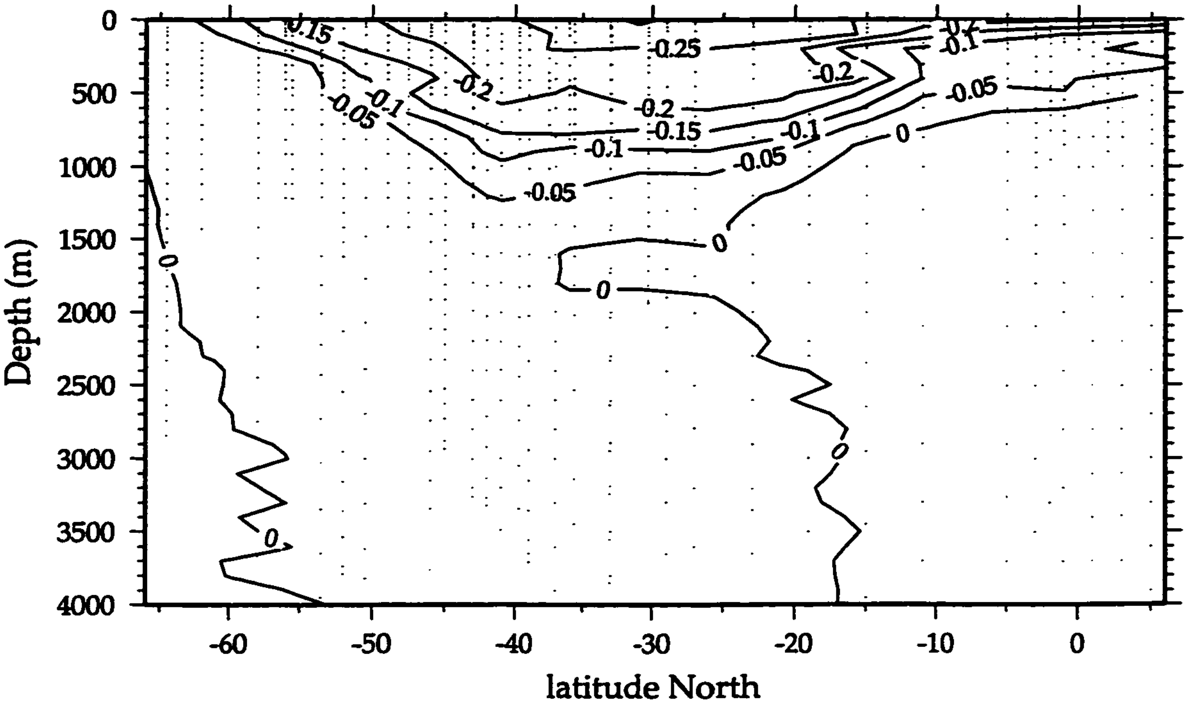

Figure 4.10. The $\delta^{13}C$ change (‰) between the GEOSECS (1978) and WOCE (1995) expeditions in the Indian Ocean. The $\delta^{13}C$ change is the difference between the $\delta^{13}C$ values predicted from the WOCE tuned MLR and the GEOSECS tuned MLR using WOCE θ, S, O_2, PO_4 and AOU data. A deepwater offset of -0.038 ‰ was removed prior to plotting, see text for discussion.

about ± 0.08 ‰ decade^{-1} at 56°S and decreased northwards to ± 0.06 ‰ decade^{-1} north of 40°S (Fig. 4.8). Despite the large uncertainties, there was little scatter in the calculated $\delta^{13}C$ change versus latitude trends for surface waters (Fig. 4.11).

The MLR derived surface water time rates of $\delta^{13}C$ change between 35°S and 55°S agreed well with rates calculated from the preformed $\delta^{13}C$ versus

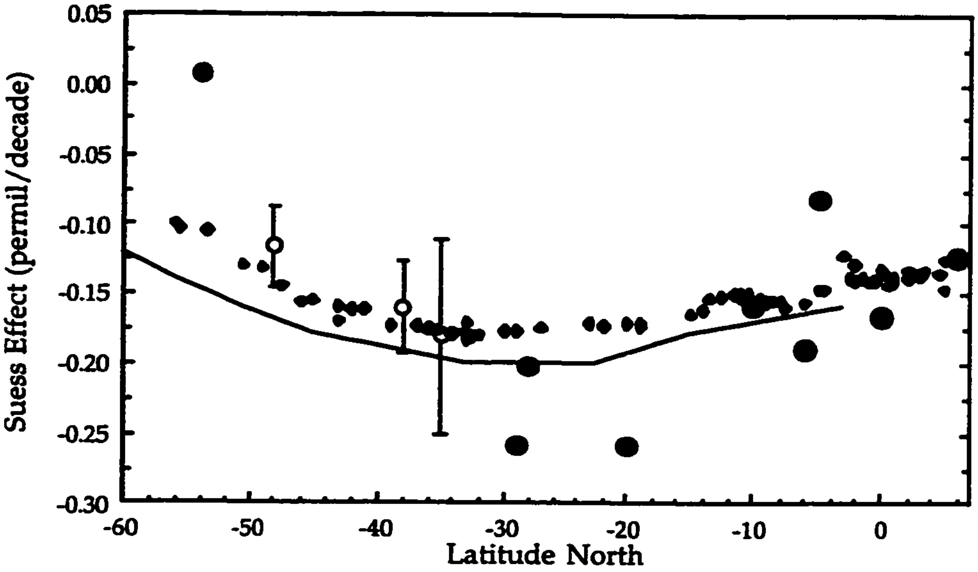

Figure 4.11. The surface water $\delta^{13}C$ time rate of change derived from the MLR approach between 1978-1995 (◆), reconstructed from preformed $\delta^{13}C$ vs. CFC ages for the time period ~1970-1990 (o, chapter three), calculated directly from the specific station comparisons between GEOSECS (1978) and WOCE (1994-1995) surface water $\delta^{13}C$ values (●, locations listed in Table 2), and predicted along 90°E by an ocean general circulation model's simulation of the global carbon cycle between 1983 and 1993 (solid line, Bacastow et al., 1996).

CFC age regressions (chapter three). The Hamburg model prediction of the $\delta^{13}C$ Suess effect during the time period 1983-1993 along 90°E (Bacastow et al., 1996) showed a similar meridional trend but at a faster (~ -0.02 ‰ decade^{-1}) $\delta^{13}C$ change rate.

The MLR derived surface water $\delta^{13}C$ change did not agree well with the surface water $\delta^{13}C$ change calculated by comparing surface $\delta^{13}C$

measurements at specific stations during GEOSECS with nearby WOCE reoccupations (Fig. 4.11). This disagreement likely results because the direct $\delta^{13}C$ subtractions are affected by the substantial seasonal and spatial variability in surface water $\delta^{13}C$ (Bacastow et al., 1996; Kroopnick, 1985). For example, in comparing GEOSECS station 452 (20°S, 80°E) with WOCE I8N station 51 (19°S, 80°E) we found a $\delta^{13}C$ decrease of -0.45 ‰ in surface water $\delta^{13}C$. However, surface waters at the WOCE station (sampled October 1995) were 3.4°C colder than during the GEOSECS occupation (sampled April 1978). Since surface water $\delta^{13}C$ is positively correlated with temperature at any one site (Bacastow et al., 1996), this temperature difference likely led to an overestimate of the GEOSECS-WOCE $\delta^{13}C$ decrease. If we assume that the $\delta^{13}C$ versus θ and O_2 correlations (Table 4.1) apply in time as well as in space, we can correct the $\delta^{13}C$ difference from the direct comparison for the GEOSECS-WOCE temperature and associated oxygen difference using the MLR coefficients. This reduced the $\delta^{13}C$ change rate to -0.17 ‰ decade^{-1}, which agreed with the time-series MLR result. Similar correlations between the discrepancy between MLR-derived versus direct $\delta^{13}C$ comparison-derived surface water $\delta^{13}C$ changes and GEOSECS-WOCE surface water temperature and oxygen differences were observed at all of the direct $\delta^{13}C$ data comparison locations. The results of this analysis indicate that seasonal as well as spatial variability in surface water $\delta^{13}C$ must be accounted for when estimating the surface ocean Suess effect by comparing snapshots of $\delta^{13}C$ data. This could be accomplished either by comparing sections occupied in the same season, as we did in chapter three, or via corrections that account for variations in sea surface temperature (Bacastow et al., 1996).

Depth-integrated ^{13}C change

To calculate the total $\delta^{13}C$ inventory change in the Indian Ocean, we depth-integrated the $\delta^{13}C$ changes (Fig. 4.10) calculated by the MLR method at each WOCE station (Fig. 4.1). The depth-integrated $\delta^{13}C$ change was sensitive to even slight calibration offsets between the GEOSECS and WOCE $\delta^{13}C$ predictions because any offsets are integrated over depths up to 1400 m. The mean offset between the GEOSECS and WOCE MLR calculated $\delta^{13}C$ changes over 2000 to 4000 m depth was subtracted from the $\Delta\delta^{13}C$ depth profile at each individual station. The station offsets decreased northwards from about -0.056 ‰ at 39°S to about -0.009 ‰ at 5°N. South of 40°S where some deep anthropogenic $\delta^{13}C$ change may have occurred, as evidenced by detectable CFC levels to the bottom (Fig. 4.8), we assumed that the offset of -0.056 ‰ observed in CFC-free waters at 39°S and deeper than 2000 m, applied.

At all stations the integration depth was selected, by hand, as the first depth where the MLR derived $\delta^{13}C$ change between GEOSECS and WOCE was no longer discernible from the residual scatter in deep water $\delta^{13}C$ change values (Fig. 4.12). Although this approach is subjective, the integrated values were relatively insensitive to the maximum depth chosen because, relative to the large surface changes and overall uncertainties, the $\delta^{13}C$ changes were small in the vicinity of the integration depth. The integration depths ranged from 100 - 300 m south of 50°S, and increased northwards to ~ 1400 m at 35°S - 45°S and and decreased northwards to ~ 1200 m at 20°S. In the tropics, the $\delta^{13}C$ changes were typically integrated down to 500 - 800 m (Fig. 4.12). When we adopted an alternate approach of integrating only down to the depth where the WOCE-GEOSECS change was larger than -0.05 ‰, i.e., the smallest significant $\delta^{13}C$ change as discussed above, the integration depths were ~ 200 m shallower at all latitudes.

Throughout the subtropics (20°S to 40°S), the MLR derived depth-integrated $\delta^{13}C$ change rate was ~ -12 ‰ m yr^{-1} and was significantly larger than its typical uncertainty of ± 5 ‰ m yr^{-1} (Figs. 4.12 and 4.13). South of 40°S, the integrated ^{13}C change rate decreased polewards from ~ -12 ‰ m yr^{-1} to ~ -5 ± 5 ‰ m yr^{-1} at ~ 48°S (Fig. 4.13). South of 50°S the $\delta^{13}C$ change was larger than uncertainties in very shallow waters only (Fig. 4.12), and the depth integrated $\delta^{13}C$ change rate was less than -2.5 ‰ m yr^{-1} (Fig. 4.13). North of 20°S, the $\delta^{13}C$ changes were larger than uncertainties at depths < 500 m only (Fig. 4.12), and the depth-integrated change rate decreased to around -3 ± 3 ‰ m yr^{-1} north of 10°S (Fig. 4.13). When we instead integrated the depth profiles of the WOCE-GEOSECS $\delta^{13}C$ change (Fig. 4.12) down to the -0.05 ‰ cutoff, as discussed above, the depth integrated $\delta^{13}C$ changes were < 5 % smaller in the subtropics and about 10 % smaller at high latitudes (south of 45°S) and in the tropics (north of 15°S).

We compared the MLR derived depth-integrated $\delta^{13}C$ change to the depth-integrated Indian Ocean preformed $\delta^{13}C$ reconstructions (chapter three) and to the depth-integrated change calculated by subtracting GEOSECS $\delta^{13}C$ depth profiles from nearby WOCE reoccupations (Fig. 4.1, Table 4.2). At each station, any offset in the GEOSECS vs. WOCE $\delta^{13}C$ values between 2000 m and 4000 m was calculated (Table 4.2). After this deep water correction was applied, the difference between the $\delta^{13}C$ profiles was integrated down to the

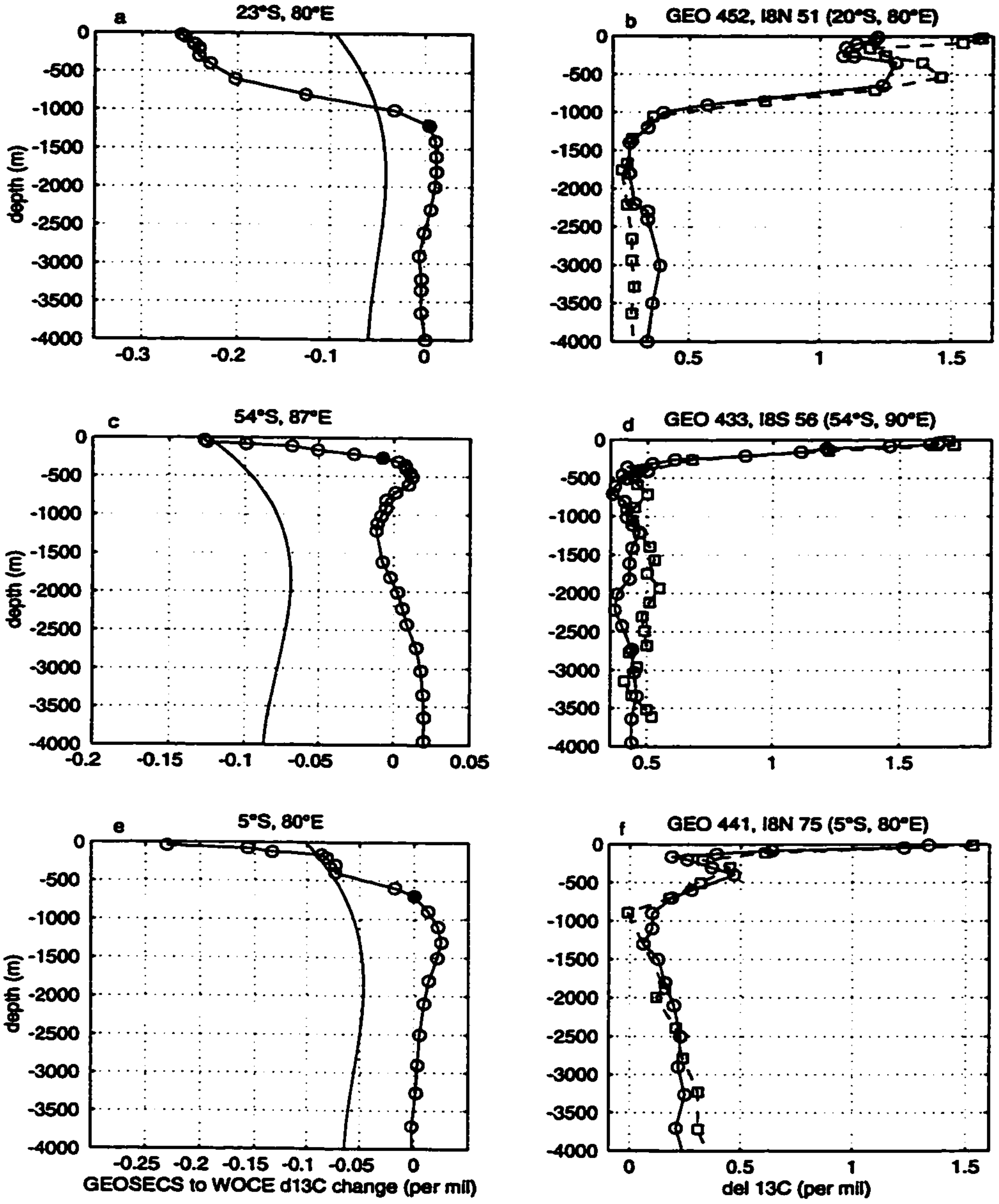

Figure 4.12. Depth profiles of the $\delta^{13}C$ residual difference (the $\delta^{13}C$ Suess effect) between GEOSECS and WOCE (o) at a) 23°S, c) 54°S and e) 5°S. The asterisk represents the depth to which the $\delta^{13}C$ change was integrated. The solid lines are the uncertainties in the difference calculated from the gridded GEOSECS and WOCE MLR baseline residuals, see text for discussion. Included are nearby direct (station-to-station) $\delta^{13}C$ depth profile comparisons between GEOSECS (□) and WOCE (o) from b) 20°S, 80°E, d) 54°S, 90°E and f) 5°S, 80°E.

Table 4.2. Depth integrated $\delta^{13}C$ change calculated by subtracting GEOSECS $\delta^{13}C$ depth profiles from nearby profiles reoccupied during WOCE. The GEOSECS stations were occupied during January - April 1978. The WOCE I7N, I8N and I8S stations were occupied during March-April 1995, September-October 1995 and December 1994, respectively. The integration depth was defined as the first depth where the $\delta^{13}C$ versus depth profiles intersected after having corrected the GEOSECS data for any deep water ($Z > 2000$ m) offset (see text for discussion).

GEOSECS Station	Modern Station	$\delta^{13}C$ Offset, $Z >$ 2000 m (‰)	Integration Depth (m)	Integrated $\delta^{13}C$ Change (‰ m)
#418 6°N, 64°E	WOCE I7N #117 5°N, 60°E	-0.065	600	-91
#420 0°, 51°E	WOCE I7N # 104 0°, 56°E	-0.048	400	-63
#421 6°S, 51°E	WOCE I7N # 90 8°S, 53°E	-0.019	400	-123
#424 12°S, 54°E	WOCE I7N # 70 12°S, 55°E	-0.014	1000	-145
#427 28°S, 57°E	WOCE I7N # 40 28°S, 55°E	-0.0098	1400	-249
#452 20°S, 80°E	WOCE I8N # 51 19°S, 80°E	-0.062	1000	-216
#441 5°S, 92°E	WOCE I8N # 75 5°S, 80°E	0.046	350	-29
#450 10°S, 80°E	WOCE I8N # 63 11°S, 80°E	-0.0074	600	-43
#436 29°S, 110°E	WOCE I8N # 41 29°S, 80°E	-0.14	1400	-253
# 433 53°S, 103°E	WOCE I8S # 56 54°S, 87°E	0.054	175	-7.6
#435 40°S, 110°E	WOCE I8N # 5 41°S, 95°E	-0.080	1000	-327

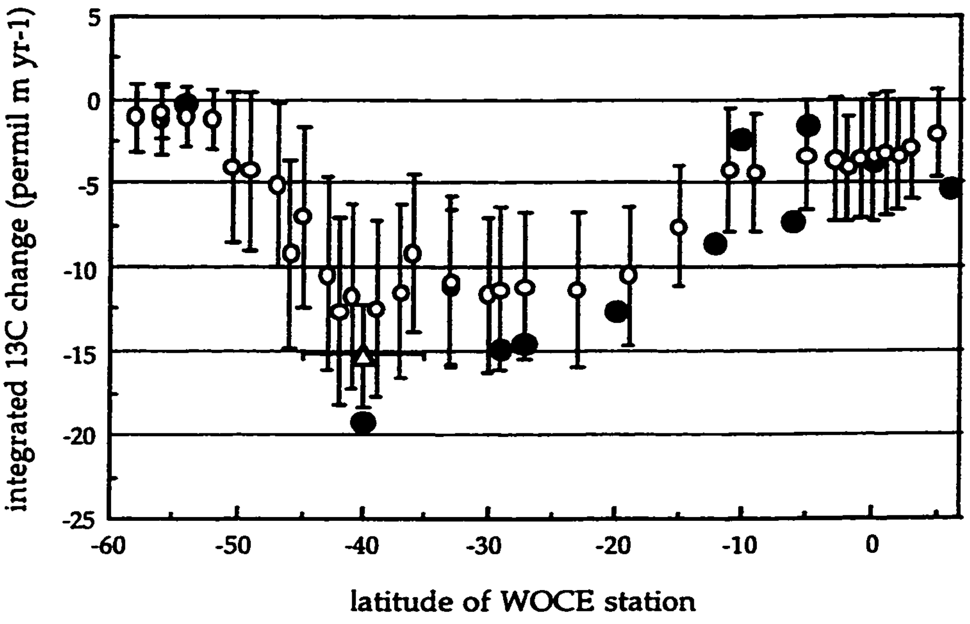

Figure 4.13. The depth-integrated $\delta^{13}C$ change rate calculated at each WOCE station using the MLR approach (o), the preformed $\delta^{13}C$ reconstructions (Δ, chapter three), and by subtracting GEOSECS $\delta^{13}C$ depth profiles from nearby WOCE reoccupations (●).

depth where no $\delta^{13}C$ change was measurable (Fig. 4.12). Unlike the situation for the surface water $\delta^{13}C$ change calculations, the MLR-derived and preformed $\delta^{13}C$-derived depth-integrated $\delta^{13}C$ changes agree within uncertainties with $\delta^{13}C$ changes calculated by the direct subtractions (Fig. 4.13). The good agreement suggests that depth-integrated direct $\delta^{13}C$ data comparisons, such as those published by Quay et al. (1992), are relatively unaffected by aliasing of spatial and temporal variability in $\delta^{13}C$ at depth.

Implications for oceanic CO_2 uptake

Based on our time-series MLR calculations, the mean rate of change of surface water $\delta^{13}C$ between 1978 and 1995 was -0.157 ± 0.008 ‰ decade^{-1} between 55°S and the equator along 80°E and 115°E (Fig. 4.11). The Hamburg model simulation yielded a larger surface ocean $\delta^{13}C$ rate of change of -0.176 ‰ decade^{-1} between 55°S and the equator along 90°E (Bacastow et al., 1996, Fig. 9a). The Hamburg model predicted a global surface ocean average $\delta^{13}C$ change rate of -0.171 ‰ decade^{-1} between 1983 and 1995 (Bacastow et al., 1996). We estimated a global average surface ocean Suess effect between 1978 and 1995 of -0.153 ± 0.008 ‰ decade^{-1} by scaling our surface $\delta^{13}C$ changes along 80°E and 115°E by the factor -0.171/-0.176. The box-diffusion model simulation results of Bacastow et al. (1996) indicate that a global surface ocean $\delta^{13}C$ Suess effect of -0.153 ± 0.008 ‰ decade^{-1} implies an ocean uptake rate of CO_2 of about 2.5 ± 0.5 Gt. C yr^{-1} over the time period 1984-1993. The uncertainty reported reflects the CO_2 uptake rate's sensitivity to error in our global mean surface ocean Suess effect only.

In chapter three we compared the surface ocean Suess effect calculated from the difference between a 1970 $\delta^{13}C$ section along 150°W in the Pacific Ocean (Kroopnick et al., 1977) with the same section reoccupied in the same season in 1993, and from reconstructions of preformed $\delta^{13}C$ changes in the Pacific, South Indian, and North Atlantic Oceans, with the Hamburg model simulation of the $\delta^{13}C$ change (Bacastow et al., 1996). We found that the Hamburg model tends to overestimate the time rate of $\delta^{13}C$ change in the surface South Pacific and South Indian Oceans by about ~ 0.05 ‰ decade^{-1} and ~ 0.03 ‰ decade^{-1}, respectively (Fig. 3.9). At the same time, the model results agreed with observations in the North Pacific and North Atlantic Oceans. The fact that the model tends to overestimate the $\delta^{13}C$ change in the southern hemisphere only means that the global surface ocean extrapolation factor we used here, -0.171/-0.176, was likely too small. This may have caused us to underestimate the global surface ocean time rate of $\delta^{13}C$ change, and thus overestimate the global ocean's CO_2 uptake rate. Based on more extensive global coverage, in chapter three we estimated a global surface ocean rate of $\delta^{13}C$ change of -0.15 ± 0.04 ‰ decade^{-1}. Since the MLR-derived South Indian Ocean $\delta^{13}C$ changes were in good agreement with, but slightly faster (< 0.02 ‰ decade^{-1}) than, the reconstructed changes (Fig. 4.11), we speculate that the global surface ocean $\delta^{13}C$ Suess effect lies in the range of -0.15 to -0.17 ‰ decade^{-1}, with an uncertainty on the order of ± 0.025 ‰ decade^{-1}. Bacastow et al.'s (1996) box-diffusion model simulation results imply a corresponding ocean uptake rate of CO_2 of ~ 1.8 to ~ 2.5 Gt. C yr^{-1} over the time period 1984-1993.

The average depth-integrated time rate of $\delta^{13}C$ change along the 80°E to 115°E section was -6.9 ± 0.5 ‰ m yr^{-1} from 58°S to 5°N (Fig. 4.13). This was somewhat smaller than the Quay et al. (1992) global mean 1970-1990 perturbation estimate of -10.4 ± 2.3 ‰ m yr^{-1}. To extend the global significance of our Indian Ocean $\delta^{13}C$ change estimate, we adopted the Quay et al. (1992) scaling approach by using the global bomb ^{14}C inventory determined during GEOSECS (Broecker et al., 1985) and the relationship between GEOSECS bomb ^{14}C inventories and depth-integrated ^{13}C changes at all of the stations available to us at this time (Fig. 4.14). The regression-derived trend between depth-integrated $\delta^{13}C$ changes during the 1970s, 1980s

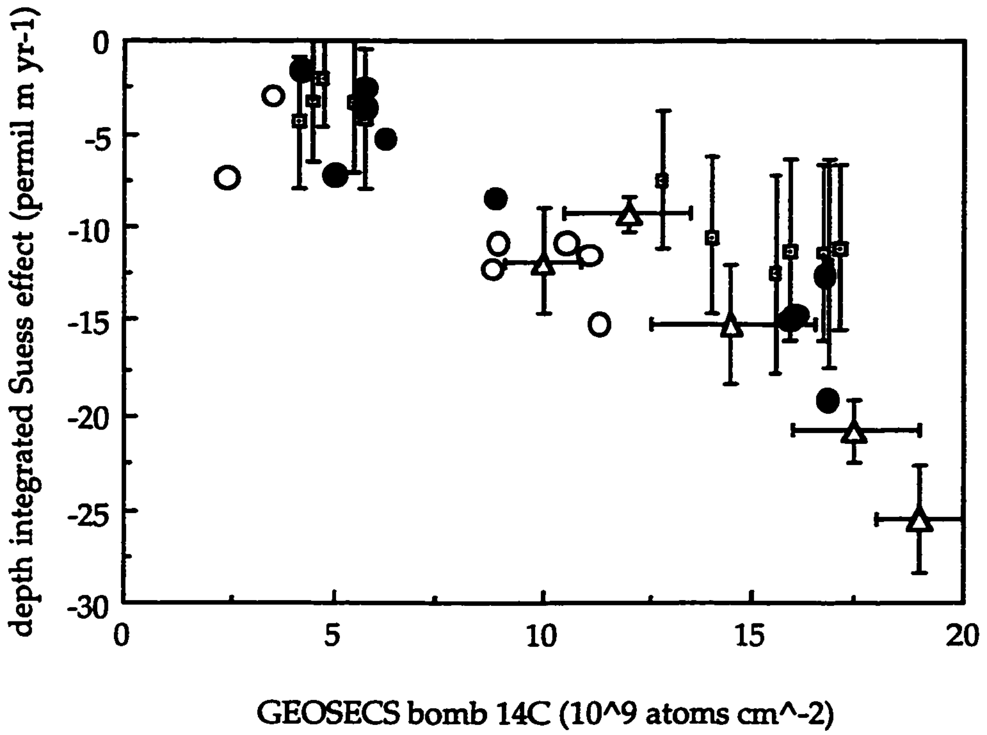

Figure 4.14. The depth-integrated $\delta^{13}C$ change plotted against nearby GEOSECS bomb ^{14}C Inventories for the GEOSECS-WOCE direct $\delta^{13}C$ comparisons in the Indian Ocean (●), from the GEOSECS-WOCE MLR comparison approach (□), from a 1970-1990 direct $\delta^{13}C$ data comparison in the Pacific Ocean (o, Quay et al., 1992), and from preformed $\delta^{13}C$ versus CFC-age reconstructions in the Pacific, South Indian, and North Atlantic Oceans (Δ, chapter three).

and early 1990s and GEOSECS bomb ^{14}C inventories was $\Delta\delta^{13}C$ (‰ m yr^{-1}) = -0.22 - 0.91 $\Delta\Delta^{14}C$ (10^9 atoms cm^{-2}). A global ocean average depth-integrated $\delta^{13}C$ Suess effect of -7.9 ± 3.1 ‰ m yr^{-1} was determined by applying the global ocean average bomb ^{14}C inventory of 8.4 x 10^9 atoms cm^{-2} measured during

Table 4.3. Global carbon cycle parameters used to derive an oceanic CO_2 uptake rate from atmospheric $^{13}CO_2$ and $^{12}CO_2$ budgets following the approach of Quay et al. (1992). All values, except our estimated depth-integrated oceanic $\delta^{13}CO_2$ change, are from Heimann and Maier-Reimer (1996).

Carbon Cycle Parameter 1970-1990	**Value**
Atmospheric CO_2 inventory	715 ± 7 Gt. C
Change in atmospheric CO_2 inventory	60 ± 6 Gt. C
$\delta^{13}C$ of atmospheric CO_2	-7.55 ± 0.1 ‰
Change in $\delta^{13}C$ of atmospheric CO_2	-0.4 ± 0.2 ‰
$\delta^{13}C$ of anthropogenic CO_2 source	-28.1± 0.5 ‰
$\delta^{13}C$ of oceanic dissolved inorganic carbon (DIC)	1.8 ± 0.5 ‰
Depth-integrated change of $\delta^{13}C$ of oceanic DIC	-158 ± 64 ‰ m
Suess effect in the terrestrial biosphere	-18 ± 12 Gt. C ‰ yr^{-1}

GEOSECS (Broecker et al., 1985) to this regression relationship. The error reported reflects uncertainties in the regression only.

To determine an oceanic CO_2 uptake rate we used our estimate of the depth-integrated oceanic $\delta^{13}C$ Suess effect in the atmosphere-ocean-terrestrial biosphere budgets of $^{12}CO_2$ and $^{13}CO_2$ developed by Quay et al. (1992). Using the carbon cycle parameters (Table 4.3) of Heimann and Maier-Reimer (1996), this implied an oceanic CO_2 uptake rate of 1.3 ± 1.0 Gt. C yr^{-1} during the time period ~1970 - 1990, smaller than the rate of 2.1 ± 0.8 Gt. C yr^{-1} calculated by Quay et al. (1992), the IPCC estimate of 2.0 ± 0.8 Gt. C yr^{-1} (Houghton et al.,

1995) and Keeling et al.'s (1996) estimate of 1.7 ± 0.9 Gt. C yr^{-1} based on secular changes in atmospheric O_2 concentrations during 1991-1994. A slightly greater oceanic CO_2 uptake rate of ~ 2.0 ± 1.0 Gt. C yr^{-1} was calculated using our integrated time rate of change of $\delta^{13}C$ and Heimann and Maier-Reimer's (1996) "dynamic constraint" method.

Chapter 5 : Recommendations for future research

Introduction

Our purpose here is to summarize the relative strengths and weaknesses of the three methods used to determine the $\delta^{13}C$ Suess effect in this dissertation: the snapshot comparison approach (chapters three and four), the preformed $\delta^{13}C$ versus CFC age approach (chapter three) and the multiple parameter regression (MLR) approach (chapter four). Because one of the major sources of uncertainty in our CO_2 uptake determinations derives from the use of a bomb ^{14}C analogy to globally extrapolate local Suess effect estimates (chapters three and four), we begin by taking a closer look at the relations among the $^{14}CO_2$, $^{13}CO_2$ and $^{12}CO_2$ perturbations in the oceans. Next we investigate the possibility of combining reconstructed oceanic $\delta^{13}C$ changes with reconstructed oceanic DIC changes to constrain the ocean-atmosphere CO_2 disequilibrium and carbon fluxes through the terrestrial biosphere. Finally, we make recommendations on how to improve the MLR and preformed $\delta^{13}C$ methods, and highlight their most promising future applications.

Relations among the oceanic $^{12}CO_2$, $^{14}CO_2$ and $^{13}CO_2$ perturbations

$\Delta^{14}C$ versus $\Delta^{13}C$

The average depth integrated $\delta^{13}C$ change ($\int\Delta\delta^{13}C$) calculated from the 22 WOCE I8N and I8S/I9S stations from 40°S to 5°N using the MLR approach (chapter four) was -7.8 ± 0.6 ‰ m yr^{-1}. Over the same latitude range, the average Indian Ocean bomb ^{14}C inventory ($\int\Delta\Delta^{14}C$) during GEOSECS was 11.3 x 10^9 atoms cm^{-2}. The $\int\Delta\delta^{13}C$ versus $\int\Delta\Delta^{14}C$ trend for the MLR-derived $\delta^{13}C$ changes was $\int\Delta\delta^{13}C$ (‰ m yr^{-1}) = -0.06 - 0.7 $\int\Delta\Delta^{14}C$ (10^9 atoms cm^{-2}) at the 11 locations where we could make the comparison. Applying the GEOSECS average bomb ^{14}C from 40°S to 5°N in the Indian Ocean to the regression relationship above yielded an average depth integrated $\delta^{13}C$ change of -7.9 ‰ m. The agreement with the depth-integrated change calculated using $\delta^{13}C$ data alone suggests that the bomb ^{14}C strategy, which was based on a smaller dataset, yields robust extrapolations within this region. However, in using the global bomb ^{14}C extrapolation, we are uncertain how the $\int\Delta\delta^{13}C$ versus $\int\Delta\Delta^{14}C$ relationship calibrated in the oceanic regions where we do have Suess effect estimates relates to the global ocean's $\int\Delta\delta^{13}C$ versus $\int\Delta\Delta^{14}C$ relationship. For example, the $\int\Delta\delta^{13}C$ versus $\int\Delta\Delta^{14}C$ relationship determined for the subtropical and tropical Pacific Ocean agrees (within uncertainties) with the relationship determined in the South Indian Ocean (Fig. 4.14). However, the depth-integrated $\delta^{13}C°$ reconstructions in the North Atlantic imply that a slightly higher $\int\Delta\delta^{13}C$ to $\int\Delta\Delta^{14}C$ ratio might apply there (Fig. 4.14).

Ultimately, the global extrapolation using $\int\Delta\Delta^{14}C$ is limited by the different time histories of the two tracers in the atmosphere. The atmospheric $\delta^{13}C$ perturbation (Fig. 1.3) is an ongoing, quasi-exponential forcing on the surface ocean, and the ocean-atmosphere $\delta^{13}C$ disequilibrium appears to have been increasing during 1970-1990, as discussed below. The bomb ^{14}C perturbation, on the other hand, more closely resembles a 1963-1964 spike in atmospheric $\Delta^{14}C$ values (Fig. 1.2) that manifested itself, due to the slow gas-exchange equilibration time for isotopes of oceanic DIC, as a broader peak in surface ocean $\Delta^{14}C$ values (Fig. 2.15). Both the atmospheric and surface ocean $\Delta^{14}C$ perturbations are relaxing to a somewhat higher than pre nuclear value (Figs. 1.2 and 2.15). The fact that atmospheric $\Delta^{14}C$ is decreasing more quickly than surface ocean $\Delta^{14}C$ means that the ocean-atmosphere $\Delta^{14}C$ disequilibrium has been decreasing since 1970, in contrast to the situation for $\delta^{13}C$. Heimann and Maier-Reimer (1996) have shown that, because of their different characteristic atmospheric histories and perturbation times, the oceanic $^{13}CO_2$ and $^{14}CO_2$ perturbations predicted by an ocean general circulation model correlate poorly (Fig. 5.1). In contrast, the oceanic $^{13}CO_2$ and $^{12}CO_2$ perturbations were highly correlated (r^2=0.96) because of their similar atmospheric source histories (Fig 5.1).

Most of the uncertainty (77 %) in the fossil-fuel CO_2 uptake rate of 1.3 ± 1.0 Gt. C yr^{-1} calculated from the oceanic $\delta^{13}C$ change stems from the ± 40 % uncertainty in the global depth integrated $\delta^{13}C$ change (Table 4.3). The primary source of uncertainty in the global $\int\Delta\delta^{13}C$ value, in turn, stems from uncertainty in the global ocean's $\int\Delta\delta^{13}C$ versus $\int\Delta\Delta^{14}C$ relationship. The correlation between anthropogenic $\delta^{13}C$ and $\Delta^{14}C$ changes determined using WOCE instead of GEOSECS ^{14}C measurements would likely improve the situation because the time-scale of bomb-^{14}C penetration into the ocean in the 1990s is closer to the time constant of the evolution of the ^{13}C signal in the

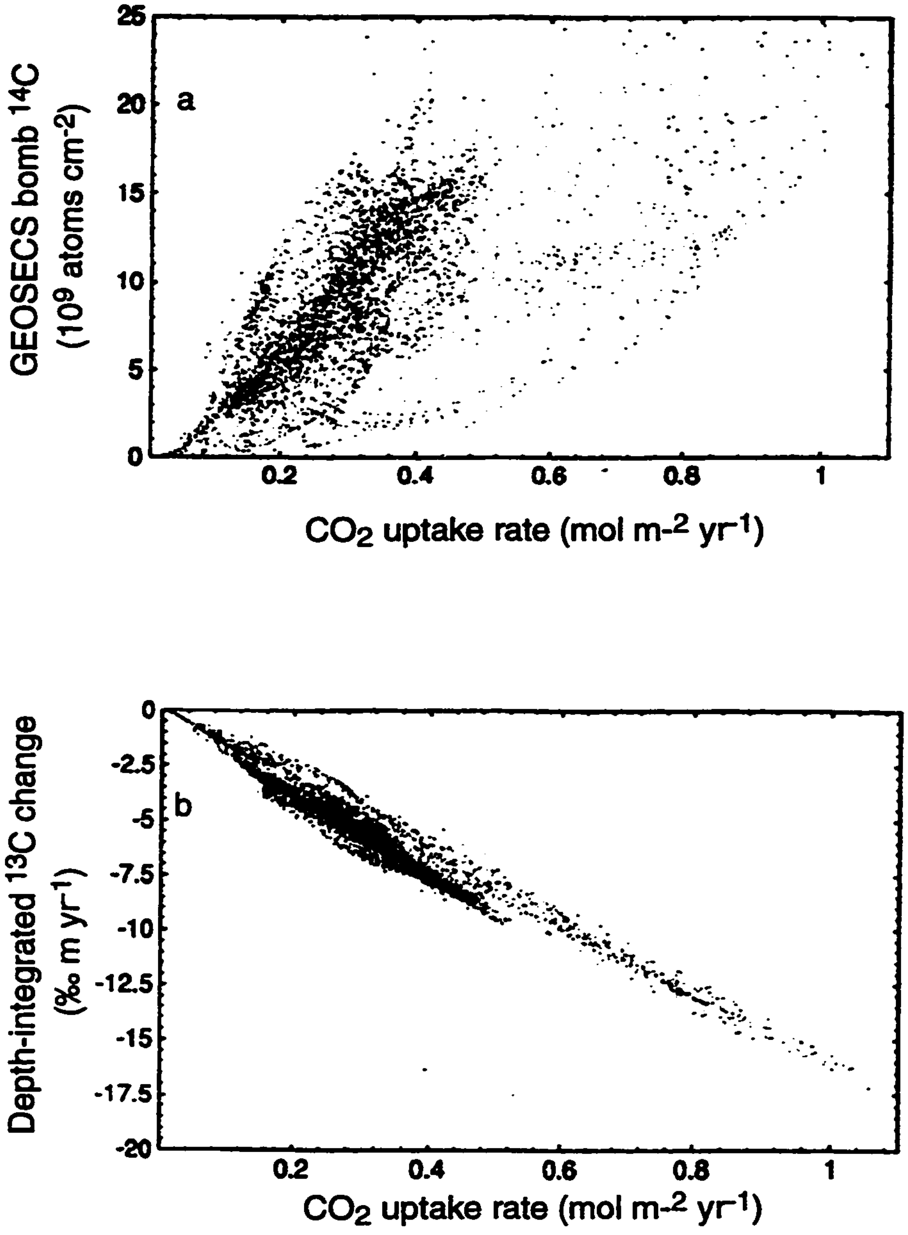

Figure 5.1. Bomb radiocarbon inventory (a) and vertically integrated rate of change of $\delta^{13}C$ during 1970-1990 (b) plotted against vertically integrated rate of change of carbon inventory per unit area in a Hamburg model simulation of the global carbon cycle (Heimann and Maier-Reimer, 1996).

atmosphere, i.e., ~ 30 years. An improved determination of the $\int\Delta\delta^{13}C$ versus $\int\Delta\Delta^{14}C$ relationship, therefore, awaits a redetermination of the global ocean $\int\Delta\Delta^{14}C$ using WOCE ^{14}C data.

When our preformed $\delta^{13}C$ and MLR-derived $\int\Delta\delta^{13}C$ observations were added to the seven depth-integrated snapshot comparisons of Quay et al. (1992), the uncertainty in the regression of $\int\Delta\delta^{13}C$ versus $\int\Delta\Delta^{14}C$ actually increased (chapters three and four). This indicates that the uncertainty in the oceanic $\int\Delta\delta^{13}C$ versus $\int\Delta\Delta^{14}C$ relationship is not data limited. The ocean general circulation model (OGCM) results of Heimann and Maier-Reimer (1996) suggest that even with a large number of precise $\int\Delta\delta^{13}C$ and $\int\Delta\Delta^{14}C$ determinations, the correlation between $\int\Delta\delta^{13}C$ and $\int\Delta\Delta^{14}C$ will not improve by much (Fig. 5.1). The Hamburg model results indicate that the best estimate of depth-integrated oceanic $\delta^{13}C$ changes will likely be derived from global coverage of the $\delta^{13}C$ changes alone and won't rely on an oceanic $\int\Delta\delta^{13}C$ to $\int\Delta\Delta^{14}C$ relationship. The preformed $\delta^{13}C$ Suess effect reconstructions, however, are currently limited geographically to the subtropical and subpolar regions and have not been attempted in tropical waters. As a result, the reconstructed depth-integrated ^{13}C changes derived to date are biased towards the subtropical regions which exhibit higher than average depth-integrated ^{13}C (and ^{14}C) changes (Quay et al., 1992; Broecker et al., 1985). Similarly, uncertainties in the MLR method limited robust depth-integrated $\delta^{13}C$ change estimates to regions where the signal was large, i.e., the subtropical regions. At this time, therefore, we still rely on the $\int\Delta\Delta^{14}C$ extrapolation to obtain the best global $\int\Delta\delta^{13}C$ estimate.

Based on our three estimates of the $\delta^{13}C$ Suess effect, i.e., snapshot comparisons, MLR and preformed $\delta^{13}C$ reconstructions, the global mean penetration depth of the ^{13}C perturbation from 1970-1990, defined as the depth-integrated ^{13}C change (-158 ± 64 ‰ m) divided by the average surface change (-0.32 ± 0.05 ‰), was 490 ± 210 m, similar to the 520 ± 110 m reported by Quay et al. (1992). Broecker and Peng (1993) estimated a ^{13}C perturbation penetration depth of 570 m by 1990 by adjusting the global mean GEOSECS bomb ^{14}C penetration depth of 360 m (Broecker et al., 1985) for a longer "characteristic" time scale (~ 30 years, Fig. 1.1) of the atmospheric ^{13}C perturbation. Using a more appropriate characteristic ^{13}C perturbation time of ~ 20 years, i.e., the average time over which we quantified the $\delta^{13}C$ change, and the same square root of penetration time scaling as Broecker and Peng (1993), and Broecker et al.'s (1995) redetermination of the average GEOSECS bomb ^{14}C penetration depth, 391 m, yielded a ^{13}C perturbation penetration depth estimate that is similar to ours, i.e., 510 m, although the uncertainties in all of these estimates are substantial. Thus the $\delta^{13}C$ Suess effect changes we estimated by three methods for surface and thermocline waters yielded a mean penetration depth in good agreement with GEOSECS bomb ^{14}C measurements. A redetermination of the bomb ^{14}C penetration depth using WOCE data from the 1990s, as discussed above, should provide an additional useful comparison.

The Hamburg model results (Heimann and Maier-Reimer, 1996) highlight the biggest advantage of using $\int\Delta\delta^{13}C$ determinations rather than $\int\Delta\Delta^{14}C$ to determine oceanic CO_2 uptake rates. Based on Fig. 5.1, a precise determination of the oceanic Suess effect predicts the global ocean CO_2 uptake rate to within ± 0.3 Gt. C yr^{-1}, while the best you could hope to achieve using bomb ^{14}C would be a determination to within ~ ± 1.5 Gt. C yr^{-1}. Bomb ^{14}C inventories are attainable to within ± 10 % (Broecker et al., 1995), the same degree of precision attained in calculating $\int\Delta\delta^{13}C$ changes in the Indian Ocean using the MLR approach. Thus it appears likely that eventually, once better global coverage of the $\delta^{13}C$ Suess effect is attained, $\int\Delta\delta^{13}C$ will complement and perhaps replace bomb ^{14}C as a calibration tool for models studying oceanic uptake of fossil-fuel CO_2.

$^{13}CO_2$ versus $^{12}CO_2$

A ^{13}C budget for the ocean, atmosphere and terrestrial biosphere indicates that the ratio of the anthropogenic $\delta^{13}C$ perturbation to the anthropogenic DIC perturbations ($\Delta\delta^{13}C/\Delta DIC$) in the oceans depends on the turnover time of the terrestrial biosphere (Broecker and Peng, 1993; Keir et al., 1998). This dependence implies that combined reconstructions of the oceanic $\delta^{13}C$ and DIC changes would yield an estimate of the turnover time of the terrestrial biosphere. Highly accurate reconstructions of the anthropogenic $\delta^{13}C$ and $DI^{12}C$ changes, the latter done using modern coulometric DIC data (Gruber et al., 1996), could, potentially, provide an accurate determination of this ratio. To investigate this possibility, we calculated how well one could determine the $\Delta\delta^{13}C/\Delta DIC$ ratio using isopycnal trends in preformed DIC and $\delta^{13}C$ (equations 3.1 and 3.2, respectively). First, we assumed a representative surface ocean $\delta^{13}C$ Suess effect of -0.15 ‰ $decade^{-1}$ (chapters three and four). Next, since uncertainties in $\delta^{13}C^{\circ}$ and DIC° are both dependent on AOU (Table 3.2), we assumed an average oxygen utilization rate on the isopycnal of

4 μmol kg^{-1} yr^{-1} (chapter two). Assuming an average $\Delta\delta^{13}C/\Delta DIC$ ratio of -0.017 ‰ μmol^{-1} kg^{-1} (Fig. 5.1), we used a Monte Carlo procedure to evaluate how well one could determine $\Delta\delta^{13}C/\Delta DIC$ from isopycnal regressions of $\delta^{13}C°$ against DIC° values. We used a ± 1 σ uncertainty of 2 μmol kg^{-1} for coulometric DIC values and the uncertainties outlined in Table 3.2 for the remaining terms in equations 3.1 and 3.2.

For a typical isopycnal $\delta^{13}C°$ reconstruction (Table 3.4), where AOU was < 100 μmol kg^{-1}, the $\Delta\delta^{13}C/\Delta DIC$ ratio calculated by regressing ten calculated $\delta^{13}C°$ values against ten calculated DIC° values was -0.017 ± 0.003 ‰ μmol^{-1} kg^{-1}. The uncertainty improves to -0.017 ± 0.002 ‰ μmol^{-1} kg^{-1} when the number of samples collected is increased to ~ 25 and was relatively insensitive to the error in the DIC measurements. Additional samples (> 25) do not improve the $\Delta\delta^{13}C/\Delta DIC$ determination. At this level of precision, however, the preformed $\Delta\delta^{13}C/\Delta DIC$ ratio determination would constrain the terrestrial biosphere's Suess effect (Tables 3.5 and 4.3) to ± 30 % (Keir et al., 1998). The current uncertainty on this term is ± 60 % (Heimann and Maier-Reimer, 1996). Thus, evaluations of $\Delta\delta^{13}C°$ and $\Delta DIC°$ trends in the ocean could provide an improved constraint on the turnover time of the terrestrial biosphere. This would contribute another valuable piece of information to the global budget of fossil-fuel CO_2.

Another potentially useful application of oceanic $\Delta\delta^{13}C/\Delta DIC$ ratio determinations stems from the fact that the ocean-atmosphere $\delta^{13}C$ disequilibrium has been much easier to determine than the ocean-atmosphere pCO_2 disequilibrium. The average global air-sea $\delta^{13}C$

disequilibrium is presently -0.6 ± 0.15 ‰ (P. Quay, unpublished data), which is significantly larger than typical seasonal/spatial variability in surface water $\delta^{13}C$ values. This is in contrast for the situation for pCO_2, where the average disequilibrium, ~ 10 μatm, is significantly smaller than surface ocean seasonal and spatial variability (Takahashi, 1997).

The relationship between air-sea pCO_2 disequilibrium and $\Delta\delta^{13}C/\Delta DIC$ results from the observation that the oceanic $\Delta\delta^{13}C/\Delta DIC$ to a close approximation equals the ratio of the net air-sea $^{13}CO_2$ and $^{12}CO_2$ gas fluxes. The ocean average air-sea pCO_2 disequilibrium, in turn, is related to the net $^{13}CO_2$ and $^{12}CO_2$ gas exchange fluxes as follows:

$$\frac{Gas_{flux}{}^{13}CO_2}{Gas_{flux}{}^{12}CO_2}=\frac{G\gamma\alpha_{diff}\left\{pCO_2^{atm}R^{atm}\alpha_{gas}^{aq}-pCO_2^{aq}R^{DIC}\alpha_{DIC}^{CO_2g}\alpha_{gas}^{aq}\right\}}{G\gamma\left\{pCO_2^{atm}-pCO_2^{aq}\right\}} \tag{5.1}$$

Here, G represents the air-sea gas exchange rate, γ is CO_2 solubility, $pCO_2{}^{atm}$ and R^{atm}, and $pCO_2{}^{aq}$ and R^{DIC} represent CO_2 partial pressures and $^{13}C/^{12}C$ ratios in the atmosphere and surface ocean, respectively. The isotopic fractionation during CO_2 diffusion in seawater, α_{diff}, the fractionation during CO_2 dissolution, α_{gas}^{aq}, and the fractionation during seawater DIC to CO_2 gas speciation, $\alpha_{DIC}^{CO_2g}$, have been experimentally determined (Zhang et al., 1995).

The ratio of the net $^{13}CO_2$ and $^{12}CO_2$ gas fluxes can be determined from the oceanic $\Delta\delta^{13}C/\Delta DIC$ perturbation ratios via a simple mass-balance calculation. If $\Delta\delta^{13}C/\Delta DIC$ can be determined to within ± 0.003 ‰ $\mu mol^{-1}\ kg^{-1}$, as discussed above, the average ocean-atmosphere ΔpCO_2 ($pCO_2^{atm}-pCO_2^{aq}$)

was determined to 8.4 ± 2.6 μatm by solving equation (5.1) for pCO_2^{aq} using the air-sea $\delta^{13}C$ disequilibrium and uncertainty above. Coupled with a global ocean average CO_2 gas exchange rate ($G\gamma$ in equation (5.1)) of 0.067 moles CO_2 m^{-2} yr^{-1} μatm^{-1} (Tans et al., 1990), this yielded a relatively precise net oceanic CO_2 uptake rate estimate of 2.2 ± 0.7 Gt. C yr^{-1}. The above calculations neglected riverine carbon fluxes which add about 0.5 Gt. C yr^{-1} (Sarmiento and Sundquist, 1992) of organic carbon whose $\delta^{13}C \approx -28$ ‰ (Heimann and Maier Reimer, 1996) to the oceans. Accounting for this carbon flux by including it in equation 5.1 reduced the air-sea ΔpCO_2 only slightly (to 7.8 ± 2.6 μatm) although the total (rivers + net gas flux) ocean CO_2 uptake rate increased to 2.5 ± 0.7 Gt. C yr^{-1}.

The primary source of uncertainty in the above CO_2 uptake rate calculations was in the determination of the $\Delta\delta^{13}C/\Delta DIC$ ratio. Thus we recommend that some target isopycnals be sampled at very high resolution for $\delta^{13}C$, DIC, O_2, and nutrient and hydrographic data such that the highest possible precision $\delta^{13}C°/DIC°$ regressions can be achieved. Since CFC ages are not required for this determination, the reconstructions can be extended to older waters. The Hamburg model results discussed above (Fig. 5.1) indicate that the $\Delta\delta^{13}C/\Delta DIC$ ratio in the oceans is reasonably uniform. Isopycnals or water masses exhibiting a range of $\delta^{13}C$ change rates (Table 3.4) should be sampled to confirm this and establish the range of likely oceanic $\Delta\delta^{13}C/\Delta DIC$ values. Because this approach does not rely on CFC ages, the geographic and depth range of the $\delta^{13}C°/DIC°$ approach should be extended to deeper waters where $\delta^{13}C°$ reconstructions (chapter three) were not attempted.

$\delta^{13}C$ Suess effect estimates based on preformed $\delta^{13}C$ reconstructions

In order to improve the accuracy of oceanic CO_2 uptake rates based on $\delta^{13}C$, we need improved Suess effect determinations. An error of ± 1 Gt. C yr^{-1} is derived from uncertainties of ± 0.02 ‰ $decade^{-1}$ in the global ocean surface water $\delta^{13}C$ Suess effect (Bacastow et al., 1996) and ± 3 ‰ m yr^{-1} in the depth-integrated $\delta^{13}C$ Suess effect (Quay et al., 1992). A Suess effect estimate precise to within ± 0.02 ‰ $decade^{-1}$ was achieved at some locations, including the South Pacific south of 55°S, using the preformed ^{13}C reconstruction method (chapter three). Since high quality $\delta^{13}C$ data from the past is limited in many regions, like the North Atlantic, the only available estimates of the $\delta^{13}C$ change are based on $\delta^{13}C$ reconstructions (chapter three; Keir et al., 1998). In the South Atlantic, there is very little recent high quality $\delta^{13}C$ of DIC data south of 40°S so even $\delta^{13}C^{\circ}$ reconstructions cannot be made. A modern meridional South Atlantic section that included $\delta^{13}C$ of DIC and CFCs would make a significant improvement to the global data base of oceanic Suess effect estimates presented in this dissertation. Based on the South Atlantic Antarctic Intermediate Water salinity and CFC distributions mapped by Warner and Weiss (1992), a CFC, $\delta^{13}C$ of DIC, θ, S and O_2 section sampled intensively, and perhaps focused by continuously monitoring CFC-derived ages, on a few target isopycnals within and above the Antarctic Intermediate Water along the prime meridian between 60°S and 20°S would provide an optimal data set for $\delta^{13}C^{\circ}$ versus CFC age reconstructions.

Certainly there are opportunities to improve the $\delta^{13}C^{\circ}$ reconstruction method. For example, in some instances mixing limitations could be overcome, or at least evaluated, by using along-isopycnal ventilation models such as the one-dimensional model presented in chapter two. Such modeling efforts would also allow estimates of $\delta^{13}C$ changes in waters whose mean ages are older than 1970. CFC-113 has the potential to extend the useful dating range to waters ventilated after 1991. Similarly, recent developments in quantifying the non-conservative behavior (Lee, 1998) and solubility (Bullister and Wisegarver, 1999) of CCl_4 potentially allow dating of waters subducted prior to 1970 (Fig. 5.2). At the very least, the influence of along-isopycnal mixing with other end members could potentially be excluded using S or NO, as discussed in chapter three, if the excluded waters contain no CCl_4, and thus have likely experienced no anthropogenic $\delta^{13}C$ change. Deep water reconstructions over more extensive age ranges than those performed in chapter three offer the best potential for accurately determining the oceanic $\Delta\delta^{13}C/\Delta DIC$ ratio, as discussed above.

Another possible application of the $\delta^{13}C^{\circ}$ approach is in providing estimates of the time-history of the ocean-atmosphere $\delta^{13}C$ disequilibrium. Since oceanic uptake of fossil fuel CO_2 can be determined from this disequilibrium at any one point in time, using either an atmospheric $^{12}CO_2$ and $^{13}CO_2$ budget (Tans et al. 1993) or the $\Delta\delta^{13}C/\Delta DIC$ ratio as discussed above, these estimates could be applied, potentially, to provide a rough estimate of temporal changes in oceanic CO_2 uptake rates. In chapters three and four, we found that during the 1970s and 1980s, the time rate of change of surface water $\delta^{13}C$ at high latitudes, ~ -0.1 ‰ decade^{-1}, lagged the change rate in the atmosphere, -0.23 ‰ decade^{-1} (Fig. 1.3; Keeling et al., 1989). Based on

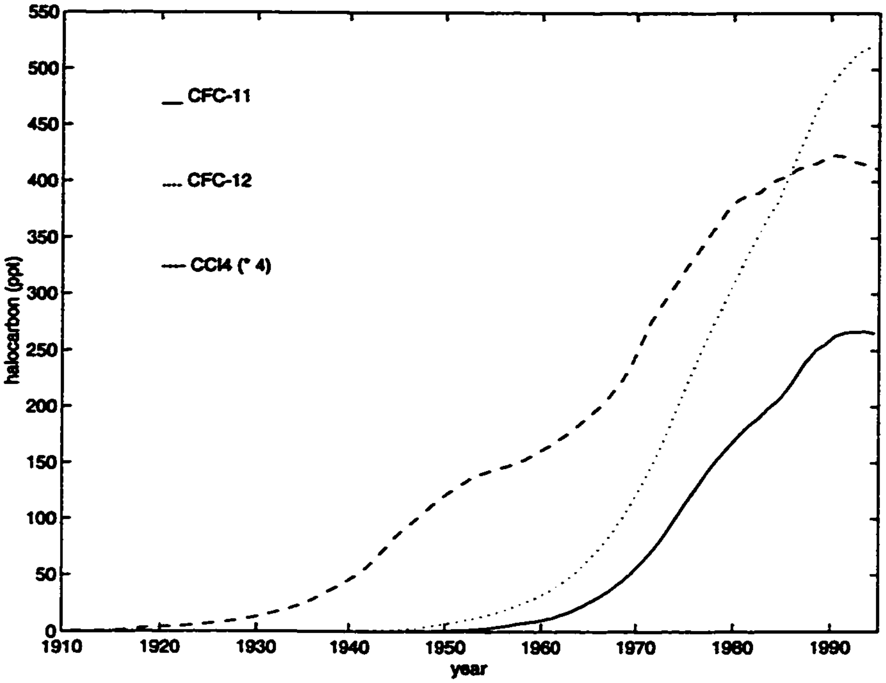

Figure 5.2. Atmospheric CFC-11 (solid line), CFC-12 (dotted line) and CCl_4 (dashed line) in the Northern Hemisphere. During the time period 1920-1980, these values are based on industrial production and release estimates, while the post-1980 values are based on direct measurements (Walker et al., 1995).

$\delta^{13}C°$ reconstructions, snapshot comparisons and the MLR approach the average surface ocean $\delta^{13}C$ is decreasing by -0.15 ‰ decade^{-1}. Thus the atmosphere-ocean $\delta^{13}C$ disequilibrium, on average, is increasing by ~ - 0.08 ‰ decade^{-1}, a rate of change that is detectable in $\delta^{13}C°$ distributions.

Multiparameter-linear regression based data set comparisons

In the Indian Ocean, the minimum uncertainty in our MLR-derived surface water $\delta^{13}C$ change estimates was ± 0.1 ‰ north of 40°S. The calculated Suess effect of ~ 0.15 ‰ decade^{-1}, indicates that the time interval between the Indian Ocean GEOSECS and WOCE expeditions (about 17.5 years) was the minimum necessary to resolve the $\delta^{13}C$ Suess effect using the MLR approach. Although the uncertainties in the Suess effect calculated using this approach are relatively large, however, the MLR approach is more robust from a practical and statistical viewpoint than the preformed $\delta^{13}C$ approach because no a-priori assumptions about Redfield ratios of remineralization or the $\delta^{13}C$ of organic matter are required. More importantly, the MLR approach explicitly handles oceanic mixing problems provided that overall oceanic circulation patterns remain relatively constant in time. Finally, the approach does not rely on transient-tracer derived dating methods. Thus, this approach can be applied over geographical and depth ranges where the preformed $\delta^{13}C$ approach was not applicable. Although the MLR approach does rely on $\delta^{13}C$ data sets from the past, it affords greater geographical coverage than the direct station-to-station comparisons allow. The MLR approach's most promising application is validating, correcting and extrapolating the more precise snapshot comparison and preformed $\delta^{13}C$ approaches. In the Pacific Ocean, for example, there were only seven high quality $\delta^{13}C$ of DIC depth profiles from > 15 years ago available (Quay et al., 1992). Because the seasonal timing and locations of the 1970 $\delta^{13}C$ measurements (Kroopnick et al., 1977; Kroopnick, 1974) do not coincide well with WOCE $\delta^{13}C$ measurements made in the 1990s, the MLR approach should definitely be applied in the Pacific basin. There the MLR approach is currently the only means available for estimating the $\delta^{13}C$ Suess effect in high latitude, tropical and deep waters. The spatial distribution of the $\delta^{13}C$ Suess effect that can be derived from the

MLR approach (Fig. 4.10) may provide the most useful Suess effect estimates for evaluating OGCM simulations of $\delta^{13}C$ uptake.

The primary limitation of the MLR approach is the relatively large uncertainties in the calculated $\delta^{13}C$ differences between the two sampling times. The signal-to-noise ratio for the MLR comparison performed in the Indian Ocean was < 3 (chapter four). The primary source of error was uncertainty in the regression predicted $\delta^{13}C$ values, which was more than twice the uncertainties in measured $\delta^{13}C$ values. Likely sources of uncertainties in predicted $\delta^{13}C$ values may have been variability in the surface ocean gas exchange boundary condition for $\delta^{13}C$, variability in carbon isotopic composition of phytoplankton in the Southern Ocean (Goericke and Fry, 1994), and uncertainties in determining composite deep water offsets between cruises. As discussed in chapter four, deep water CCl_4 measurements would be helpful in diagnosing the causes for the offsets between deep water $\delta^{13}C$ values predicted by the 1970s and 1990s tuned MLR equations.

Generally, there is a trade off between predictive skill and spatial coverage in applying the MLR approach. When the MLR equation is applied to data over more limited spatial scales, the quality of the fit improves markedly. For example, when we tuned the MLR equation to the entire WOCE I8N and I8S/I9S $\delta^{13}C$, θ, S, O_2, PO_4 and AOU data set, the 1 σ error in the was ± 0.11 ‰ (chapter four). When we tuned the MLR equation to the WOCE I8N θ, S, O_2, PO_4 and AOU data from 20°S to 30°S only, the fit improved to ± 0.044 ‰. This level of accuracy is very close to the measurement precision. Thus, more accurate Suess effect determinations than those presented in chapter four are possible if the geographical scale of the predictions are reduced. In some instances, several limited scale predictions could be combined to yield a more accurate large scale $\delta^{13}C$ change prediction. Also, a more geographically limited, and thus more accurate, MLR calculation of the $\delta^{13}C$ and DIC change between GEOSECS and WOCE could, potentially, yield highly accurate regional estimates of the oceanic $\Delta\delta^{13}C/\Delta DIC$ ratio. This ratio could be used to derive improved ocean-atmosphere ΔpCO_2 and terrestrial biosphere Suess effect estimates, as discussed above.

Concluding remarks

In calculating the surface ocean Suess effect in the Indian Ocean we found that although the MLR and $\delta^{13}C^{\circ}$ approaches agreed with each other (Fig. 4.11), they did not agree with the $\delta^{13}C$ changes deduced from two snapshot measurements in 1978 and 1995. The discrepancy likely arises from the snapshot approach's susceptibility to aliasing of seasonal and spatial variability in surface $\delta^{13}C$ values. In contrast, the surface ocean $\delta^{13}C$ changes reconstructed from preformed $\delta^{13}C$ distributions and CFC ages agreed well with direct measurements of the $\delta^{13}C$ change in the Pacific when the two sections were occupied in the same locations *and* in the same season 23 years apart (Figs. 3.7 and 3.8). Also, we found excellent agreement among all three approaches in determining the depth-integrated $\delta^{13}C$ Suess effect (chapter four). Given that the uncertainties in all of the approaches are large, the agreement is encouraging because each method relies on considerable, yet independent, assumptions. Furthermore, the observed agreement in the Pacific and Indian Oceans provides confidence in both the surface and depth-integrated ^{13}C reconstructions made for the Atlantic Ocean using the $\delta^{13}C^{\circ}$ approach, where the only available estimate of the oceanic δ^{13}C Suess effect was the time series of surface water δ^{13}C at Bermuda (Bacastow et al., 1996).

When Quay et al. (1992) published their work calculating the integrated δ^{13}C DIC change in the Pacific Ocean, there was a significant signal-to-noise advantage in determining the oceanic δ^{13}C of DIC change over determining changes in DIC (Tans et al., 1993). Recent improvements in the accuracy and precision of DIC determinations (Johnson et al., 1993) have narrowed this gap. The ratio of the $\Delta\delta^{13}$C to ΔDIC perturbations in the oceans is probably about ~ -0.016 ‰ per μmol kg^{-1} (Keir et al., 1998). Since modern DIC and δ^{13}C determinations are typically precise to ± 2 μmol kg^{-1} (Goyet and Brewer, 1993) and ± 0.03 ‰, respectively, the signal-to-noise ratios in using either of these tracers to determine the anthropogenic perturbation are, based on analytical limitations alone, equivalent. There is, however, a signal-to-noise advantage in calculating changes in preformed δ^{13}C rather than in preformed DIC. For example, in a water sample whose AOU is 100 μmol kg^{-1}, the signal-to-noise in the calculated $\delta^{13}C^{\circ}$ and DIC° changes since the sample left the surface are ~ 8 and ~ 5, respectively, using the uncertainties calculated in chapter three and by Gruber et al. (1996). Also, in comparing modern day data to older data, δ^{13}C's signal-to-noise advantage is more pronounced because older δ^{13}C data were measured to about the same precision, ± 0.03 ‰, and the older δ^{13}C data were normalized to the same Pee-Dee Belemnite standard (Kroopnick et al., 1977). Older DIC data, on the other hand, is rarely accurate to better than ± 10 μmol kg^{-1} (Brewer, 1978) and universal calibration standards for DIC determinations have only recently been developed (Dickson, 1990). Still, the fact that coulometric DIC data are less expensive and therefore more plentiful than $\delta^{13}C$ of DIC data, coupled with the need for either modeling or budgeting approaches to derive an estimate of the $^{12}CO_2$ change in the ocean from $\delta^{13}C$ changes, means that ultimately the most extensive oceanic CO_2 perturbation estimates will be derived from reconstructions or calculations of the $^{12}CO_2$ change. However, at present the $\delta^{13}C$ perturbation provides an independent estimate of the still highly uncertain rate of CO_2 uptake in the oceans. In the future, oceanic $\delta^{13}C$ change determinations will likely replace bomb ^{14}C as a benchmark for fossil fuel CO_2 uptake in ocean models. Finally, determinations of the ratio of the $\delta^{13}C$ to DIC perturbations in the ocean promise better constraints on the ocean-atmosphere CO_2 disequilibrium, and will be useful in constraining CO_2 fluxes through the terrestrial biosphere.

Citations

Anderson, L. A. and J. L. Sarmiento (1994) Redfield ratios of remineralization determined by nutrient data analysis. *Global Biogeochem. Cycles,* **8**, 1, 65-80.

Armi, L. and H. Stommel (1983) Four views of a portion of the North Atlantic subtropical gyre. *J. Phys. Ocean.,* **13**, 828-857.

Bacastow, R. B., C. D. Keeling, T. J. Lueker, M. Wahlen and W. G. Mook (1996) The $\delta^{13}C$ Suess effect in the world surface oceans and its implications for oceanic uptake of CO_2: analysis of observations at Bermuda. *Global Biogeochem. Cycles,* **10**, 2, 335-346.

Bonneau, M. -C., C. Bergnaud-Grazzini and W. H. Berger (1980) Stable isotope fractionation and differential dissolution in recent planktonic foraminifera from Pacific box cores. *Oceanologica Acta,* **3**, 377-382.

Brandes, J. A. G. (1996) Isotopic effects of denitrification in the marine environment. *Ph. D. Dissertation,* University of Washington.

Brewer, P. G., C. Goyet and G. Friederich (1997) Direct observation of the oceanic CO_2 increase revisited. *Proc. Natl. Acad. Sci. USA,* **94**, 8308-8313.

Brewer, P. G. (1978) Direct observation of the oceanic CO_2 increase. *Geophys. Res. Lett.,* **5**, 12, 997-1000

Broecker, W. S., S. Sutherland, W. Smethie, T. -H. Peng and G. Östlund (1995) Oceanic radiocarbon: separation of the natural and bomb components. *Global Biogeochem. Cycles,* **9**, 2, 263-288.

Broecker, W. S. and T. -H. Peng (1993) Evaluation of the ^{13}C constraint on the uptake of fossil-fuel CO_2 by the ocean. *Global Biogeochem. Cycles,* **7**, 3, 619-626.

Broecker, W. S., T. -H. Peng, G. Östlund and M. Stuiver (1985) The distribution of bomb radiocarbon in the Ocean. *J. Geophys. Res.,* **90**, C4, 6953-6970.

Broecker, W. S. and T. -H. Peng (1982) *Tracers in the Sea.* Eldigio Press, Lamont-Doherty Geological Observatory, Palisades, N.Y., 690 pp.

Broecker, W. S. (1974) "NO", a conservative water mass tracer. *Earth Planet. Sci. Lett.,* **23**, 100-107

Bullister, J. L. and D. P. Wisegarger (1999) The solubility of carbon tetrachloride in water and seawater, *Deep-Sea Res.,* **46**, in press.

Bullister, J. L. and R. F. Weiss (1988) Determination of CCl_3F and CCl_2F_2 in seawater and air. *Deep-Sea Res.*, **35**, 5, 839-853.

Böhm, F., M. M. Joachimski, H. Lehnert, G. Morgenroth, W. Kretschmer, J. Vacelet and W. -Chr Dullo (1996) Carbon isotope records from extant Caribbean and South Pacific sponges: Evolution of $\delta^{13}C$ in surface water DIC. *Earth Planet. Sci. Lett.*, **139**, 291-303.

Castle, R. D., R. Wanninkhof, J. L. Bullister, S. C. Doney, R. A. Feely, B. E. Huss, E. Johns, F. J. Millero, D. Frazel, D. Wisegarver, D. Greely, F. Menzia, M. Lamb, G. Berberian and L. D. Moore Jr. (1998) Chemical and Hydrographic Profiles and Underway Measurements from the Eastern North Atlantic during July and August of 1993. NOAA Data Report ERL AOML-32, 53 pp.

Chavez, F. P. and R. T. Barber (1987) An estimate of new production in the Equatorial Pacific. *Deep-Sea Res.*, **34**, 7, 1229-1243.

Ciais, P., P. P. Tans, M. Trolier, J. W. C. White and R. J. Francey (1995) A large northern hemisphere terrestrial CO_2 sink indicated by the $^{13}C/^{12}C$ ratio of atmospheric CO_2. *Science*, **269**, 1098-1102.

Chen, C. -T. A. and R. M. Pytkowicz (1979) On the total CO_2-titration alkalinity-oxygen system in the Pacific Ocean. *Nature*, **281**, 362-365.

Chen, C. -T. and F. J. Millero (1979) Gradual increase of oceanic CO_2. *Nature*, **277**, 205-206.

Chen, C. -T. A. (1982) Oceanic penetration of excess CO_2 in a cross section between Alaska and Hawaii. *Geophys. Res. Lett.*, **9**, 2, 117-119.

Chen, C. -T. A., F. J. Millero and R. M. Pytkowicz (1982) Comment on calculating the oceanic CO_2 increase: as need for caution by A. M. Shiller. *J. Geophys. Res.*, **87**, C3, 2083-2085.

Coats, D. A. (1981) An estimate of absolute geostrophic velocity from the density field in the northeastern Pacific Ocean. *J. Geophys. Res.*, **86**, C9, 8031-8036.

Codispoti, L. A. and F. A. Richards (1973) An analysis of the horizontal regime of denitrification in the eastern tropical North Pacific. *Limnol. Oceanogr.*, **21**, 379-388.

Craig, H. (1957) Isotopic standards for carbon and oxygen and correction factors for mass spectrometric analysis of carbon dioxide. *Geochim. Cosmochim. Acta*, **6**, 186-196.

Cunnold, D. M., P. J. Fraser, R. F. Weiss, R. G. Prinn, P. G. Simmonds, B. R. Miller, F. N. Alyea and A. J. Crawford (1994) Global trends and annual releases of CCl_3F and CCl_2F_2 estimated from ALE/GAGE and other measurements from July 1978 to June 1991. *J. Geophys. Res.*, **99**, D1, 1107-1126.

Dickson, A. G. (1990) The oceanic carbon dioxide system: planning for quality data. *U. S. JGOFS News*, **2**, 2.

Doney, S. C. and J. L. Bullister (1992) A chlorofluorocarbon section in the eastern North Atlantic. *Deep-Sea Res.*, **39**, 1857-1883.

Druffel, E. R. M., P. M. Williams, J. E. Bauer and J. R. Ertel (1992) Cycling of dissolved and particulate organic matter in the open ocean. *J. Geophys. Res.*, **97**, C10, 15639-15659.

Druffel, E. R. M. and L. M. Benavides (1986) Input of excess CO_2 to the surface ocean based on $^{13}C/^{12}C$ ratios in a banded Jamaican sclerosponge. *Nature*, **321**, 58-61.

Emerson, S., P. Quay, D. Karl, C. Winn, L. Tupas and M. Landry (1997) Experimental determination of the organic carbon flux from open-ocean surface waters. *Nature*, **389**, 951-954.

Fine, R. A., J. L. Reid and H. G. Östlund (1981) Circulation of tritium in the Pacific Ocean. *J. Phys. Ocean.*, **11**, 3-14.

Fletcher, C. A. J. (1988) *Computational techniques for fluid dynamics*, Springer-Verlag, New York 409 pp.

Folsom, T. R. (1979) Some measurements of global fallout suggesting characteristics of the North Pacific controlling dispersal rates of certain surface pollutants. U. S. Department of Energy Environmental Quarterly Reports, EML-356, 99 pp.

Frees, E. W. (1996) *Data analysis using regression models.* Prentice Hall, Englewood Cliffs, NJ.

Friedli, H., H. Lötscher, H. Oeschger, U. Siegenthaler and B. Stauffer (1986) Ice core record of the $^{13}C/^{12}C$ ratio of atmospheric CO_2 in the past two centuries. *Nature*, **324**, 237-238.

Gammon, R. H., J. Cline and D. Wisegarver (1982) Chlorofluoromethanes in the Northeast Pacific Ocean: measured vertical distributions and application as transient tracers of upper ocean mixing. *J. Geophys. Res.*, **87**, C12, 9441-9454.

Goericke, R. and B. Fry (1994) Variations of marine plankton $\delta^{13}C$ with latitude, temperature, and dissolved CO_2 in the world ocean. *Global Biogeochem. Cycles,* **8**, 1, 85-90.

Goyet, C. and P. G. Brewer (1993) Biochemical properties of the oceanic carbon cycle. In: *Modeling Oceanic Climate Interactions,* J. Willebrand and D. L. T. Anderson, editors. NATO series I11, Springer, Berlin, pp. 271-297.

Gruber, N., J. L. Sarmiento and T. F. Stocker (1996) An improved method for detecting anthropogenic CO_2 in the oceans. *Global Biogeochem. Cycles,* **10**, 4, 809-837.

Gruber, N. (1998) Anthropogenic CO_2 in the Atlantic Ocean. *Global Biogeochem. Cycles,* **12**, 1, 165-191.

Hansell, D. A. and T. Y. Waterhouse (1997) Controls on the distributions of organic carbon and nitrogen in the eastern Pacific Ocean. *Deep-Sea Res. I,* **44**, 5, 843-857.

Hecht, M. W., W. R. Holland and P. J. Rasch (1995) Upwind-weighted advection schemes for ocean tracer transport: an evaluation in a passive tracer context. *J. Geophys. Res.,* **100**, C10, 20763-20778.

Heimann, M. and E. Maier-Reimer (1996) On the relations between the oceanic uptake of CO_2 and its carbon isotopes. *Global Biogeochem. Cycles,* **10**, 1, 89-110.

Hellerman, S. and M. Rosenstein (1983) Normal monthly wind stress over the world ocean with error estimates. *J. Phys. Ocean.,* **13**, 1093-1104.

Houghton, J. T., L. G. Meira Filho, J. Bruce, Hoesung Lee, B. A. Callander, E. Haites, N. Harris and K. Maskell (Eds.), *Climate Change 1994: Radiative Forcing of Climate Change and An Evaluation of the IPCC IS92 Emission Scenarios,* Cambridge University Press, New York, 1995.

Huang, R. X. and B. Qiu (1994) Three-dimensional structure of the wind-driven circulation in the subtropical North Pacific. *J. Phys. Ocean.,* **24**, 1608-1622.

Jenkins, W. J. (1991) Determination of isopycnal diffusivity in the Sargasso Sea. *J. Phys. Ocean.,* **21**, 1058-1061.

Jenkins, W. J. (1987) ^3H and ^3He in the Beta Triangle: observations of gyre ventilation and oxygen utilization rates. *J. Phys. Ocean.,* **17**, 763-783.

Johnson, K. M., K. D. Wills, D. B. Butler, W. K. Johnson and C. S. Wong (1993) Coulometric total carbon dioxide analysis for marine studies: maximizing the performatnce of an automated gas-extraction system and coulometric detector. *Mar. Chem.*, **44**, 167-188.

Jones, G. A., A. R. Gagnon, R. J. Schneider, K. F. von Reden and A. P. McNichol (1994) High-precision AMS radiocarbon measurements of central Arctic Ocean sea waters. *Nuclear Instruments and Methods in Physics Research*, **B92**, 426-430.

Joos, F. and M. Bruno (1998) Long-term variability of the terrestrial and oceanic carbon sinks and the budgets of the carbon isotopes ^{13}C and ^{14}C. *Global Biogeochem. Cycles*, **12**, 2, 277-295.

Karl, D. M., R. Letelier, D. Hebel, L. Tupas, J. Dore, J. Christian and C. Winn (1995) Ecosystem changes in the North Pacific subtropical gyre attributed to the 1991-1992 El Niño. *Nature*, **373**, 230-234.

Keeling, C. D., R. B. Bacastow, A. F. Carter, S. C. Piper, T. P. Whorf, M. Heimann, W. G. Mook and H. Roeloffzen (1989) A three-dimensional model of atmospheric CO_2 transport based on observed winds: 1. Analysis of observational data. In: *Aspects of climate variability in the Pacific and the Western Americas*, D. H. Peterson, editor, American Geophysical Union, Monograph #55, 165-236.

Keeling, R. F., S. C. Piper and M. Heimann (1996) Global and hemispheric CO_2 sinks deduced from changes in atmospheric O_2 concentration. *Nature*, **381**, 218-221.

Keir, R. S., G. Rehder, E. Suess and H. Erlenkeuser (1998) The $\delta^{13}C$ anomaly in the Northeastern Atlantic. *Global Biogeochem. Cycles*, **12**, 3, 467-477.

Kroopnick, P. M. (1985) The distribution of $\delta^{13}C$ of ΣCO_2 in the world oceans. *Deep-Sea Res.*, **32**, 1, 57-84.

Kroopnick, P. (1980), The distribution of ^{13}C in the Atlantic Ocean. *Earth Planet. Sci. Lett.*, **49**, 469-484.

Kroopnick, P. M., S. V. Margolis and C. S. Wong (1977) In: *The Fate of Fossil Fuel CO_2 in the oceans*, N. Andersen and A. Malahoff, editors, Plenum Publishing Company, New York, 295-321.

Laws, E. A. (1991) Photosynthetic quotients, new production and net community production in the open ocean. *Deep-Sea Res.*, **38**, 1, 143-167.

Ledwell, J. R., A. J. Watson and C. S. Law (1993) Evidence for slow mixing across the pycnocline from an open-ocean tracer-release experiment. *Nature*, **364**, 701-703.

Lee, B. S. (1998) Uses of chlorofluorocarbons as ocean tracers and for estimating the removal rates of CFC-11 and carbon tetrachloride in certain marine environments. *Ph. D. Dissertation,* University of Washington.

Levitus, S., R. Burgett and T. Boyer (1994), NOAA Atlas NESDIS 3: World ocean atlas 1994, vol. 3, Salinity. Tech. Rep., Natl. Oceanic and Atmos. Admin., Silver Spring, Md.

Levitus, S. and T. Boyer (1994a) NOAA Atlas NESDIS 3: World ocean atlas 1994, vol. 4, Temperature. Tech. Rep., Natl. Oceanic and Atmos. Admin., Silver Spring, Md.

Levitus, S. and T. Boyer (1994b) NOAA Atlas NESDIS 2: World ocean atlas 1994, vol 2., Oxygen. Tech Rep., Natl. Oceanic and Atmos. Admin., Silver Spring, Md.

Levitus, S. (1982) Climatological atlas of the world ocean. NOAA Professional Paper No. 13, U.S. Dept. of Commerce, Washington, D.C., 173 pp.

Linick, T. W. (1978) La Jolla measurements of radiocarbon in the oceans. *Radiocarbon,* **20,** 3, 333-359.

Luyten, J. R., J. Pedlosky and H. Stommel (1983) The ventilated thermocline. *J. Phys. Ocean.,* **13,** 292-309.

Lynch-Stieglitz, J., T. F. Stocker, W. S. Broecker and R. G. Fairbanks (1995) The influence of air-sea exchange on the isotopic composition of oceanic carbon: Observations and modeling. *Global Biogeochem. Cycles,* **9,** 653-665.

Martin, J. H., G. A. Knauer, D. M. Karl and W. W. Broenkow (1987) VERTEX: carbon cycling in the Northeast Pacific. *Deep-Sea Res.,* **34,** 2, 267-285.

Masuzawa, J. (1969) Subtropical mode water. *Deep-Sea Res.,* **16,** 463-472.

McNichol, A. P. and G. A. Jones (1991) Measuring ^{14}C in seawater by accelerator mass spectrometry. WOCE Hydrographic Operations and Methods Manual, WOCE Hydrographic Programme Office, WOCE Report No. 68/91, Woods Hole Oceanographic Institution, Woods Hole, MA.

McNichol, A. P., G. A. Jones, D. L. Hutton, D. L. Gagnon and R. M. Key (1994) The rapid preparation of seawater TCO_2 for radiocarbon analysis at the National Ocean Sciences AMS Facility. *Radiocarbon,* **36,** 2, 243-246.

McCartney, M. S. (1982) The subtropical recirculation of Mode Waters. *J. Mar. Res.,* **40,** suppl., 427-464.

Michel, R. L. and H. E. Suess (1975) Bomb tritium in the Pacific Ocean. *J. Geophys. Res.,* **80,** 4139-4152.

National Ocean Sciences AMS Facility (NOSAMS)(1994a) Radiocarbon results, WOCE report 1 (P16N). Data report #94-091.

National Ocean Sciences AMS Facility (1994b) Radiocarbon results, WOCE report 3 (P17C). Data report #94-093.

National Ocean Sciences AMS Facility (1995) Radiocarbon results, WOCE report 8 (P13). Data report #95-085.

National Ocean Sciences AMS Facility (1996) Radiocarbon results, WOCE report 9 (P16C and P16S). Data report #96-019.

Oeschger, H., U. Siegenthaler, U. Schotterer and A. Gugelmann (1975) A box diffusion model to study the carbon dioxide exchange in nature. *Tellus*, **27**, 168-192.

Östlund, H. G. and M. Stuiver (1980) GEOSECS Pacific radiocarbon. *Radiocarbon*, **22**, 25-53.

Quay, P. D., B. Tilbrook and C. S. Wong (1992) Oceanic uptake of fossil-fuel CO_2: carbon-13 evidence. *Science*, **256**, 74-79.

Reid, J. L. Jr. (1973) The shallow salinity minima of the Pacific Ocean. *Deep-Sea Res.*, **20**, 51-68.

Reid, J. L. Jr. (1969) Sea-surface temperature, salinity, and density of the Pacific Ocean in summer and in winter. *Deep-Sea Res.*, **16** suppl., 215-224.

Reid, J. L. Jr. (1965) Intermediate waters of the Pacific Ocean. *Johns Hopkins Oceanographic Studies*, **2**, 85 pp.

Roemmich, D. and T. McCallister (1989) Large scale circulation of the North Pacific Ocean. *Prog. Ocean.*, **22**, 171-204.

Sabine, C. L, A. G. Dickson, C. Goyet, P. Guenther, K. M. Johnson, R. M. Key, F. J. Millero, J. L. Sarmiento, D. R. Wallace and C. D. Winn (1998) The role of the Indian Ocean as a sink for anthropogenic carbon dioxide. *EOS, Trans., Am. Geophys. Union.*

Sarmiento, J. L. and E. T. Sundquist (1992) Revised budget for the oceanic uptake of anthropogenic carbon dioxide. *Nature*, **356**, 589-593.

Shaffer, G., J. Bendtsen and O. Ulloa (1998) Fractionation during remineralization of organic matter in the Ocean. *Deep-Sea Res.*, in press.

Shiller, A. M. (1981) Calculating the oceanic CO_2 increase: a need for caution. *J. Geophys. Res.*, **86**, C11, 11083-11088.

Siegenthaler, U. and J. L. Sarmiento (1993) Atmospheric carbon dioxide and the ocean. *Nature*, **365**, 119-125.

Slansky, C. M., R. A. Feely and R. Wanninkhof (1997) The stepwise linear regression method for calculating anthropogenic CO_2 invasion into the North Pacific Ocean. In: *Biogeochemical Processes in the North Pacific*, S. Tsunogai, editor. Japan Marine Science Foundation, pp. 70-79.

Smith, W. H. F. and P. Wessel (1990) Gridding with continuous curvature splines in tension. *Geophysics*, **55**, 293-305.

Stommel, H. M. (1979) Determination of water mass properties of water pumped down from the Ekman layer to the geostrophic flow below. *Proc. Natl. Acad. Sci. USA*, **76**, 3051-3055.

Suga, T., K. Hanawa and Y. Toba (1989) Subtropical mode water in the 137°E section. *J. Phys. Ocean.*, **19**, 1605-1618.

Takahashi, T., R. A. Feely, R. F. Weiss, R. H. Wanninkhof, D. W. Chipman, S. C. Sutherland and T. T. Takahashi (1997) Global air-sea flux of CO_2: an estimate based on measurements of sea-air pCO_2 difference. *Proc. Natl. Acad. Sci. USA*, **94**, 8292-8299.

Takahashi, T., W. S. Broecker and S. Langer (1985) Redfield ratio based on chemical data from isopycnal surfaces. *J. Geophys. Res.*, **90**, C4, 6907-6924.

Talley, L. D. (1995) Some advances in understanding of the general circulation of the Pacific Ocean, with emphasis on recent U. S. contributions. *Rev. Geophys.*, suppl., 1335-1352.

Talley, L. D. (1993) Distribution and formation of North Pacific intermediate water. *J. Phys. Ocean.*, **23**, 517-537.

Talley, L. D. (1988) Potential vorticity distribution in the North Pacific. *J. Phys. Ocean.*, **18**, 89-106.

Talley, L. D. (1985) Ventilation of the subtropical North Pacific: the shallow salinity minimum. *J. Phys. Ocean.*, **15**, 1-17.

Tans, P. P., and J. W. C. White (1998) In balance, with a little help from plants. *Science*, **281**, 183-184.

Tans, P. P., J. A. Berry and R. F. Keeling (1993) Oceanic $^{13}C/^{12}C$ observations: a new window on ocean CO_2 uptake. *Global Biogeochem. Cycles*, **7**, 2, 353-368.

Tans, P. P., I. Y. Fung and T. Takahashi (1990) Observational constraints on the global atmospheric CO_2 budget. *Science*, **247**, 1431-1438.

Thiele, G. and J. L. Sarmiento (1990) Tracer dating and ocean ventilation. *J. Geophys. Res.*, **95**, C6, 9377-9391.

Toole, J. M., K. L. Polzin and R. W. Schmitt (1994) Estimates of diapycnal mixing in the abyssal ocean. *Science*, **264**, 1120-1123.

Tsuchiya, M. and L. Talley (1992) An eastern Atlantic section from Iceland southward across the equator. *Deep-Sea Res.*, **39**, 1885-1917.

Tsuchiya, M. (1982) On the Pacific upper-water circulation. *J. Mar. Res.*, **40** suppl., 777-799.

Van Scoy, K. A. and E. R. M. Druffel (1993) Ventilation and transport of thermocline and intermediate waters in the Northeast Pacific during recent El-Niños. *J. Geophys. Res.*, **98**, C10, 18083-18088.

Van Scoy, K. A., R. A. Fine and H. G. Östlund (1991) Two decades of mixing tritium into the North Pacific Ocean. *Deep-Sea Res.*, **38** suppl., 191-219.

Walin, G. (1982) On the relation between sea-surface heat flow and thermal circulation in the ocean. *Tellus*, **34**, 187-195.

Walker, S., P. Salameh and R. Weiss (1995) Table of reconstructed atmospheric F-11 and F-12 histories. personal communication.

Wallace, D. W. R. (1995) Monitoring global ocean carbon inventories. Ocean Observing System Development Panel, Texas A&M University, College Station, TX, 54 pp.

Wallace, D. W. R. and J. R. N. Lazier (1988) Anthropogenic chlorofluoromethanes in newly formed Labrador Sea water. *Nature*, **332**, 61-63.

Warner, M. J., J. L. Bullister, D. P. Wisegarver, R. H. Gammon and R. F. Weiss (1996) Basinwide distributions of chlorofluorocarbons CFC-11 and CFC-12 in the North Pacific: 1985-1989. *J. Geophys. Res.*, **101**, C9, 20525-20542.

Warner, M. J. and R. F. Weiss (1992) Chlorofluoromethanes in South Atlantic Antarctic intermediate water. *Deep-Sea Res.*, **39**, 2053-2075.

Warner, M. J. and R. F. Weiss (1985) Solubilities of chlorofluorocarbons 11 and 12 in water and seawater. *Deep-Sea Res.*, **32**, 1485-1497.

Watanabe, Y. W., K. Harada and K. Ishikawa (1994) Chlorofluorocarbons in the central North Pacific and southward spreading time of North Pacific intermediate water. *J. Geophys. Res.*, **99**, C12, 25195-25213.

Weiss, R. F. (1970) The solubility of nitrogen, oxygen, and argon in water and seawater. *Deep-Sea Res.*, **17**, 347-359.

Woods, J. D. (1985) The physics of thermocline ventilation. In: *Coupled Ocean-Atmosphere Models*, Chapter 34. J. C. J. Nihoul, editor, Elsevier, Amsterdam, 767 pp.

Yuan, X. and L. D. Talley (1992) Shallow salinity minima in the North Pacific. *J. Phys. Ocean.*, **22**, 1302-1316.

Zhang, J., P. D. Quay and D. O. Wilbur (1995) Carbon isotope fractionation during gas-water exchange and dissolution of CO_2. *Geochim. Cosmochim. Acta,* **59**, 1, 107-114.

VITA

Rolf Erik Sonnerup

University of Washington

1999

Education

Institution	*Degree*	*Year*	*Field of Study*
Princeton University Princeton NJ	B.A. (honors)	1987	Chemistry
University of Washington Seattle WA	Ph. D.	1999	Chemical Oceanography

Research Experience

Position	*Years*	*Organization*
U.W. Space grant fellowship	1991	University of Washington
National Defense Science and Engineering fellowship	1991-1994	University of Washington
Research Associate	1994-1999	University of Washington

Teaching Experience

Teaching Assistant, (introductory physical oceanography)	1994	University of Washington
Guest Lecturer, (graduate course in geochemical modeling)	1997	University of Washington

Employment Experience

Associate Chemist	1987-1988	Remediation Technologies, Inc. Seattle WA
Chemist	1988-1989	PTI Environmental Consultants, Inc. Bellevue WA
Commercial Fisherman (month of July)	1989-	independent owner/operator in Bristol Bay (AK) salmon fishery

Publications

Sonnerup, R.E., P. D. Quay, and J. L. Bullister, (1999), Thermocline Ventilation and Oxygen Utilization Rates in the Subtropical North Pacific Based on CFC Distributions During WOCE, *Deep Sea Research,* **46**, 5, 777-805.

Sonnerup, R. E., P. D. Quay, T. A. Westby, H. Anderson, A. P. McNichol and J. L. Bullister (1999) "Reconstructing the Oceanic ^{13}C Suess Effect" *Global Biogeochemical Cycles.,* (in press).

Sonnerup, R. E. and P. D. Quay. The ^{13}C Suess Effect in the Indian Oceans. Manuscript in preparation for *Global Biogeochemical Cycles,* draft available upon request.

Presentations

"Reconstructing the Oceanic ^{13}C Suess Effect." U W Chemical Oceanography Departmental Seminar, March 1999.

"Thermocline ventilation and oxygen utilization rates in the North Pacific". Danish Center for Earth System Science, Departmental Seminar, November 1998.

"Reconstructing the Oceanic ^{13}C Suess Effect Using Preformed ^{13}C." American Geophysical Union Ocean Sciences Meeting, February 1998.

"Oceanic Uptake of Fossil-Fuel CO_2 Determined Via Preformed ^{13}C." U W Chemical Oceanography Departmental Seminar, December 1997.

"Oceanic Uptake of Anthropogenic CO_2 Based on $^{13}C/^{12}C$ of Total CO_2 in the Oceans, a Synthesis". Carbon Modeler's Consortium, Princeton University, February 1997.

"Thermocline Ventilation and Oxygen Utilization Rates in the North Pacific" Maurice Ewing Symposium on the Applications of Trace Substance Measurements to Oceanographic Problems, Biosphere 2, October 1995.

"Anthropogenic Chlorofluorocarbons and Radiocarbon in the Subtropical North Pacific Thermocline." U W Chemical Oceanography Departmental Seminar, January 1995.

"Thermocline Ventilation Rates in the North Pacific" American Geophysical Union Fall Meeting, December 1994.

IMAGE EVALUATION
TEST TARGET (QA-3)

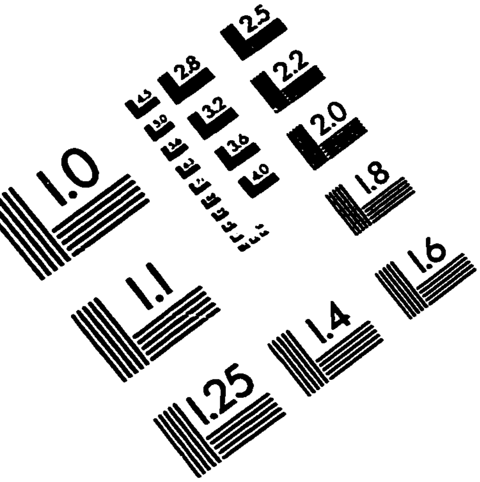

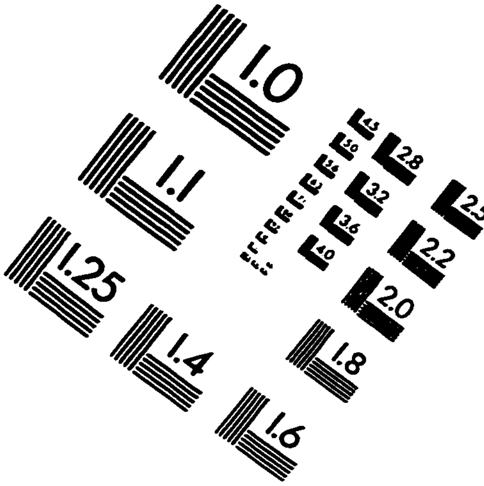

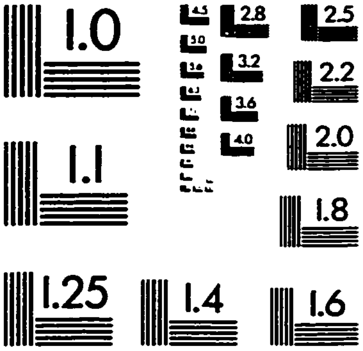

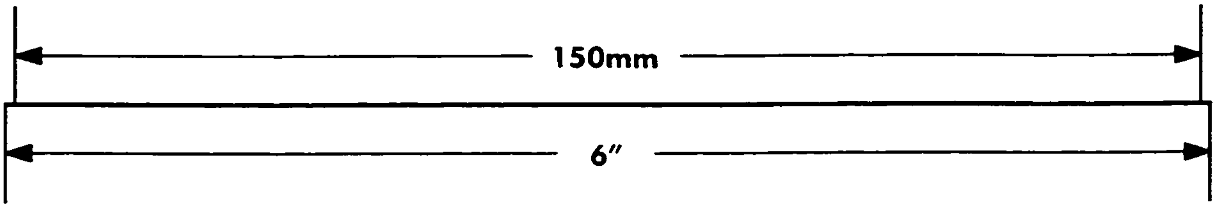

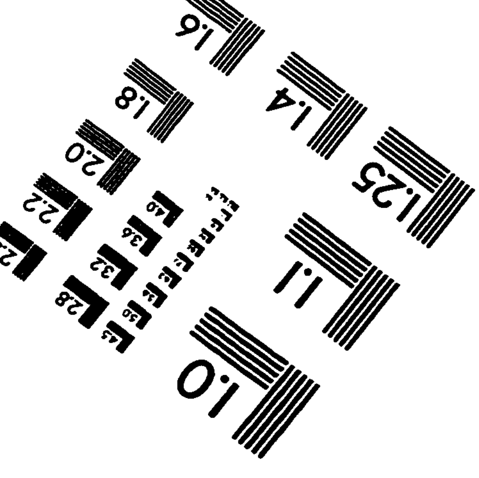

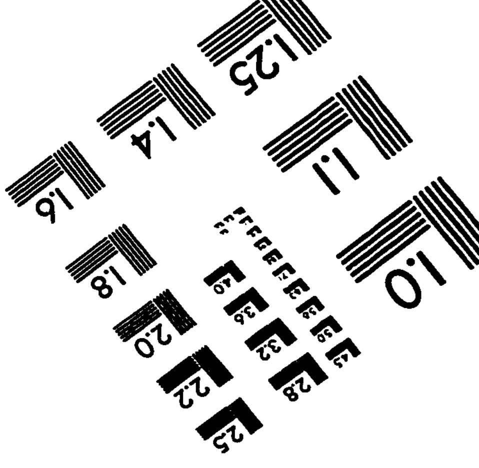

APPLIED IMAGE . Inc
1653 East Main Street
Rochester, NY 14609 USA
Phone: 716/482-0300
Fax: 716/288-5989